

論文 / 著書情報  
Article / Book Information

題目(和文)	
Title(English)	The Influence of Rebar Corrosion on Steel-to-Concrete Bond and Stress Transfer of Damaged Concrete Around Rebar and Its Implementation into Structural Analysis Model
著者(和文)	栗原遼大
Author(English)	Ryouta Kurihara
出典(和文)	学位:博士(工学), 学位授与機関:東京工業大学, 報告番号:甲第11809号, 授与年月日:2022年3月26日, 学位の種別:課程博士, 審査員:千々和 伸浩,岩波 光保,高橋 章浩,佐々木 栄一,河野 進,牧 剛史
Citation(English)	Degree:Doctor (Engineering), Conferring organization: Tokyo Institute of Technology, Report number:甲第11809号, Conferred date:2022/3/26, Degree Type:Course doctor, Examiner:,,,,,
学位種別(和文)	博士論文
Type(English)	Doctoral Thesis

*The Influence of Rebar Corrosion on Steel-to-Concrete Bond and Stress Transfer of Damaged Concrete Around Rebar and Its Implementation into Structural Analysis Model*

鋼材—コンクリート間の付着及び鉄筋周囲のコンクリートの応力伝達特性に与える鉄筋腐食の影響と構造解析モデルへの導入

Ryota Kurihara

Supervisor: Associate Professor Nobuhiro Chijiwa

Department of Civil and Environmental Engineering

Tokyo Institute of Technology

A dissertation submitted in partial fulfillment of the requirements for the degree of doctor of engineering

February 2022

## Abstract

Evaluation of residual structural performance on existing reinforced concrete structures is important for maintenance of sound infrastructures. Rebar corrosion is one of the typical deterioration phenomena in reinforced concrete structures, and many previous researches tried to understand rebar corrosion and its influence on the structural behavior. FE analysis is one of effective tools for quantitative evaluation on the structural performance of RC structures. FE analysis has been become possible with reproduction of real scale structures due to remarkable evolution in information technology, thus appropriate FE model for reinforce concrete subjected to rebar corrosion is required for the evaluation of existing structures. The objective was to develop a FE analytical model of bond degradation and corrosion cracking which can apply on real scale model.

In order to make clear bond deterioration behavior, the static beam loading test and the pull-out test of rebars with different bond conditions were conducted. Mechanical bond by interlock between lug of deformed bar and concrete is the dominant in bond components. Thus, interlock condition was focused in this investigation. FE analysis reproducing the shape of the rebars with hexahedral elements was also performed. It was mainly shown that bond was maintained as long as parts of regions of interlock remained, sound bond can be assumed. A FE model was proposed to derive the critical corrosion rate at which sound bond can be assumed, and to express the bond deterioration by changing the tension stiffening. It was verified that the model tracked the behavior of degraded beam members well even with a coarse mesh.

To make clear the influence of various scale cracks on structural performance and development of shear transfer model subjected to corrosion crack were also aimed. Before the model development, analytical investigation on the structural behavior of RC member with shrinkage cracking was conducted in order to confirm the accuracy of the evaluation of micro-cracking. The results suggested that shrinkage crack was the cause of the stiffness reduction observed in real structures, and it was confirmed that the evaluation accuracy for micro-crack was sufficient. On the other hand, corrosion cracks are formed along rebars with large openings, thus it has a deviation from the assumption of the smeared crack model. The proposed model for corrosion crack induction considered the non-uniformity of corrosion crack width, the non-penetration state in a finite element, and discharge of corrosion product from concrete surface through corrosion cracks with corrosion progress. The model was based on the results of shear test for concrete block with artificial crack and analytical investigation with fine mesh for tracking corrosion crack elongation. Based on the proposed corrosion model, analytical accuracy of structural behavior of the beam subjected to rebar corrosion was improved.

# Table of Contents

## Chapter 1

### *Introduction*

1.1 Background	2
1.2 Objectives	2
1.3 Previous researches and significance of this thesis	3
1.3.1 Deterioration mechanism of reinforced concrete caused by rebar corrosion	
1.3.2 Modeling of section loss	
1.3.3 Modeling of bond deterioration	
1.3.4 Modeling of corrosion crack	
1.3.5 Significance of this thesis	
1.4 Introduction of the analytical system and basic constitutive laws	6
1.5 Contents of this thesis	9

## Chapter 2

### *Investigation on the bond property change due to rebar corrosion and development of averaged bond deterioration model*

2.1 Abstract of chapter 2	16
2.2 Experimental program on the static loading test for RC beam	16
2.2.1 Specimens and materials	
2.2.2 Procedure of loading test	
2.3 Experimental results and discussion	19
2.3.1 Load-deflection relationship and behavior of crack distribution	
2.3.2 Strain distribution of main rebar	
2.3.3 Summary of experimental results	
2.4 FE analysis for reproduction on beam loading experiment	24
2.4.1 Outline of FE analytical model	
2.4.2 Segregated modeling of mortar and coarse aggregate with fine mesh	
2.4.3 Model of joint element	



2.4.4 Validation of analytical modeling by reproduction for pull out test for a rebar	
2.4.5 Results of reproduction analysis for beam loading test	
2.5 Analytical case study assuming lug loss due to rebar corrosion	33
2.5.1 Analysis cases	
2.5.2 Investigation on the effect of lug height loss	
2.5.3 Investigation on the effect of nonuniform lug loss region on cross section of rebar	
2.5.4 Investigation on the effect of non-uniform lug loss in the axial direction of rebar	
2.5.5 Summary of the analytical case study	
2.6 Discussions from experimental and analytical investigations	39
2.7 Equivalent modeling of bond deterioration	40
2.7.1 The modeling concept and the proposal	
2.7.2 The influence of bond deterioration model on structural behavior	
2.8 Summary of chapter 2	43

### Chapter 3

#### *Investigation on the influence of various scale cracks on structural performance and development of shear transfer model subjected to corrosion crack*

3.1 Abstract of chapter 3	47
3.2 The influence of distributed cracks on RC structures	49
3.2.1 Drying shrinkage effects on structural performance in full scale structures	
3.2.2 Drying shrinkage effects on structural performance in member scale structures	
3.2.2 Outcomes from analytical investigations on distributed fine cracks	
3.3 The influence of concentrated crack due to corrosion expansion	57
3.3.1 Organization of issues on modeling of corrosion crack	
3.3.2 The conventional model for shear transfer on crack surface of concrete	
3.3.3 The conventional model for corrosion expansion induction	
3.3.4 Variation of shear stiffness reduction behavior with dependence on mesh size	
3.4 Development of shear transfer model before crack penetration	62
3.4.1 Experimental program focusing on the shear stiffness with non-penetrated crack	
3.4.2 Experimental results and proposal of the shear transfer model	
3.4.3 Determination method of cracked area ratio to uncracked area in a finite element	

3.5 Development of shear transfer model after crack penetration .....	70
3.5.1 Equivalent crack width model considering nonuniformity of crack	
3.5.2 Crack width model considering crack opening limit	
3.6 Structural behavior change by proposed shear transfer model on a RC member ...	74
3.6.1 The target member and outline of static loading test	
3.6.2 Reproduction FE analysis by the conventional corrosion crack induction model	
3.6.3 Application of the proposed model considering the discharge limit	
3.6.4 The influence of the equivalent crack width model on shear transfer	
3.6.5 Structural behavior change with corrosion progress	
3.7 Summary of chapter 3 .....	83

## Chapter 4

### *Conclusions*

4.1 Conclusions .....	89
4.2 Future recommendations .....	91

# Chapter 1

## Introduction

- Backgrounds
- Objective and Significance of this thesis
- Review of previous researches
- Basic constitutive laws of the FE analysis
- Contents of this thesis

## 1.1 Background

Many reinforced concrete structures which were constructed in the high economic growth period in Japan have been elapsed for more than 50 years from completion. Deteriorations by the influence of environmental action or external force have been reported, and repairment or strengthening are strongly required as a social demand. Residual performance evaluation for deteriorated RC structures is necessary for determination of appropriate maintenance strategy. FE analysis which can reproduce invisible stress stream in detail can greatly help it. Application of FE analysis for RC structures had been tried from 1960s and various modeling and constitutive laws were proposed for reproducing nonlinear and time-dependent behavior of reinforced concrete [1-2]. Applicable range for various dimension and phenomenon and acceptable computation load of FE analysis has improved with remarkable evolution in computation technology, and real scale FE analysis reproducing existing structures directly has become possible in recent years [3-5].

When deterioration of RC structure is focused, rebar corrosion is one of the typical deteriorations in reinforced concrete structures. It is caused by various factors such as chloride attack, carbonation, and can lead to serious degradation of structural performance such as load-bearing capacity or ductility. [6-9]. It is strongly required to develop methods to evaluate the current and future structural performance of reinforced concrete structures with rebar corrosion. Rebar corrosion is meso-scale phenomena such as bond deterioration between rebar and concrete, section loss of rebar, or local cracking induced by expansive strain around rebar. There are many researches focusing on FE analytical model for RC structure with rebar corrosion [10-14], but most of the models developed in same scale as corrosion phenomena by discrete RC model or fine mesh strategy. In real scale FE analysis, it is required to perform FE analysis by rough mesh model for the purpose investigating structural performance as averaged behavior with practical computation load. Thus, real scale FE analysis should conflict against rebar corrosion modeling in scale problem.

Current evaluation methods on the residual structural performance for existing structures with rebar corrosion are based on the visual inspection and the grading of deterioration stage semi-qualitatively. Therefore, the quantitative evaluation method is greatly required for effective and efficient maintenance under limited resource. Development of an equivalent model for rebar corrosion in rough mesh size, which can be applicable in real scale FE model with low computation load, can greatly promote the establishment of a quantitative evaluation method for the structural performance.

## 1.2 Objectives

Under a social demand of FE modeling which is applicable for real scale analysis with rebar corrosion, this thesis focused on the development of structural FE analytical model for reinforced concrete with rebar corrosion, which is applicable in rough mesh. The objectives of this research are summarized as follows.

(1) Objectives in Chapter 2 (Bond deterioration)

- To make clear the bond deterioration behavior by interlock loss due to section loss of rebar
- Development of bond deterioration model base on the precise understanding of bond mechanism

(2) Objectives in Chapter 3 (Shear transfer on the crack surface)

- To make clear the influence of distributed cracks due to drying shrinkage on the structural performance in various dimension
- To make clear the shear transfer behavior of concrete with nonuniformity in crack elongation progress, crack width, and crack direction.
- Development of shear transfer model of concrete with macro crack due to corrosion determined from corrosion ratio

### **1.3 Previous researches and significance of this thesis**

#### **1.3.1 Deterioration mechanism of reinforced concrete caused by rebar corrosion**

Rebar in concrete is covered by passivation film generated by high alkali condition of hardened cement in the sound condition. It can shut electron movement between rebar and concrete and steel corrosion can be prevented. However, passivation film can be destructed due to low alkali condition caused by carbonation or anion attack such as chloride ion [15]. Therefore, oxidation reaction of steel can start at passivation film destructed region. Rebar corrosion is electro chemical change from iron to corrosion product such as iron oxide or iron oxyhydroxide. In other word, rebar corrosion causes the generation of corrosion product and section loss of rebar. The volume of corrosion product is larger than that of iron, thus corrosion product exerts an expansion force from inside of concrete around rebar inducing cracks of concrete around rebar. After inside cracks reach the concrete surface, deterioration factors from the concrete surface can easily ingress, thus corrosion crack speeds up rebar corrosion and degradation of durability [16-18]. During this corrosion process, the bond between the rebar and the concrete deteriorates, which affects the load bearing mechanisms [19-22].

Changes of the structural performance due to rebar corrosion had been focused by many previous researches, and most of them conducted structural performance evaluation tests on the RC member with accelerated rebar corrosion. It was known that section loss, bond deterioration, and corrosion crack induced by rebar corrosion were mainly have influence on structural performance. These effects complexly mixed in the situation with actual corroded rebar, and few previous researches separated out each phenomenon induced by rebar corrosion.

Section loss of rebar is equivalent as reduction of steel amount in the cross section of RC structures, thus it causes degradation of yielding load and load capacity. Deterioration of bond, which is stress transfer function between rebar and concrete, causes decrease of flexural capacity, stiffness, crack dispersibility, and resistance against crack elongation of reinforced concrete members [23-24].

On the other hand, when the anchorage of main rebar is sound, bond deterioration can improve shear capacity by the formation of the tied arch mechanism due to uniform strain distribution of lateral rebar [25-27]. Corrosion crack causes stiffness degradation of RC members due to reduction of shear stress transfer between cracks, and eventually leads to spalling of cover concrete due to the complete separation of concrete by complete crack elongation. Corrosion crack also causes bond degradation because local bearing pressure strength around rebar was reduced. While researches focusing on structural performance change due to corrosion crack with artificial crack for considering cracking effects were very few [28], but positive effects such as increase of shear crack formation load by inhibition of propagation of flexural crack or shear crack by external force were also reported.

### 1.3.2 Modeling of section loss

Most models of the representation for section loss due to rebar corrosion were based on reduction of rebar ratio or the mechanical performance of the rebar such as yield strength [10, 29-31]. It is because section loss of rebar means that reduction of rebar amount in the cross section, thus direct reproduction such as reduced amount of rebar, or indirect reproduction such as reduced equivalent yield strength was applied. In the case of serious corrosion level, rupture of rebar occurs at corrosion pit even under lower tensile stress than the value calculated from averaged section loss. Coronelli *et al.* suggested that declination of rebar performance by pit corrosion can be considered as implementation of the ratio of pit point area to cross section area of sound bar [10].

### 1.3.3 Modeling of bond deterioration

Sound bond between rebar and concrete is an important factor of load bearing mechanism of RC structure, and bond consists of three main components: mechanical interlock, chemical adhesion, and friction resistance. Among these, mechanical interlock, which is caused by bearing pressure between the uneven surface of the rebar and surrounding concrete, is highly effective, and interlock leads dispersion of inside crack around rebar [32- 35]. In order to obtain strong mechanical interlock, deformed bars with lugs are used in general reinforced concrete structures.

Bond deterioration mechanism is different in each bond component. Chemical adhesion between rebar and concrete should be lost immediately after rebar corrosion starting, because rebar is covered by corrosion product and rebar and concrete is detached in this situation. Friction resistance also reduced by corrosion product gel whose elastic modulus is greatly lower than concrete or steel. On the other hand, improvement of bond strength and stiffness by confinement of expansion stress in round bar was also reported before leak of corrosion gel from concrete surface through corrosion crack. It is because friction resistance becomes higher by increase of normal stress to rebar surface due to expansion stress. Section loss of rebar due to corrosion changes the shape of rebar, and lug shape that makes interlock is flattened [36]. Corrosion induced crack is also one of the causes of bond deterioration because crack around rebar reduces bearing pressure strength between lug and concrete

and contact area between lug and concrete by concrete deformation, resulting same condition as section loss [37].

Models of sound bond between rebar and concrete were based on investigation on one axial pull-out test of rebar, and bond behavior can be modeled from strength of concrete and slip displacement of rebar according to Shima *et al.* [35]. Here, there are two approaches for modeling of rebar in concrete in FE analysis, discrete model and smeared model. In the case that rebar is reproduced by discrete model, behavior of rebar is modeled with stress-strain relationship of steel, and embedded in concrete by beam as truss or line element. Then, stress transfer model between concrete and rebar, namely bond stress-slip relationship, is applied. Bond deterioration can be expressed by changing bond stress-slip relationship, extremely to no stress transfer [38, 39]. For reproducing stress-strain behavior as integrated material of rebar and concrete, smeared rebar model applies averaged strain-stress relationship as reinforced concrete and induction of tension stiffening can express bond behavior [40]. When bond between concrete and rebar can work, rebar strain around crack become large and uncracked region of concrete has tensile stress bearing while concrete in cracked region does not have. As a result, apparent resistance stress against tensile strain of concrete can be produced, and this mechanism is well known as tension stiffening. Stress-strain relationship after crack can be determined by stiffening parameter in averaged stress-strain relationship of reinforced concrete in smeared rebar model. Bond deterioration can be reproduced by reduced tension stiffening degree, but it has still room for investigation reduction behavior of tension stiffening with corrosion process.

#### 1.3.4 Modeling of corrosion crack

Cracked concrete model in numerical analysis is mainly divided into two approach, discrete crack model and smeared crack model. Discrete model treats crack as discontinuous surface, and re-meshing. On the other hand, smeared crack model defines the behavior of cracked concrete with distributed fine cracks in a element. In this approach, stress-strain relationship is more complex than discrete crack model, but re-meshing or crack propagation process is not required to be considered.

For modeling of corrosion crack, specific characteristics such as unevenness of expansion pressure or peculiar crack direction have to be taken into account. In discrete model, crack width by corrosion crack can be evaluated directly but crack elongation direction or crack occurrence location are difficult to be expected. Rigid Body Spring Model proposed by Kawai [41] or Lattice Model proposed by Bazant et al. [42] are one of the analytical models of major discrete crack and escaped specific expectation model of crack location or propagation for corrosion crack by applying voronoi diagram for meshing [43, 44]. In smeared crack model, modeling methods have been developed to evaluate corrosion crack caused by expansive stress caused by corrosion products, mainly by inducing forced displacement and expansion stress [45-48]. Crack propagation behavior can be controlled expansive induction directly while accuracy of model highly depends mesh size. [48]

### 1.3.5 Significance of this thesis

FE analysis for real scale structure prefers smeared model by large mesh size to discrete model or using small mesh size from the view point of modeling load or computation load especially in the evaluation simulating overall structural behavior, not fine points such as each crack elongation. For development of FE model which is applicable in real scale structure, each deterioration phenomena caused by rebar corrosion were focused. Section loss of rebar can be reproduced by reduced rebar ratio determined by corrosion amount, and this approach have been developed in previous researches.

When considering bond deterioration, most of the previous researches focused on the pull-out behavior of rebar or the response as a RC member with rebar corrosion due to exposure in actual environment or electrical acceleration. Here, bond deterioration mechanism is complexed; interlock condition changes between lug and concrete due to section loss, loss of chemical adhesion, friction resistance against rebar slip, and reduction of the bearing strength of concrete due to cracks around rebar. Previous discussions cannot evaluate the change of contribution of bond constituting components or corrosion crack. Thus, for an accurate understanding of the phenomenon, it is necessary to separate out the multiple factors of bond deterioration. Mechanical interlock is dominant factor in the three bond components and the author expects interlock condition change due to section loss by corrosion can determine total bond performance. This thesis focused on the evaluation of influence of change in interlock condition on load bearing mechanism and bond performance of RC beams through the experimental and analytical investigations. Based on the investigations, it was required to develop equivalent representation for bond, namely stress transfer degree between rebar and concrete, not direct representation such as joint element.

Representations for corrosion crack in the current smeared crack model were proposed and verified for member scale investigations by applying same scale of mesh size as cross section of rebar. Thus, crack around rebar can be reproduced directly. Basically, these approaches are based on inducing of forced expansion stress with rebar location, but the accuracy of application in large mesh size has to be discussed more because non-penetrated crack condition or unevenness of corrosion crack surface has to be considered equivalently.

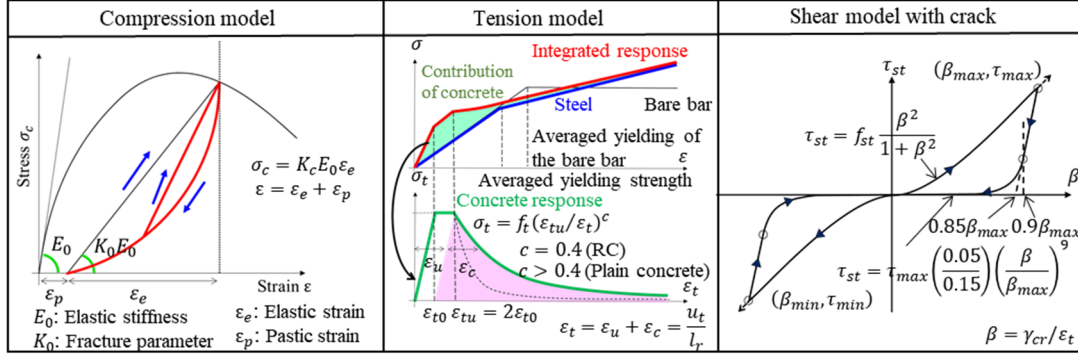
## 1.4 Introduction of the analytical system and basic constitutive laws

Through the thesis, the author used the three-dimensional nonlinear finite element analytical system “COM3” for the analysis [50]. This system introduces the six-directional fixed smeared crack model based on the active crack method [51]. Active crack concept suggested that non-linearity of concrete can be dominantly determined by widest opening crack under stress field in that time, and structure model of cracked concrete at active crack is applied for one element. Applicability of COM3 to various reinforced concrete structures in the past researches [2-5, 27-28, 47-29, 52,53]. Summary

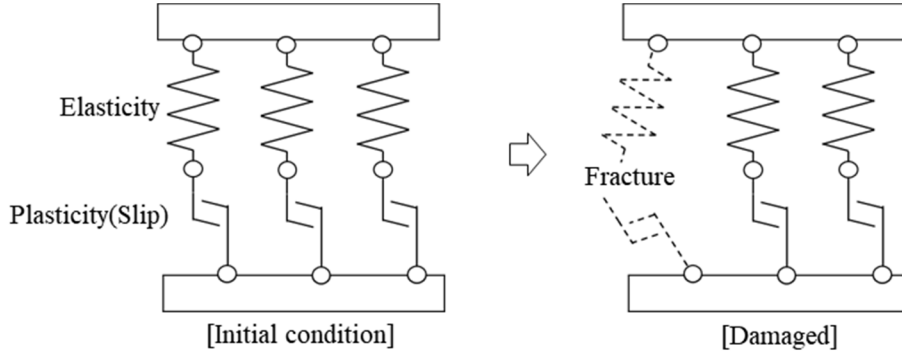


of constitutive laws of compression, tension, and cracked shear were shown in **Fig. 1.1**.

Elasto-plastic and continuum fracture model as shown in **Fig 1.2** [50, 54] was applied for concrete compression model. Compressive stiffness is modeled by multiple springs and cumulative plastic damage such as micro crack or local crush is expressed by decrease of springs, namely stiffness



**Fig 1.1** Constitutive laws of reinforced concrete in COM3



**Fig 1.2** Concept of Elasto-plastic and continuum fracture model

reduction. Under this concept, constitutive law of concrete in compression is given by **Eq. (1.1)**

$$\sigma_c' = K_c E_0 (\epsilon' - \epsilon_p') \quad (1.1)$$

Where,  $\sigma_c'$  is normalized compressive stress by compressive strength,  $E_0$  is initial tangent elastic modulus,  $\epsilon'$  is compressive strain,  $\epsilon_p'$  is plastic compressive strain, and  $K_c$  is failure parameter.  $K_c$  means the survive ratio of springs keeping load bearing function, namely stiffness ratio to sound elastic modulus. Survive ratio  $K_c$  and  $\epsilon_p'$ , that is residual strain in actual situation, are given **Eq. (1.2)** and **Eq. (1.3)** in normal strength concrete under one axial stress field, respectively.

$$K_c = \exp[-0.73(\epsilon_{max}')\{1 - \exp(-1.25\epsilon_{max}')\}] \quad (1.2)$$

$$\varepsilon'_p = \varepsilon'_{max} - (20/7) \{1 - \exp(-0.35\varepsilon'_{max})\} \quad (1.3)$$

Where,  $\varepsilon'_{max}$  is maximum compressive strain in stress hysteresis. This compression model can be expanded to three dimensions constitutive law by equivalent stress and strain composed with average stress and deviatoric stress in solid element.

Tension model of concrete is based on the averaged stress and averaged strain relationship [55]. This model has good agreement with the smeared crack model proposed by Vecchio and Collins [56], and tension softening behavior is separately considered by RC zone, which is affected by bond between rebar and concrete, and plain concrete zone defined by the zoning method [57]. In RC zone, concrete has resistance against tensile strain even after cracking because rebar stress can be transferred by bond between rebar and concrete with known as tension stiffening. Concrete tensile model after crack with tension stiffening can be given by **Eq. (1.4)**.

$$\sigma_c = f_t(\varepsilon_{tu}/\varepsilon_t)^c \quad (1.4)$$

Where,  $\sigma_c$  is averaged tensile stress,  $\varepsilon_{tu}$  cracking strain,  $\varepsilon_t$  averaged tensile strain, and  $c$  is stiffening parameter which represents bond condition. Based on the previous researches,  $\varepsilon_{tu}$  and  $c$  adopt 0.0002 and 0.4 for RC zone, respectively [57]. In plain concrete, tension softening behavior can be determined by tension fracture energy and size on which the average stress-strain relationship is defined. Stiffening parameter of plain concrete can be given by **Eq. (1.5)**.

$$\int \sigma_c d\varepsilon_t = G_f/l_r \quad (1.5)$$

Where,  $G_f$  is fracture energy of concrete and  $l_r$  is reference length of finite element. In this model, reference length is equal to finite element size.

Shear model of cracked concrete is based on the contact density function model [58]. **Equation (1.6)** shows the relationship between shear stress  $\tau$  and shear strain  $\gamma$  by shear stiffness  $G$ .

$$\tau = G\gamma \quad (1.6)$$

Shear stiffness  $G$  of cracked concrete is described as shown in **Eq. (1.7)** and **Eq. (1.18)**.

$$1/G = 1/G_{st} + 1/G_c \quad (1.7)$$

$$G_{st} = \frac{\tau_{st}}{\gamma} = f_{st} \frac{\beta^2}{1 + \beta^2}, \beta = \frac{\gamma}{\varepsilon_t} \quad (1.8)$$

Where,  $G_{st}$  is intrinsic shear stiffness,  $G_c$  is shear stiffness of uncracked concrete,  $\varepsilon_t$  is tensile strain normal to crack surface, and  $f_{st}$  is intrinsic shear strength. This shear model can describe shear stiffness by only the ratio of averaged shear strain to averaged tensile strain without absolute value of crack spacing or crack width. When cracks closed, cracked concrete should have high shear stiffness, thus uncracked shear stiffness  $G_c$  was taken into account. Because the value of  $G_c$  is greatly higher

than  $G_{st}$ , the value of  $G_{st}$  becomes dominant with large tensile strain in normal to crack surface.

For rebar model, COM3 applies tri-linear stress-strain relationship considering elastic modulus, yield strength, tensile strength, yield plateau strain, and tensile rupture strain.

## 1.5 Contents of this thesis

This thesis was organized by 4 chapters. Chapter 1 described background, objectives and significance of this thesis with the reviews of previous researches and FE modeling approaches for corroded RC structure. Basic constitutive laws in the analytical system on which this study focused was also introduced in Chapter 1.

Chapter 2 investigated influence of interlock loss due to rebar corrosion on bond performance and structural performance in member and shows the bond deterioration model under 20% of corrosion ratio. 20% is approximately maximum value in corrosion ratio in land structure, except the structure under severe environment such as coastal structure. In the investigation on influence of interlock loss, which is dominant factor of bond components on structural performance of RC member, static loading tests on beams with different interlock conditions was conducted. The loading test on beam specimens were analyzed by the FE model that reproduces the shape of rebar using solid elements precisely. This FE model applied very fine mesh, and mortar and coarse aggregate were modeled individually. These models were verified by reproduction analysis for beam loading tests and rebar pull-out tests from concrete. Then, analytical case studies simulating non-uniform or partial shape change of rebar in cross section and in axial direction were conducted. Bond deterioration with corrosion progress was proposed, and bond performance in large mesh by smeared rebar model was represented by degree of tension stiffening, which shows resistance against tensile stress after cracking. Structural performance change due to reduced tension stiffening degree with proposed bond deterioration model was also described.

Corrosion crack model was developed in Chapter 3. At first, in order to arrange the overall understanding of the influences of crack on RC structure or RC member, distributed micro crack and concentrated macro crack were discussed separately. This thesis conducted thermo-hygro analysis and integrated with structural analysis, and make clear that stiffness reduction as a structure is caused by drying shrinkage cracks by full-scale analysis. Then, the mechanism of stiffness reduction by drying and the effects of member size are investigated. The investigations showed the cracks in concrete caused stiffness reduction and it was caused by reduction of shear transfer degree of concrete between crack surface. When considering the modeling of cracks, one of the major differences between drying shrinkage crack and corrosion crack was scale. Drying shrinkage crack was distributed in an entire member as many fine cracks, thus it had affinity with smeared crack model, which assumes distributed crack in all region in an element. On the other hand, corrosion crack was concentrated meso-scale crack along rebar and unevenness in crack width or crack progress direction should be considered.

Discussion on shear transfer between corrosion crack was separated into three parts, stage 1 until corrosion crack reaches concrete surface, stage 2 after crack penetration, and stage 3 discharge of corrosion product from opened corrosion crack in concrete surface. Until penetration of crack, a finite element had both cracked and uncracked region, and uncracked concrete has high shear stiffness. However, conventional model defined cracked or uncracked model in a element with strain. In order to investigate shear stiffness with both cracked and uncracked region in a element, shear loading test for concrete blocks with inducing non-penetrated pre-cracked were conducted. Experimental result showed that shear stiffness value by corrosion crack can be determined from the ratio of cracked area of concrete to uncracked area. For defining cracked area ratio from corrosion ratio, fine mesh analysis simulating corrosion crack elongation was conducted. This analysis model reproduced a rebar embedded in the center of square concrete, and composed from steel element and concrete element, joint element between interface of steel and concrete. Corrosion expansion was applied as forced expansion strain in steel element, and ratio of cracked to uncracked area was defined as the function of corrosion ratio with referring previous experiments focusing on crack elongation due to corrosion process. After corrosion cracks penetrated through all section of concrete in a element, shear stiffness reduction was overestimated in the case that large mesh was used and distributed rebar ratio was applied. It was because that large mesh reproduced straight crack propagation along rebar even while unevenness crack width in normal and parallel direction to rebar axial had to be considered. Equivalent corrosion crack width was proposed for solving derivation of modeling from actual condition in the stage 2. In serious corrosion ratio defined as stage 3, limitation of crack opening due to release of expansion stress caused by leak of corrosion gel had to be considered. Thus, discharge limit, which represented maximum crack width were proposed. Modified corrosion model can reproduce the structural behavior of member with rebar corrosion, and proposed model can be verified.

Chapter 4 summarized the conclusions of this study. Recommendations of further studies were also listed.

## References in Chapter 1

- [1] 岡村甫, 前川宏一, (1985), 鉄筋コンクリートにおける非線形有限要素解析, 土木学会論文集, (360), 1-10
- [2] D. Ngo, A. C. Scordelis, (1967), Finite Element Analysis of Reinforced Concrete Beams, ACI Journal, 64, 152-163
- [3] Maekawa, K., Chijiwa, N., Ishida, T., (2011). Long-term deformational simulation of PC bridges based on the thermo-hygro model of micro-pores in cementitious composites. Cement and Concrete Research, 41(12), 1310-1319.
- [4] Ohno, M., Chijiwa, N., Suryanto, B., Maekawa, K., (2012). An investigation into the long-term

excessive deflection of PC viaducts by using 3D multi-scale integrated analysis. *Journal of advanced concrete technology*, 10(2), 47-58.

[5] Kurihara, R., Chijiwa, N., & Maekawa, K., (2017), Thermo-hygral analysis on long-term natural frequency of RC buildings with different dimensions. *Journal of Advanced Concrete Technology*, 15(8), 381-396

[6] Tuutti, K, (1982), Corrosion of steel in concrete, Doctoral dissertation, Lund University

[7] Page, C. L., (1975), Mechanism of corrosion protection in reinforced concrete marine structures, *Nature*, 258, 5535: 514-515

[8] C. Alonso, C. Andrade, J.A. Gonzalez, (1988), Relation between resistivity and corrosion rate of reinforcements in carbonated mortar made with several cement types, *Cement and Concrete Research*, 18(5), 687-698

[9] 青山敏幸, 下村匠, 丸山久一, (1998), 塩害により鉄筋が腐食した RC 部材の曲げ性状. *コンクリート工学年次論文報告集*, 20:2, 883-888.

[10] D. Coronelli, P. Gambarova, (2004), Structural Assessment of Corroded Reinforced Concrete Beams: Modeling Guidelines, *Journal of Structural Engineering*, Vol.130(8), 1214-1224

[11] M, Berra, A. Castellani, D, Coronelli, S. Zanni, G. Zhang, (2003), Steel - concrete bond deterioration due to corrosion: finite-element analysis for different confinement levels, *Magazine of Concrete Research*, 55(3), 237-247

[12] L. Berto, P. Simioni, A. Saela, (2008), Numerical modelling of bond behaviour in RC structures affected by reinforcement corrosion, *Engineering Structures*, 30(5), 1375-1385

[13] 富田充宏, 梶川康男, 久野和敬, (1998), 鉄筋腐食により劣化した RC ばりの剛体 ばねモデルによる非線形解析, *土木学会論文集*, 584: 267-276.

[14] 車谷麻緒, 寺田賢二郎, 加藤準治, 京谷孝史, 檜山和男, (2013), コンクリートの破壊力学に基づく等方性損傷モデルの定式化とその性能評価, *日本計算工学会論文集*, 2019, 20190007

[15] 大即信明, 横井聡之, 下沢治, (1985), モルタル中鉄筋の不動態に及ぼす塩素の影響, *土木学会論文集*, (360), 111-118

[16] C. Aldea, S. Shah, A, Karr, (1999), Effect of Cracking on Water and Chloride Permeability of Concrete, *Journal of Materials in Civil Engineering*, 11(3)

[17] L. Bertolini, (2008), Steel corrosion and service life of reinforced concrete structures, *Structure Infrastructure Engineering*, 4(2), 123-137

[18] 岡田清, 小柳洽, 宮川豊章, (1979), コンクリート部材のひびわれと鉄筋腐食に関する研究. *土木学会論文報告集*, 1979(281), 75-87

[19] G.J. Al-Sulaimani, M. Kaleemullah, I.A. Basunbul, Rasheeduzzafar, (1990), Influence of corrosion and cracking on bond behaviour and strength of reinforced concrete members, *ACI Structural Journal*, 87(2), 220-231

- [20] C. Fang, K. Lundgren, L. Chen, C. Zhu, (2004), Corrosion influence on bond in reinforced concrete, *Cement and Concrete Research*, 34(11), 2159-2167
- [21] J. Rodriguez, L.M. Ortega, J. Casal, (1997), Load carrying capacity of concrete structures with corroded reinforcement, *Construction and Building Materials*, 11(4), 239-248
- [22] J. Cairns, Y. Su, D. Law, (2008), Structural performance of corrosion-damaged concrete beams, *Magazine of Concrete Research*, 60(5), 359-370
- [23] I. Sæther, (2011), Bond deterioration of corroded steel bars in concrete, *Structure and Infrastructure Engineering*. 7(6), 415-429
- [24] Y. Auyeung, P. Balaguru, L. Chung, (2000), Bond behaviour of corroded reinforcement bars, *ACI material Journal*, 97(2), 214-220
- [25] 池田尚治, 宇治公隆, (1980), 鉄筋コンクリートはりのせん断耐荷挙動に及ぼす鉄筋の付着の影響に関する研究. 土木学会論文報告集, 1980(293), 101-109
- [26] G. R. Pndey, H. Mutsuyoshi, T. Maki, R. Tanino, (2005), Enhancing shear capacity by controlling bond of reinforcement, *Proceedings of the Japan Concrete Institute*, 27(2), 799-804
- [27] 蔡強華, 伊藤陽平, 栗原遼大, 千々和伸浩, 鉄筋腐食による局所的な付着劣化が RC 梁のせん断性能に及ぼす影響に関する研究, 第 21 回コンクリート構造物の補修, 補強, アップグレードシンポジウム, 2021.10
- [28] 山田雄太, 千々和伸浩, 岩波光保. (2017), 引張主鉄筋に沿う人工損傷の長さがせん断補強筋の無い RC はりの疲労耐荷機構に及ぼす影響. 土木学会論文集 E2 (材料・コンクリート構造), 73(3), 323-336
- [29] L.A. Lutz, P. Gergely, (1967), Mechanics of bond and slip of deformed bars in concrete, *ACI Journal*, 64(11), 711-721
- [30] J. Cairns, G.A. Plizzari, Y. Du, D.W. Law, C. Franzoni, (2005), Mechanical properties of corrosion-damaged reinforcement, *ACI Mterial Journal*, 102, p256
- [31] A.A. Almusallam, (2010), Effect of degree of corrosion on the properties of reinforcing steel bars, *Construction and Building Materials*, 15, 361-368
- [32] L.A. Lutz, P. Gergely, (1967), Mechanics of bond and slip of deformed bars in concrete, *ACI Journal*, 64(11), 711-721
- [33] Y. Goto, (1971), Cracks formed in concrete around deformed tension bars, *ACI Journal*, 68(4), 244-251
- [34] 水野高明, 渡辺明, (1963), 丸鋼, 異形丸鋼および異形ねじり鉄筋の付着に関する研究, 第 93 号, pp.23-30, 土木学会論文集
- [35] 島弘, 周礼良, 岡村甫, (1987), マッシブなコンクリートに埋め込まれた異形鉄筋の付着応力 - すべり - ひずみ関係. 土木学会論文集, (378), 165-174.
- [36] 長岡和真, 阿部哲雄, 番場俊介, 村上祐貴, (2013), 主鉄筋の腐食膨張挙動に対するコンクリートの拘束圧に基づく付着割裂性状評価. コンクリート工学論文集, 24(2), 29-42.

- [37] Cairns, J., Du, Y., & Law, D., (2006), Residual bond strength of corroded plain round bars. Magazine of Concrete Research, 58(4), 221-231.
- [38] M. Berra, A. Castellani, D. Coronelli, S. Zanni, G. Zhang, (2003), Steel - concrete bond deterioration due to corrosion: finite-element analysis for different confinement levels, Magazine of Concrete Research, 55(3), 237-247
- [39] L. Berto, P. Simioni, A. Saela, (2008), Numerical modelling of bond behaviour in RC structures affected by reinforcement corrosion, Engineering Structures, 30(5), 1375-1385
- [40] Somayaji, S. and Shah, S. P.: (1981), Bond Stress Versus Slip Relationship and Cracking Response of Tension Members, ACI Journal, pp. 217-225
- [41] 辻野哲司, 竹内則雄, 川井忠彦. (1996), 離散化極限解析プログラミング離散化極限解析プログラミング 103, 1990. 木材学会誌, 42(6), 565-573.
- [42] Bažant, Z. P., Tabbara, M. R., Kazemi, M. T., Pijaudier-Cabot, G., (1990), Random particle model for fracture of aggregate or fiber composites, Journal of engineering mechanics, 116(8), 1686-1705
- [43] P. Grassl, T. Davies, (2011), Lattice modelling of corrosion induced cracking and bond in reinforced concrete, Cem. Concr. Compos., 33, pp.918-924.
- [44] Tran, K. K., Nakamura, H., Kawamura, K., Kunieda, M. (2011), Analysis of crack propagation due to rebar corrosion using RBSM, Cement and Concrete Composites, 33(9), 906-917
- [45] 車谷麻緒, 安藏尚, 相馬悠人, 岡崎慎一郎, (2019), 損傷モデルによる 3 次元腐食ひび割れ進展解析に関する基礎的研究, 日本計算工学会論文集, 2019, 20190007
- [46] 車谷麻緒, 寺田賢二郎, 久田真, (2007), 鉄筋の腐食膨張のモデル化とコンクリートのひび割れ挙動の数値解析. 土木学会論文集 A, 63(1), 167-178.
- [47] Toongoenthong, K., Maekawa, K., (2005), Multi-Mechanical Approach to Structural Performance Assessment of Corroded RC Members in Shear, Journal of Advanced Concrete Technology, 3(1), 107-122
- [48] Toongoenthong, K., Maekawa, K., (2005), Simulation of coupled corrosive product formation, migration into crack and propagation in reinforced concrete sections. Journal of Advanced Concrete Technology, 3(2), 253-265.
- [49] Gebreyouhannes, E., Maekawa, K., (2016). Nonlinear gel migration in cracked concrete and broken symmetry of corrosion profiles. Journal of Advanced Concrete Technology, 14(6), 271-286.
- [50] Maekawa, K., Okamura, H., Pimanmas, A., Nonlinear mechanics of Reinforced Concrete, Spon Press, 2003
- [51] 福浦尚之, 前川宏一, (2009), 非線形支配ひび割れ面の三次元同定と空間平均化構成則の高度化, 土木学会論文集 E, 65(1), 118-137
- [52] Chijiwa, N., Maekawa, K., (2015), Thermo-Hygral Case-Study on Full Scale RC Building under Corrosive Environment and Seismic Actions, J. Adv. Concr. Technol., 13(10), 465-478
- [53] Song, H., You, D., Byun, K., Maekawa, K., (2002), Finite element failure analysis of reinforced

concrete T-girder bridges, Eng. Struct., 2002, 24, 151-162

[54] Maekawa, K., Takemura, J., Irawan, P., Irie, M., (1993), Triaxial Elasto-Plastic and Continuum Fracture Model for Concrete, Proc. of JSCE, 460(V-18), 131-138

[55] Okamura, H., Maekawa, K., Sivasubramaniyam, S., Verification of modeling for reinforced concrete finite element, Finite Element Analysis of Reinforced Concrete Structures, Tokyo, Japan, May 21-24, ASCE, NewYork, 1985, pp528-543

[56] Vecchio, F. J., Collins, M. P. (1986), The modified compression-field theory for reinforced concrete elements subjected to shear, ACI J., 83(2), 219-231

[57] An, X., Maekawa, K., Okamura, H., (1997), Numerical Simulation of Size Effect in Shear Strength of RC Beams, J. Materials Conc. Struct. Pavement, 564(V-35), 297-346

[58] Li, B., Maekawa, K., Okamura, H., (1989), Contact Density Model for Stress Transfer across Cracks in Concrete, Journal of the Faculty of Engineering, 40(1), 9-52



# Chapter 2

Investigation on the bond property change due to rebar corrosion and development of averaged bond deterioration model

- Experimental investigation on structural behavior change by reduction of interlock area
- Analytical investigation on the relationship between interlock condition and bond performance with corrosion process
- Development of bond deterioration model

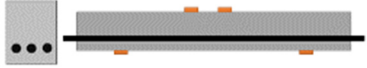
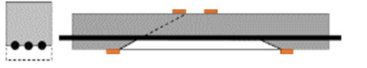


## 2.1 Abstract of Chapter 2

This chapter focused on bond between rebar and concrete and aimed development of bond deterioration model for RC structures with rebar corrosion. At first, in order to sperate out multiple bond components and to understand of bond deterioration mechanism, the author focused on the influence of interlock loss on the structural behavior and bond performance of RC member from experimental and analytical approach. Interlock was produced by bearing pressure between lug and concrete and contribution of interlock in bond is dominant in bond components. Static loading test on six RC beams and FE analysis reproducing beam tests were conducted for the investigation on the effects of reduced interlock condition, and confinement effects of stirrups against slipping of main rebar. In order to evaluate interlock effects precisely, rebar shape including lugs was reproduced by fine hexahedron elements in the FE analysis. The author also conducted analytical case studies for investigating the effects of non-uniform partial interlock loss due to section loss of rebar simulating expected situations caused by actual rebar corrosion. Through these case studies, it was showed that bond as an entire member is maintained and sound bond behavior can be assumed as long as parts of regions with interlock between lugs and concrete can work even when section loss of rebar occurs due to corrosion. Based on the investigations, bond deterioration model was proposed with tension stiffening. Sound bond can be assumed even when interlock region or interlock degree were reduced by section loss due to rebar corrosion, and reduced bond was applied in the serious corrosion ratio.

## 2.2 Experimental program on the static loading test for RC beam

In order to investigate the effect of interlock loss on the bond performance of RC beams, the static

**Table 2.1** List of the specimens

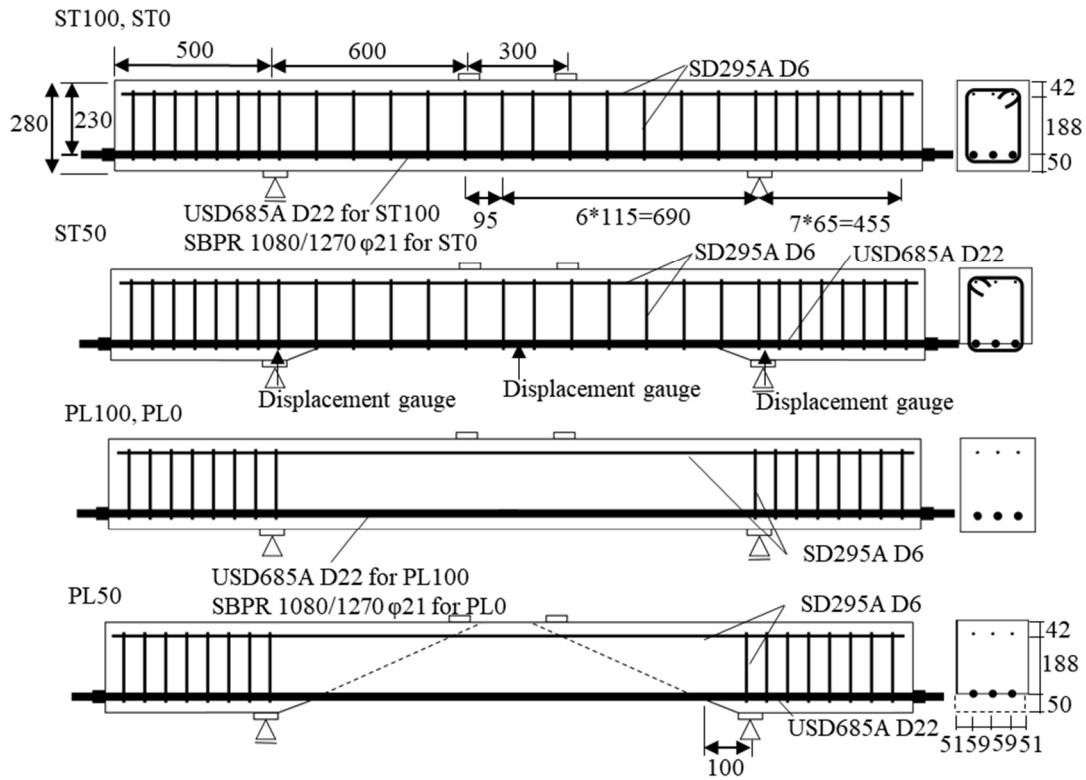
Name	Interlock area	Stirrup	Outline of experimental specimens	Remark
ST-100	100%	Placing		Sound specimen
PL-100	100%	Not placing		
ST-50	50%	Placing		 Specimen whose the underside of main rebar was exposed
PL50	50%	Not placing		
ST-0	0%	Placing		Specimen without interlock
PL-0	0%	Not placing		

loading test was conducted. Degree of bond was controlled by area with the contact between rebar lug and surrounding concrete. Interlock areas of specimens were designed as the values of 0%, 50%, and 100%. Placing of stirrup was also focused on for confirming confinement effects on deformation or slipping of main rebar by stirrup.

### 2.2.1 Specimens and materials

**Table 2.1** shows the list for specimens of a total 6 RC beams. In this test, the author focused on the interlock effects on load carrying mechanism in the bond components. For this purpose, interlock area was controlled although chemical adhesion and friction resistance was kept intact in the all cases.

The specimen with 50% interlock area had no cover concrete in the loading span, and the concrete was in contact with only the top half surface of the main rebars, and the bot-tom half side was exposed. Cases with 50% of interlock area focused on not only the effects of residual bond degree but also the reproduction in actual corrosion progress as an extreme case reproducing the situation that cover concrete was spalled but contact between upper side of main rebar and concrete was kept. The specimen with interlock area of 0% used round PC rod. Two series of specimens, the ST series with stirrup and the PL series without stirrup, were set for beams with three different interlock area. The geometry and rebar arrangement of specimens are shown in **Figure 2.1**. For the main rebars of the specimens, high strength screw bars were used in the cases of 100% and 50% interlock area cases, and



**Figure 2.1** Geometry and rebar arrangement of the specimens

round PC rod were used in the case of 0% interlock area. In all cases, D10 whose yield strength was 305MPa was used for the stirrup and compression bar. Beam specimens were designed for failing in shear with tensile rebar ratio of 1.95%, effective height of 230 mm, shear span of 600 mm, beam width of 220 mm, and anchorage length of 500 mm. For securing the solid anchorage, the main rebars were fixed by attaching nuts at the beam ends.

The six beam specimens were cast at the same time using ready-mixed concrete with the mix proportions given in **Table 2.2**. The formwork of PL-50, ST-50 were produced by Styrofoam, and cray

**Table 2.2** Mix proportions of concrete.

Conditions				Unit content(kg/m <sup>3</sup> )				
W/C (%)	s/a (%)	Slump (cm)	Air content (%)	Water	Cement	Sand	Gravel	Admixt ure
42.5	41.1	12	4.5	173	408	697	1033	4.08

Cement: Ordinary portland cement, density 3.13 g/cm<sup>3</sup>

Fine aggregate: Crushed and natural mixed sand, Specific gravity 2.60 g/cm<sup>3</sup>

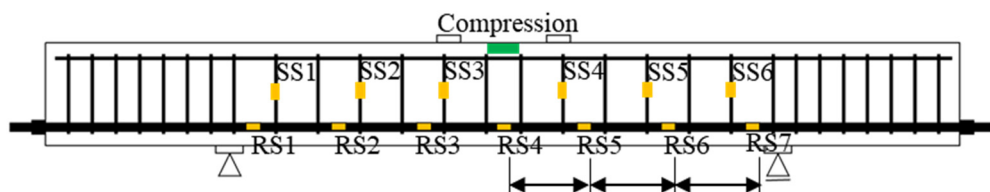
Coarse aggregate: Crushed limestone, Maximum size 20mm, Specific gravity 2.69 g/cm<sup>3</sup>

Chemical admixture: Polycarboxylic acid-based AE water reducing agent, density 1.04 g/cm<sup>3</sup>

**Table 2.3** Characteristics of materials used.

	Main rebar		Concrete	
	Screw bar	Round rebar (PC rod)		
Type	USD685A	SBPR 1080/1270	Compressive strength (N/mm <sup>2</sup> )	39.7
Yield strength (N/mm <sup>2</sup> )	710	1189	Elastic modulus (kN/mm <sup>2</sup> )	27.5
Tensile strength (N/mm <sup>2</sup> )	883	1270	Tensile strength (N/mm <sup>2</sup> )*	2.67

\*Estimated value from compressive strength based on JSCE Standard Specifications



**Figure 2.2** Measurement positions for main rebar strain

was attached in the bottom half surface of rebar in order to achieve loss of contact of rebar with concrete absolutely. The specimens were cured under sealed condition for 10 to 12 days under 20 degree of ambient temperature until the loading test. **Table 2.3** lists the mechanical properties of the concrete obtained from compression tests on cylinder specimens. 39.7 MPa of compressive strength and 27.5 kN/mm<sup>2</sup> of elastic modulus were measured. **Table 2.3** also shows the main rebar property, 710 MPa for screw bar and 1189 MPa for PC rod of yielding strength.

### 2.2.2 Procedure of loading test

Four-point static loading test was performed using a universal testing machine with the loading speed of 1kN/sec. Crack propagation was checked and marked by visual inspection every 20kN of load increasing. Total load, vertical deflection of the beam, and strain of the main rebar, stirrup and concrete were measured. The vertical deflection of the test specimen was taken as the difference from the displacement at center and supporting points. Main rebars strain in the both ST and PL series and stirrup strain in the ST series were measured by strain gauges attached on the rebars. The orange and green regions indicate the strain measurement positions of rebar and concrete in **Figure 2.2**, respectively. Strain at 7 points along main rebar were measured in order to track uniformity rebar strain indicating bond degree. Total 6 points of strain gauges were set for every other stirrup in the shear span. The strain gauges for rebar were attached before casting while the gauge for measuring the strain at compression edge of concrete was attached just before loading.

## 2.3. Experimental results and discussion

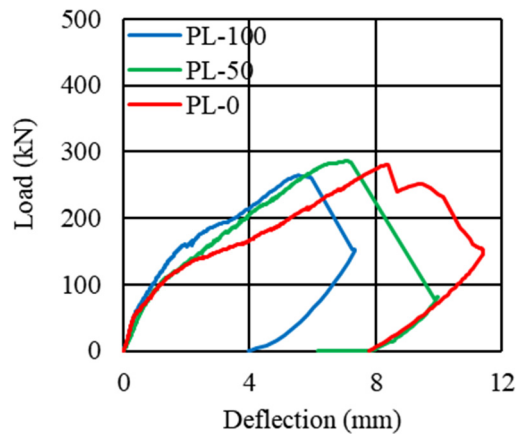
### 2.3.1 Load-deflection relationship and behavior of crack distribution

The load-deflection relationship of each specimen is shown in **Figure 2.3** and **Figure 2.4**. Comparison of maximum load with calculated load in each case with failure mode base on the JSCE code is shown in **Table 2.4**, and the designed flexure strength was 2.5 times and 1.3 times higher than that causing shear failure in PL series and ST series, respectively. **Figure 2.5** shows the crack pattern of each specimen after failure. The thick lines in the crack pattern show the dominant crack at failure. The shaded region in the PL-50 case indicates concrete crushed region at failure. Dot line and orange marks mean rebar arrangement and the strain measurement points of rebar, respectively.

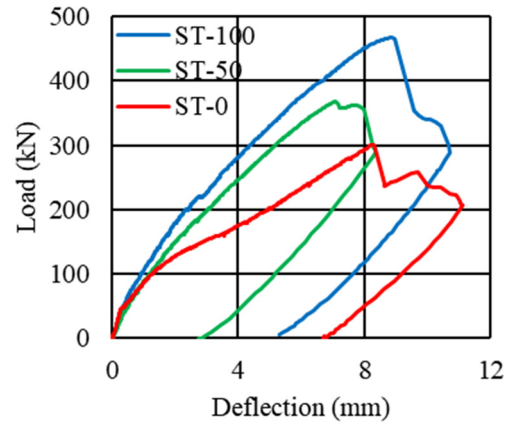
In both the PL series and the ST series, as the interlock area between the rebar and concrete decreased from 100% to 50% and 0%, the stiffness of the beam decreased after the formation of flexural crack. Initial stiffness in elastic range of the PL-50 and ST-50 specimens was lower than that of the specimens with 100% and 0% interlock area, on account of the smaller cross section of the beam due to the absence of cover concrete.

The maximum loads for the PL series were 264 kN, 285 kN, and 280 kN for PL-100, PL-50, and PL-0, respectively. Maximum load of PL-100 was 39% higher than that of design, but it was reasonable because it was well known that designed shear strength without stirrups was overestimated

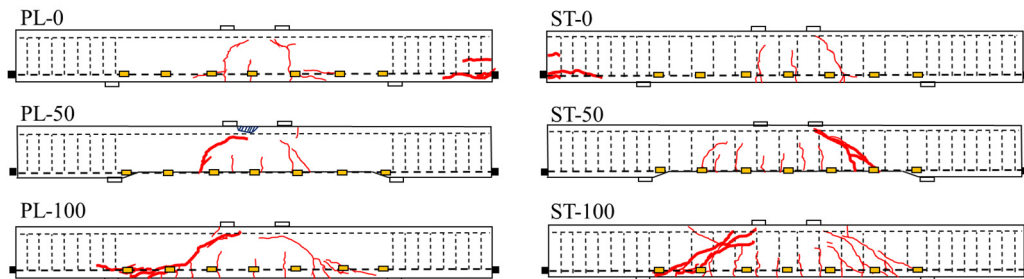
approximately at 30%. Although the maximum load of PL-50 was close to that of PL-100, load reduction of PL-50 was due to crushing at the top of the concrete at the center of the span, instead of shear failure as in PL-100. This is because that the tied arch was formed in PL-50, and the shear capacity was increased. The failure of PL-0 was caused by crushing of the concrete around the anchoring nuts.



**Figure 2.3** Load-deflection curve (PL series)



**Figure 2.4** Load-deflection curve (ST series)



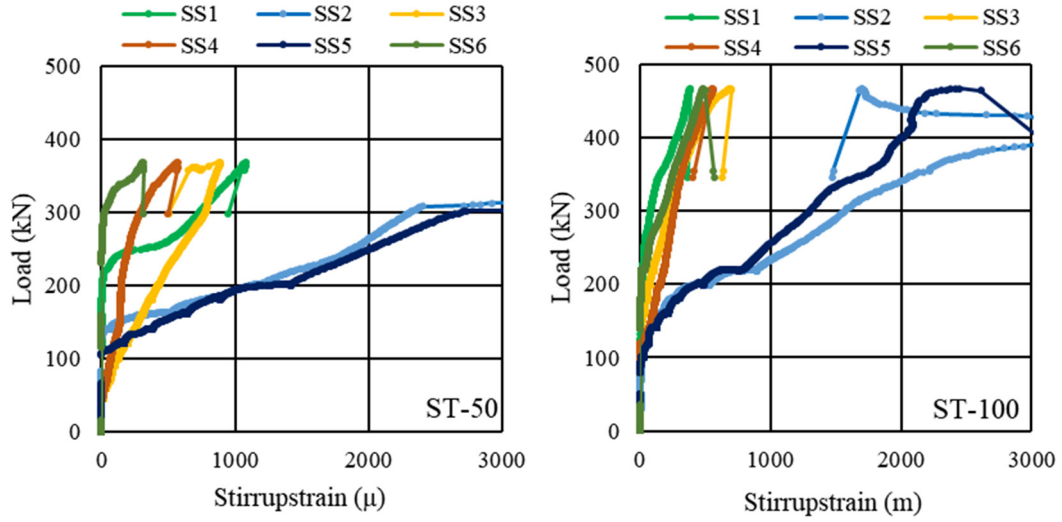
**Figure 2.5** Crack patterns by visual inspection after failure

(Thick line: dominant cracks at failure, Shaded area: concrete spoiled area at failure)

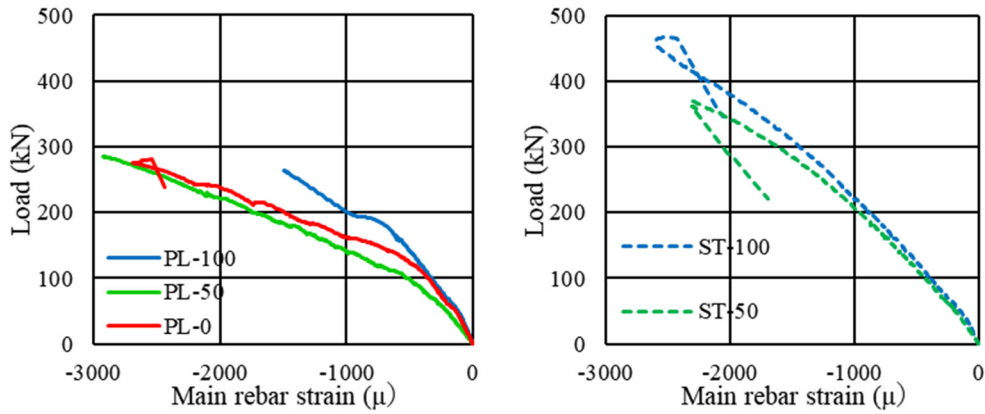
**Table 2.4** Comparison of maximum load with calculated load

Measured maximum load in the loading tests					Calculated maximum load*		
Interlock area	PL series		ST series		Mode	PL series	ST series
	Load	Failure mode	Load	Failure mode			
100%	264kN	Shear	466kN	Shear	Shear	189kN	359kN
50%	285kN	Compression	368kN	Shear	Flexure	478kN	478kN
0%	280kN	Anchorage	299kN	Anchorage			

\*Calculated values were based on JSCE Standard Specifications



**Figure 2.6** Stirrup strain (Left: ST-50, Right: ST-100)



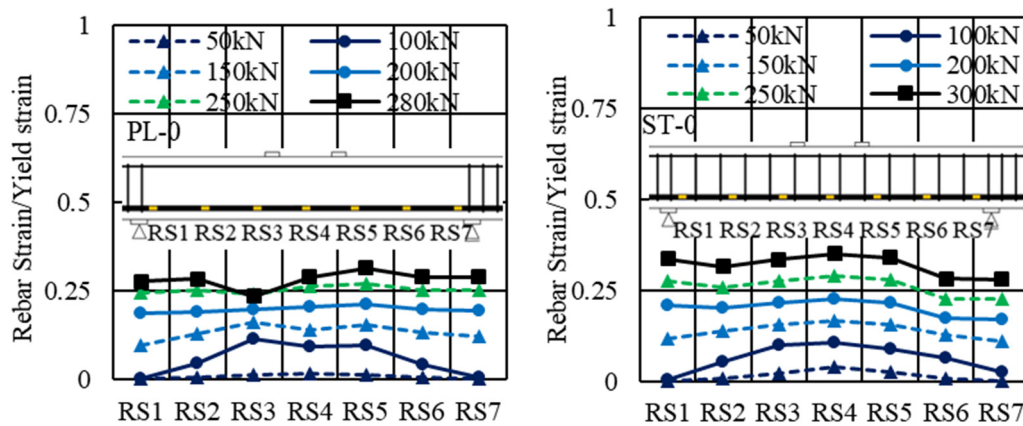
**Figure 2.7** Concrete strain behavior at compression edge (Left: PL series, Right: ST series)

The maximum loads of ST-100 and ST-50 were 466 kN and 368 kN, respectively, showing a different tendency from those of the PL series. Comparing ST-100 and ST-50, the two specimens showed similar crack propagation and both failed in shear, although the maximum load of ST-50 was approximately 20% lower than that of ST-100 while the both ST-50 and ST-100 showed higher shear strength than designed value. In the both ST-50 and ST-100, stirrup strains on shear crack exceeded yield strain at failure, it indicated shear tension failure as shown in **Figure 2.6**. Noted that strain of stirrup in the ST-0 was failed to be measured due to the trouble in the measurement system. The ST-0 beam showed 299kN of maximum load, and crack pattern, failure mode and maximum load were similar to those of PL-0. In the PL-0 and the ST-0, stiffness of beam declined markedly after cracking and dispersibility of cracks was clearly reduced. In these beams, because bond was uniformly low, stress on the anchoring parts was increased, and it ultimately caused the anchorage failure.

The difference in interlock area of the specimens also affected the dispersibility of flexural cracks. The number of flexural cracks was 8 and 7 for ST-100 and PL-100, respectively, but only 3 cracks were formed in the span center in ST-0 and PL-0. Difference in placing of stirrups was showed in the behavior of PL-50 and ST-50. In PL series without stirrup, the number of flexural cracks was reduced from 7 in PL-100 to 4 in PL-50, while the number of cracks in ST-50 with stirrup was 8, the same number as in ST-100. Placing of stirrups also affects crack location. Cracks was basically formed on or near the stirrup in ST series while cracks located randomly in PL series. Looking at **Figure 2.7**, increase behavior of compressive strain in the PL-50 was similar to the PL-0 and the PL-50 showed the highest compression strain at failure, indicating compression failure while compression strain in the PL-100 was suppressed due to shear crack. On the other hand, behavior of compressive stain with loading of ST-100 and ST-50 was almost same until failure. Compressive strain and stirrup strain in the ST-0 was failed to be measured due to the trouble in the measurement system. However, it could be considered that the behavior of the ST-0 was almost same as that of the PL-0 because there is little difference in load-deflection curve and crack behavior between PL-0 and ST-0. Thus, there is clear difference in the trend of compression strain behavior, the behavior of the PL-50 was similar to PL-0 while that of the ST-50 and the ST-100 were deviated from that of the ST-0.

### 2.3.2 Strain distribution of main rebar

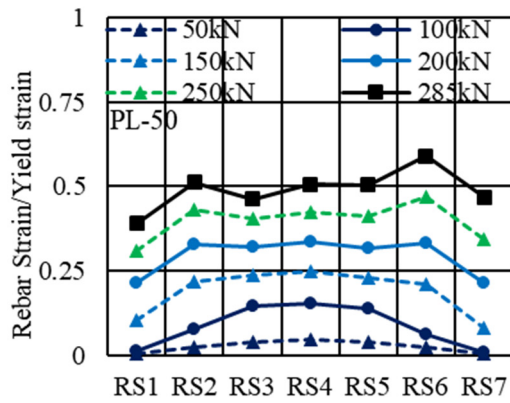
**Figure 2.8 – Figure 2.13** shows the strain distribution of the main rebar along axial direction in each specimen. In order to compare the specimens between screw bar and PC rod with different strength, vertical axis shows the ratio of measured strain to yielding strain of each main rebar. All beam specimens failed before yielding of main rebar. In the both PL-100 and ST-100, tensile strain was highest at the center of the beam and decreased as measurement points became closer to the supporting points, maintaining the correlation with the flexure moment distribution. You can find some unevenness in PL-100 and it is caused by cracks on strain gauges and cracks along rebar as shown in



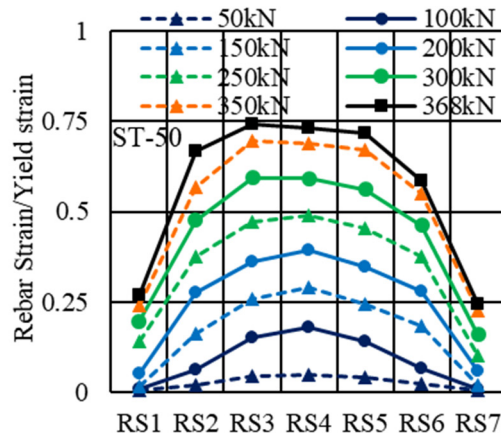
**Figure 2.8** Main rebar strain distribution (PL-0) **Figure 2.9** Main rebar strain distribution (ST-0)



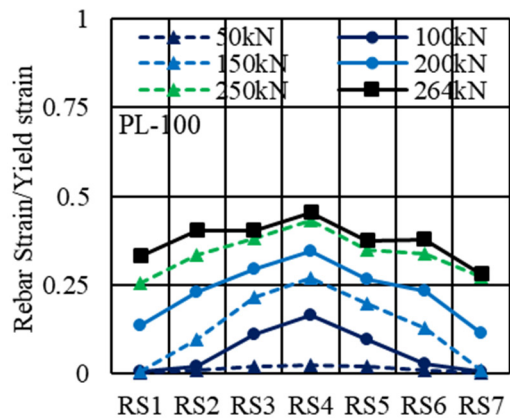
Fig. 5. In the PL-0 and ST-0 specimens, the strain distribution kept arch shape until 100 kN, but the strain along rebar became almost same value after 150 kN due to chemical bond loss. This was consistent with the result that PL-0 and ST-0 shared the same failure mode. In the cases of 100% and 0% interlocking, strain distribution trend was same regardless of placing stirrups. On the other hand, the axial strain distribution clearly differed between ST-50 and PL-50. In ST-50, the axial strain distribution was similar arch shape to that in ST-100 until beam failure. On the other hand, in PL-50, the strains at each measured point, except for the supporting points (RS1 and RS7), were almost identical past 150 kN. In the visual inspection after 150 kN, the detachment of the main rebar from the upper concrete was observed. The failure mode and the crack distribution in PL-50 al-so supported that bond was lost at 150 kN, whereas in ST-50, sound bond was maintained until failure.



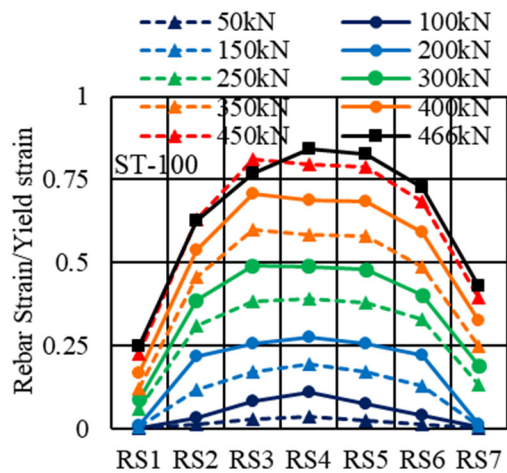
**Figure 2.10** Main rebar strain distribution  
(PL-50)



**Figure 2.11** Main rebar strain distribution  
(ST-50)



**Figure 2.12** Main rebar strain distribution  
(PL-100)



**Figure 2.13** Main rebar strain distribution  
(ST-100)

### 2.3.3 Summary of experimental results

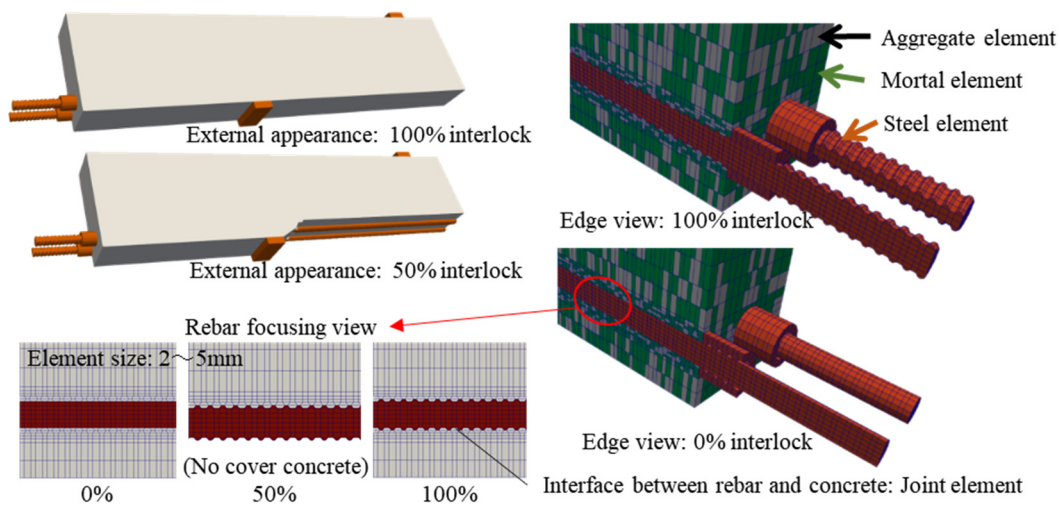
In the case of ST-50, post-cracking stiffness decreased, but the reduction degree was slight, and crack behavior, strain distribution, and failure mode were similar compared with ST-100. Even though the underside of the rebar was exposed and the half of interlock area was not available, no large bond loss is deemed to have occurred. On the other hand, in PL-50, the smaller number of cracks and uniform strain distribution as shown in the result of PL-0 clearly indicated bond loss. The detachment of main rebar suggests the interlock loss caused by contact loss between lug and concrete. However, in the case of ST-50, the main rebar kept contact with upper concrete because of the suppression of relative displacement between the main rebar and concrete by stirrups. Therefore, interlock was maintained. Stirrups affected crack location through the confinement effects on main rebar. Crack location was concentrated around stirrup because interlock between main rebar and stirrup was strong, and it causes local high unity between concrete and main rebar.

Totally, almost sound bond can be maintained even if interlock area was half as long as contact between lugs and concrete was kept. It was also confirmed that stirrup has contribute on keeping contact and unity between concrete and main rebar.

## 2.4 FE analysis for reproduction on beam loading experiment

### 2.4.1 Outline of FE analytical model

**Figure 2.14** shows the outline of the analysis models. To more precisely grasp the phenomena caused by differences in interlock conditions, the shapes of the main rebar and the anchoring nuts at beam end were reproduced using steel solid elements. Two-dimensional joint element was placed at the boundary between the steel element for main rebar and the concrete element. As the effect of interlock can be reproduced by the shape of steel elements, it is possible to separate the interlock from



**Figure 2.14** Outline of analysis model

other bond components. Chemical adhesion and frictional resistance were considered in the property of joint element. A smeared rebar model was applied for stirrup and compression reinforcement. Considering the symmetry of the beam, a quarter cut model was used for analysis.

#### 2.4.2 Segregated modeling of mortal and course aggregate with fine mesh

A small mesh size of 2 mm minimum was set to reproduce the shape of screw bars by hexahedral elements. In this model, aggregate and mortal were separately modeled and randomly placed. The mesh size was significantly smaller than the aggregate size in this model, thus it was deemed to be out of the assumption based on the composite behavior of aggregate and paste in a smeared crack model. In the experiment, the volume ratio of coarse aggregate in the concrete was 36%. Based on that, 36% of concrete elements were randomly set to the aggregate element, and the other concrete elements were set to the mortar elements as shown in **Figure 2.14**.

**Table 2.4** lists the material property values applied in the aggregate and mortar elements. Because limestone was used as the coarse aggregate in the experiment, the general values of compressive strength (140MPa) and tensile strength (10MPa) of limestone aggregate were used for the aggregate elements [1]. Since the fracture of aggregate is brittle, the parameters were set so that tensile bearing stress after occurrence of crack drops sharply with large stiffening parameter while concrete constitutive law was applied for aggregate elements. For the elastic modulus of the aggregate element, the estimated value obtained from the density of aggregate with **Eq. (2.1)** was used [2].

$$E_{ag} = (2.35\gamma_{ag} - 5.78) \times 10^5 \quad (2.1)$$

Where,  $E_{ag}$  is the elastic modulus (MPa) and  $\gamma_{ag}$  is the density of aggregate (g/cm<sup>3</sup>). The calculated elastic modulus of course aggregate had almost same value as that of general limestone aggregate [1].

The compressive strength and tensile strength of the mortar element taken from the concrete material test results shown in **Table 2.3** were applied for the properties of element property because strength of mortal was dominant for concrete failure in normal strength concrete. Elastic modulus of mortal is lower than that of concrete in general and Hashin-Hansen's equation for two-phase composite materials, shown in **Eq. (2.2)**, was used for determining the elastic modulus of mortal [3, 4].

**Table 2.4** Material property values in analysis model

	Mortar element	Aggregate element
Compressive strength (N/mm <sup>2</sup> )	39.7	140
Tensile strength (N/mm <sup>2</sup> )	2.67	10
Elastic modulus (kN/mm <sup>2</sup> )	18.8	51.8

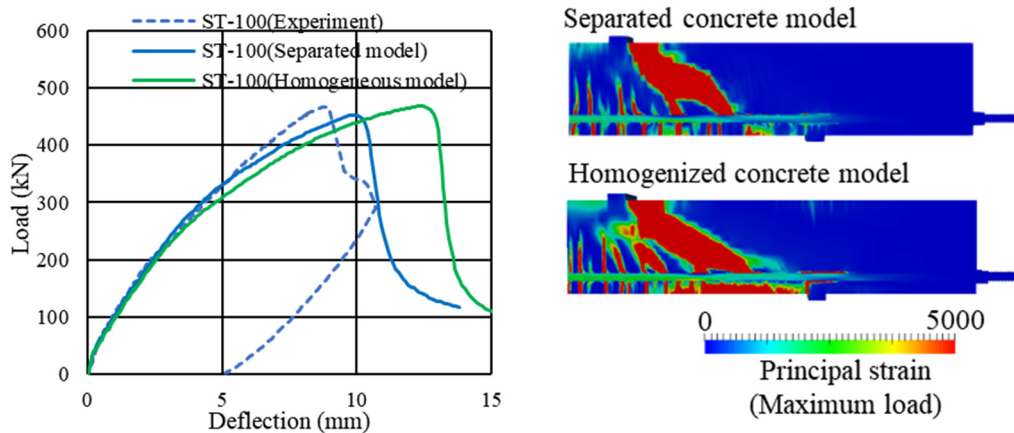
$$E_c = E_m \frac{(1 - V_g)E_m + (1 + V_g)E_g}{(1 + V_g)E_m + (1 - V_g)E_g} \quad (2.2)$$

Where,  $E_c, E_m, E_g$  is the elastic modulus of concrete, mortar, and coarse aggregate, respectively, and  $V_g$  is the volume ratio of coarse aggregate in concrete. The elastic modulus of mortar element  $E_m$  could be obtained by **Eq. (2.2)** from the measured elastic modulus of the concrete  $E_c$  and the elastic modulus of the aggregate  $E_g$  estimated by **Eq. (2.1)** in this study. Strictly speaking, it was necessary to consider the influences of the interfacial transition zone between the aggregate and mortar elements, and the contact conditions between aggregate elements according to the aggregate diameter and aggregate shape. However, in this analytical model, these influences were considered to be small because the damage was concentrated on the mortar elements, which had a lower elastic modulus and strength than aggregates.

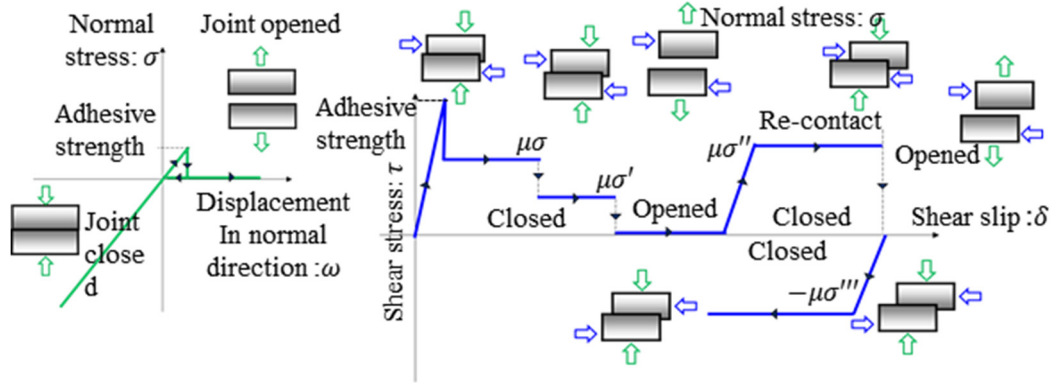
Here, **Figure 2.15** shows the comparison between homogenized concrete model and separated modeling in the beam analysis of the ST-100 case. Homogenized concrete model was composed by the same meshing and material properties as shown in **Table 2.3** given from cylinder test were applied. Post-cracking stiffness of homogenized concrete model was lower than the results of experiment or segregated model, while maximum load and crack distribution in ultimate state were almost same. It seemed to be because that homogenized concrete model cannot reproduce high resistance of crack progress in the local region by aggregate directly. Accurate averaged strain and averaged stress relationship or equivalent fracture energy in extremely fine mesh reproduced by homogenized concrete model required more consideration.

#### 2.4.3 Model of joint element

For reproducing the mechanical behavior chemical adhesion and friction resistance between steel and concrete, FE model in this study applies 2D joint element. In general, steel-concrete interface



**Figure 2.15** Comparison of separated and homogenized concrete modeling



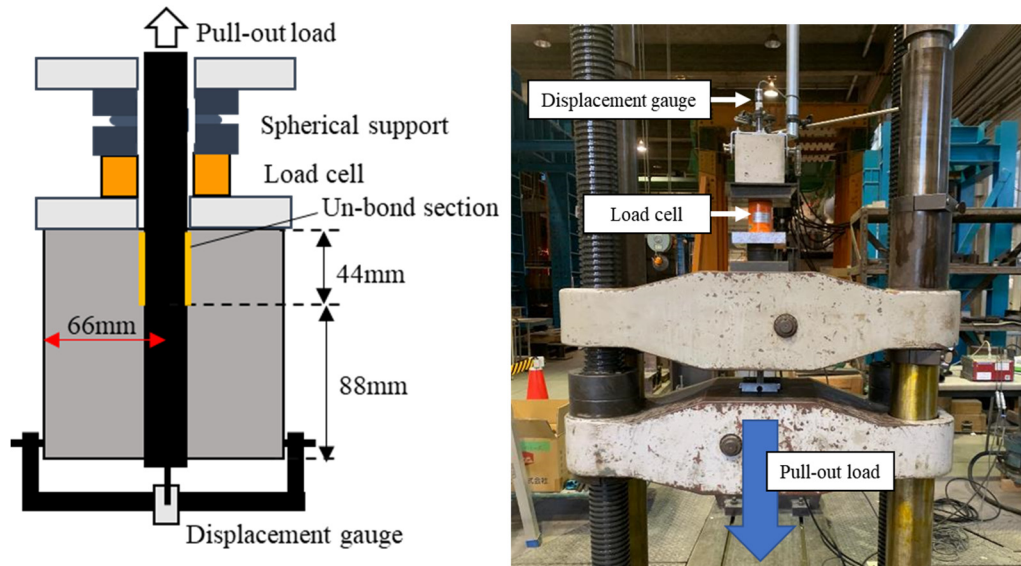
**Figure 2.16** Model of joint element

shows contact friction behavior in shear with initial adhesive strength. Thus, the author applied Mohr-Coulomb friction law in the shear direction on the contact surface with initial adhesive strength in the both normal and shear direction. Summary of joint element model is shown in **Figure 2.16**. Recovery of chemical adhesion is not considered when joint surface contacts again. In other word, after stress in joint element in shear or open direction exceeds its chemical adhesion strength, no normal stress is considered when the interface is opened, and shear stress follows only the Mohr-Coulomb friction law [5]. The friction coefficient  $\mu$  of 0.4 was applied in this study according to the past research focusing smooth interface between steel and concrete [6]. Applicability of this joint model had been verified in previous research for evaluation on composite structures [7-9].

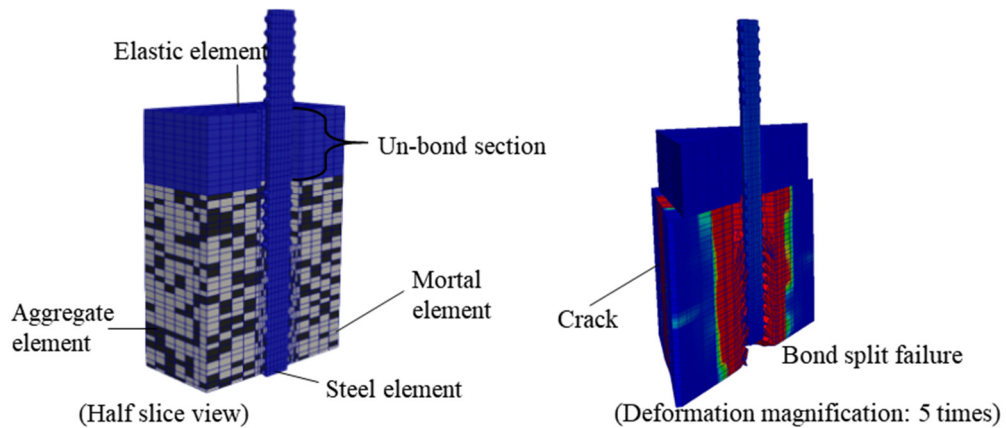
#### 2.4.4 Validation of analytical modeling by reproduction for pull out test for a rebar

In order to check the validity of the FE model such as reproduction of rebar shape by hexahedron elements, the parameters applied for the joint element between steel and concrete, and the parameters of aggregate and mortar elements, a pull-out test of rebar embedded in concrete was reproduced by FE analysis. The pull-out test was based on JSCE-G 503-2013 (Test for bond strength between concrete and steel reinforcement by pull-out test). **Figure 2.17** shows the outline of the pull-out test. The specimens for the pull-out test were the concrete cubes of 132 mm on each side with a rebar embedded in the center. The length of one side being six times the diameter of the rebar. An unbonded zone of twice the rebar diameter in length was provided on the pull-out side. The relative displacement between the rebar and the concrete cube was measured as the pull-out displacement at bottom side of specimens. The pull-out test was conducted on a total of four specimens, consisting of two specimens with reinforcement consisting of the screw bar, and two specimens with round PC rod. The properties of steel bars were same as the beam loading test.

**Figure 2.18** shows the reproduction analysis model. As same as the beam model, it consisted of mortar element, aggregate element, and steel element. Two-dimensional joint elements were placed at



**Figure 2.17** Outline of pull-out test

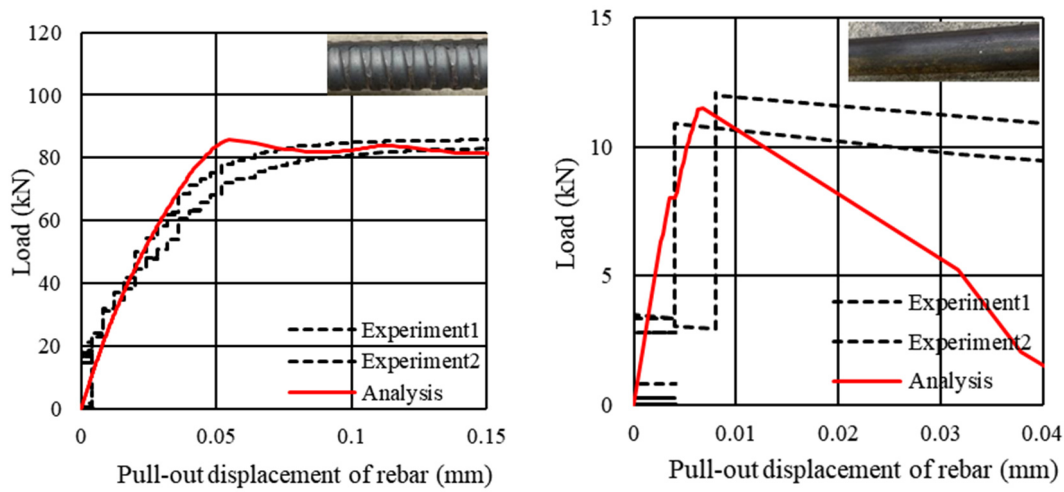


**Figure 2.18** Analysis model and strain distribution under pull-out load (Screw bar)

the boundaries around the steel element.

**Figure 2.19** shows the comparison of the test results and analytical results in the load-pull-out displacement relationship. In the both screw bar and round PC rod cases, the analysis was able to reproduce the behavior until applied load reached the maximum value. Deformed bar was pulled out at approximately 80kN, and crack along rebar occurred and concrete block was split in the both experiment and analysis, namely bond split fracture. On the other hand, split of concrete was not observed in pull-out behavior of round PC rod. Bond fracture was occurred between smooth surface of rebar and surrounding concrete due to chemical bond loss at 11 kN of applied pull-out load. In this pull-out test, displacement measurement around and after failure did not have high reliability. It is because that specimens bounced or split at failure and it affected measurement of displacement gauge fixed on the concrete cube surfaces. Thus, there was slight difference in softening behavior between



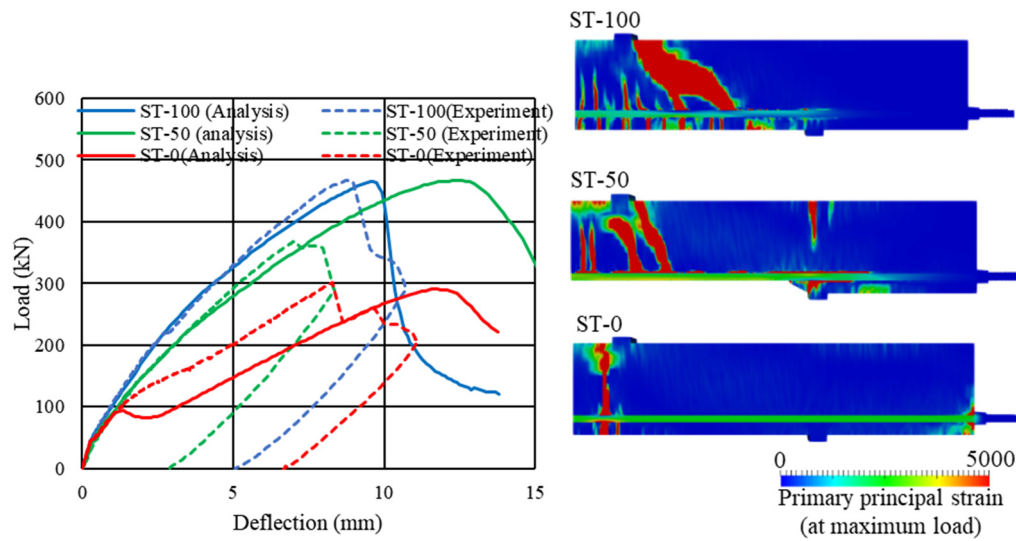


**Figure 2.19** Rebar pull-out test reproduction analysis results (Left: Screw bar, Right: Round PC bar)

experiment and analysis especially for round bar. Dynamic analysis considering local contingency of slipping can improve slip behavior reproduction between smooth surface due to bond fracture [8]. There was still room for improving fitting accuracy softening behavior of round bar after bond slipping, but these influences were considered to be greatly small compared with bond fracture with interlock. Thus, the author concluded that those models, such as the material properties of the aggregate and mortar elements, and the stiffness, chemical adhesion strength, friction coefficient of the joint element, were valid enough to evaluate the structural behavior of RC member with interlock.

#### 2.4.5 Results of reproduction analysis for beam loading test

**Figure 2.20** shows the comparison between the analytical and experimental load-deflection curves and the primary principal strain distribution. For ST-100, the analysis was able to reproduce the initial stiffness, load capacity, strain distribution of main rebar and crack distribution observed in the experiment. For ST-50, analytical stiffness value became lower than experimental value past approximately 250kN, and shear failure occurred at a higher load than that in the experiment. As the analytical model uses a smeared reinforcement model for the shear reinforcement, the confinement effect by the stirrup for main rebar cannot be considered directly. In this analysis, among the joint elements in the ST-50 model, a high value was applied to the chemical adhesive strength at the locations of the stirrup in the experiment to reproduce the confinement effect by the stirrup. However, as the load increased, the stress for the detachment was concentrated around the joint elements which have high adhesive strength, and at a load of approximately 250kN, the rebar detachment occurred. The shear capacity of beam increased, as a result, the maximum load is considered to have been higher than that recorded in the experiment. ST-50 in analysis failed in shear, but the angle of the shear cracks was large and the crack shape was similar to those of PL-50 in the experiment. If interlock between

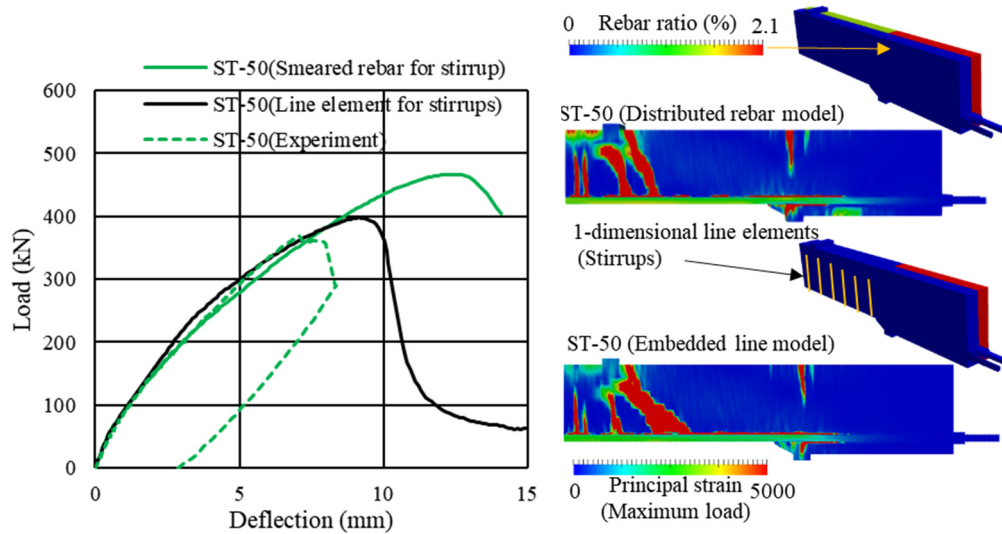


**Figure 2.20** Results of reproduction FE analysis for beam loading test

the top concrete and the lugs on the rebar can be maintained by the discrete representation of the stirrups mechanically, the detachment can be prevented and the accuracy can be improved. In order to reproduce the confinement effect of stirrup in analytical model, the author reproduced stirrup as line element without distributed rebar model and embedded in concrete elements. Line elements were placed at same regions as that in the experiment in each main rebar dividedly with half cross section in order to reproduce confinement effect by surrounding geometry of each stirrup because strain-stress relationship of line element was modeled only in the axial direction without flexure resistance. No bond slip behavior was modeled between concrete and line element, thus complete bond between stirrups and concrete was assumed in the analytical model. **Figure 2.21** shows the comparison in load-deflection curves and strain distribution, and analytical results with embedded stirrup model reproduced experimental results well in the load capacity, the failure mode, and the shear crack angle. It was because that detachment of main rebar was confined by line element, and bond condition measured in the experiment were reproduced well. From these investigations, it was showed that whether contact between concrete and lug worked or not had large influences on sound bond. Though embedded rebar reproduction succeeded to track load-deflection relationship better than distributed rebar model, it was still required to develop another constitutive law of line element or bond slip behavior between line elements and solid elements. Thus, the author used distributed rebar model for stirrup following case studies because they focused on only various lug loss condition and did not consider the situation causing detachment of main rebar such as corrosion crack or spoiling of cover concrete.

The analytical result of the ST-0 showed a different behavior from the experiment, a decrease

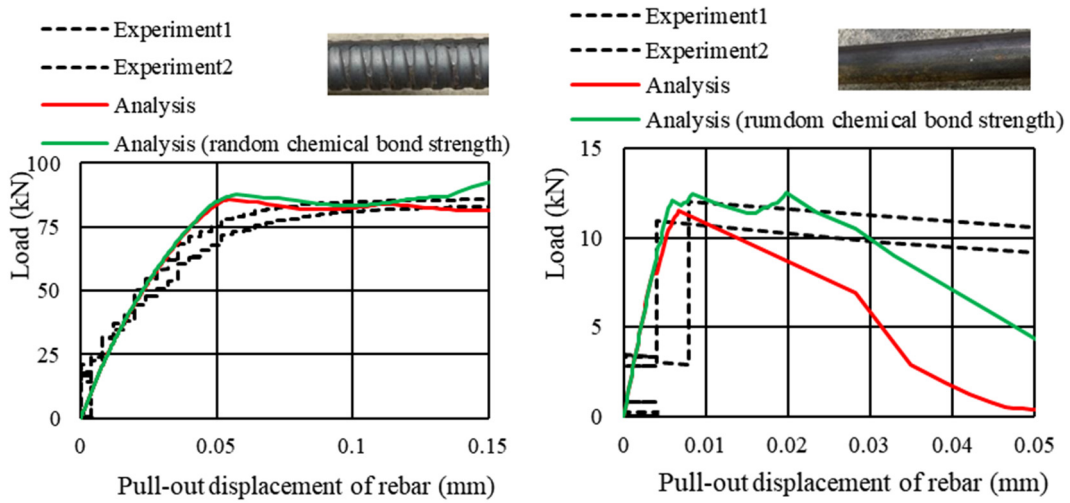




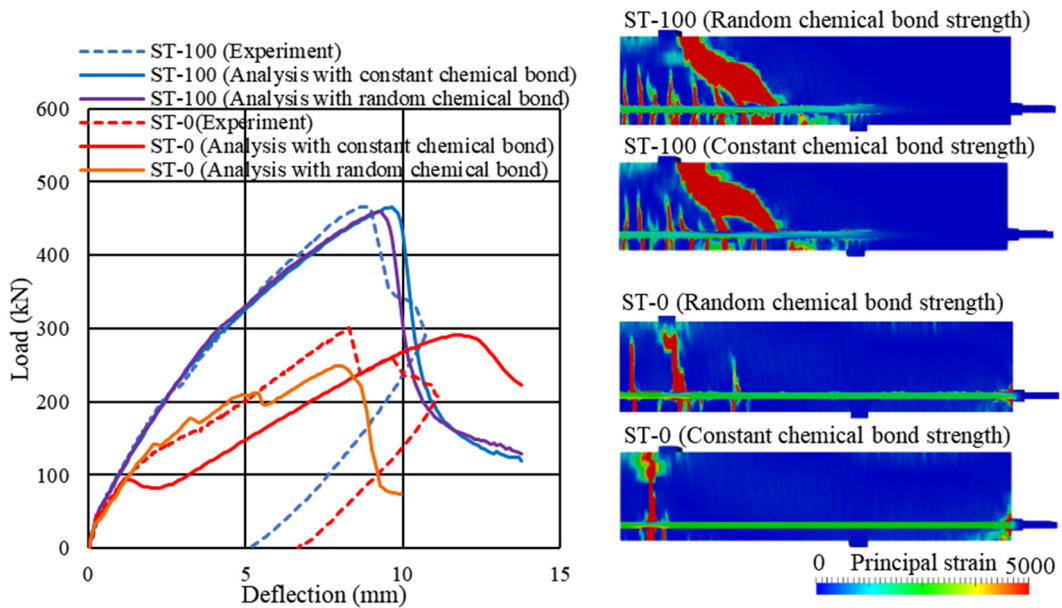
**Figure 2.21** Comparison between distributed and embedded stirrup model in ST-50

in load occurred at a load of approximately 110kN, and later the load increased again. In the analysis, slip between the rebar and concrete observed pull out test for round bar occurred at a load of approximately 110kN, and rebar slip occurred instantaneously in most surface of the rebars. On the other hand, in the experiment, slip between the rebar and concrete occurred locally and it was intermittent as the load increased, which may have caused the difference in the load-deflection curves. In the load-deflection curve obtained from the ST-0 experiment, the slope of the curve began to decrease from approximately 120kN. Slip sound was intermittently heard from approximately 100kN during the loading test, presumably indicating that the rebar began to slip. The load at which slip of the rebar started was consistent between experiment and analysis. The strain distribution of ST-0 clearly showed a decrease in the number of cracks and the concentration of strain in the concrete at the anchoring parts at the beam ends compared with the sound case, reproducing the crack behavior and the failure mode in the experiment. Although there was a difference in stiffness after rebar slip, the maximum load was almost the same as that in the experiment. Rebar slipping was a dynamic phenomenon of intermittent local slipping, and it is difficult to track it in static analysis. The reproduction accuracy of ST-0 should be improved by introducing dynamic analysis, setting parameters non-uniformly for the joint elements, or introducing viscous behavior. In order to reproduce non-uniform distribution of bond condition, the author conducted the reproduction analysis on pull-out test for deformed and round bar, and on the static loading test for ST-0 and ST100 case with 2 degree of chemical bond strength randomly. 90% of bond elements in that in the beam model was set to 80% of original value of bond chemical strength, and the others were 2.8 times larger value, thus total bond strength was same as original model. Stiffness in the both open and closure condition, friction coefficient in joint elements, and the property of mortar or aggregate elements were not

changed. Comparison between models with constant and random chemical bond strength was shown in **Figure 2.22** on the pull-out test and **Figure 2.23** on the static loading test, respectively. When pull-out behavior was focused on, load was kept constant at maximum load in the case with non-uniform chemical bond strength just after rebar slipping occurred because region with higher strength can resist against pull-out slip while pull-out stiffness and bond strength were almost same in the both cases. On the other hand, the difference in pull-out behaviors of deformed bar by uniform and nonuniform



**Figure 2.22** Comparison between constant and random distribution of chemical bond strength with the reproduction analysis of pull-out test (Left: Screw bar, Right: Round PC bar)



**Figure 2.23** Comparison between constant and random distribution of chemical bond strength with the reproduction analysis of static loading test

distribution of chemical bond strength, thus it was confirmed that contribution of interlock for bond between rebar and concrete also from this investigation. Pull-out behavior of rebar around chemical bond fracture was reproduced well by random distribution of chemical bond strength, and structural behavior of member in static loading could also be succeeded to reproduce. Gradual chemical bond loss at local regions was reproduced, as a result, the matching between analytical and experimental results in the ST-0 case was improved as shown in the load-deflection curve and strain distribution in **Figure 2.23**. Nevertheless, difference in structural behaviors of member in the ST-100 was greatly slight, thus properties of joint elements were insensitive due to solid bond caused by interlock. As long as a member uses deformed bar, and beam model showed in **Figure 2.14** resulting the structural behavior in **Figure 2.20** was valid enough because that stress transfer by lug can be reproduced well and contribution of interlock on bond was outstanding compared with chemical adhesion and friction action, which was also supported by previous researches [10]-[13].

## 2.5. Analytical case study assuming lug loss due to rebar corrosion

### 2.5.1 Analytical cases

Analysis reproducing the change of interlocking condition that is expected to occur due to rebar corrosion was conducted. The shape of the screw rebar, geometry of beam, the rebar arrangement, and the loading conditions were the same as the reproduction FE analysis for the ST series in Chapter 4. The analysis cases shown in **Table 2.5** were set up focusing on three points: lug height loss, non-uniform lug loss region on cross section of rebar, and non-uniform lug loss region in axial direction of rebar. In those case studies, the influence of corrosion cracking is not considered. Strictly speaking, when the corrosion gel is infiltrated into corrosion crack, low density area is generated on the corroded part. However, this case study focuses on the interlock condition to deepen the understanding of bond deterioration, as the same as discussed in the previous chapter

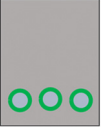

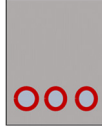
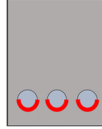
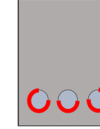
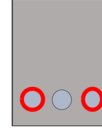
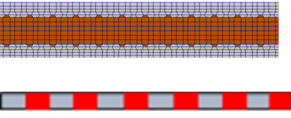
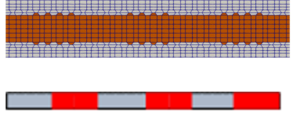
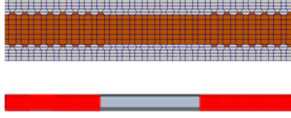
#### -Lug height loss-

As the corrosion of the rebar progresses, the rebar lug is flattened gradually. However, because the surface of the bar is uneven, the bar surface never become smooth as round PC rods by corrosion. Degree of interlock by lugs is affected by the reduction of contact area between the lugs and the surrounding concrete. The beams with different lug height was analyzed using the cases of 75% (LugH-75%), 50% (LugH-50%), and 25% (LugH-25%). The height of the lug in the sound case was 2.0 mm, which was the same as that of the screw rebars used in the experiment.

#### -Non-uniform lug loss region on cross section of rebar-

Since the deterioration factors that cause rebar corrosion ingress from the surface of RC member, the corrosion starts from the region close to the concrete surface [14]. Three cases were analyzed: The

**Table 2.5** List of analysis cases.

Focus	Lug height loss			Non-uniform lug loss region on cross section		
name	LugH-75%	LugH-50%	LugH-25%	Bottom-0%	Outer-0%	Side-0%
Lug loss region						
Lug loss ratio	25%	50%	75%	50%	66.6%	66.6%
Remark	75% of lug height (1.5mm)	55% of lug height (1.0mm)	25% of lug height (0.5mm)	Loss in Bottom side	Loss in bottom side and outside	Loss in two outer rebars
Focus	Non-uniform lug loss region on axial direction					
Name	LugInt-1cm		LugInt-3.5cm		LugInt-7cm	
Lug loss region						
Lug loss ratio	50%		50%		50%	
Remark	Intermittent lug loss (1 cm interval)		Intermittent lug loss (3.5 cm interval)		Intermittent lug loss (7 cm interval)	

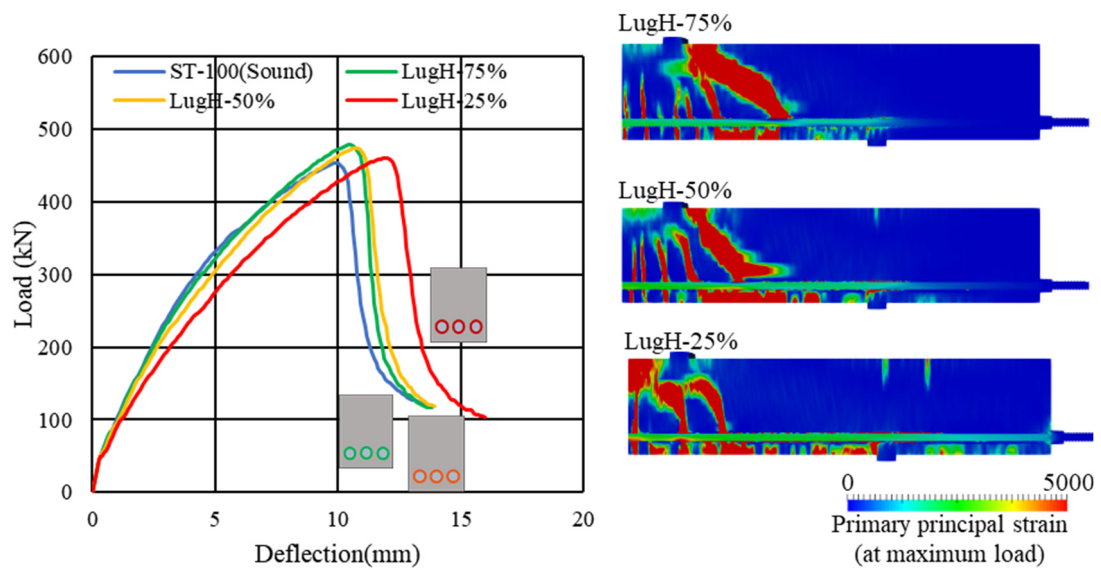
case in which only the lugs on the bottom side of all main rebars was lost (Bottom-0%), the case in which the lugs on the bottom side of all main rebars were lost as well as the lugs on the lateral sides of the outer two main rebars (Outer-0%), and the case in which the lugs on the outer two main rebars were lost (Side-0%). Actually, interlock remaining part of Bottom-0% is same as ST-50 appeared in the previous chapters, and the difference is only whether cover concrete exists or not.

#### -Non-uniform lug loss in axial direction-

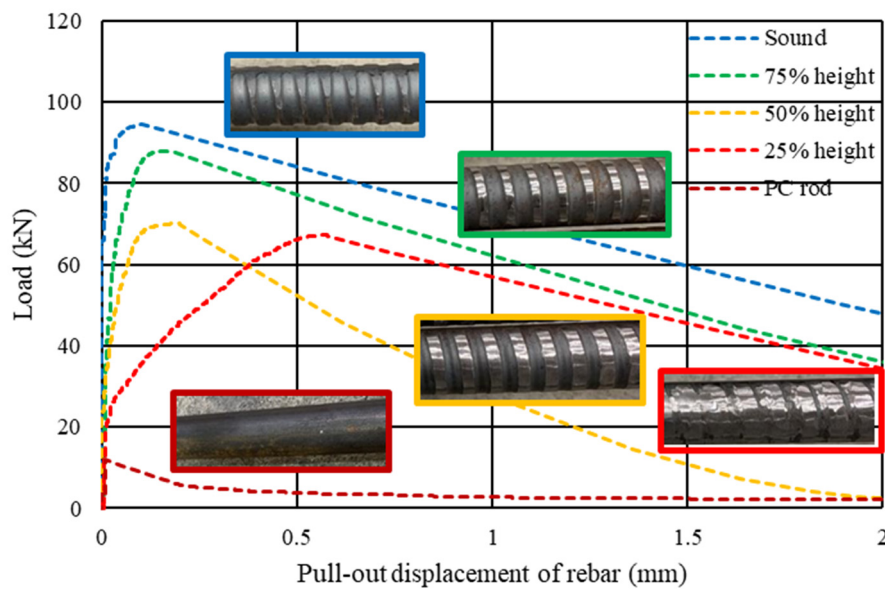
Since the non-uniformity of corrosion also appears in the axial direction of the rebar [15], the beams with alternating regions of lost lugs and sound lugs were analyzed. Three cases were set up, and the intervals of lug lost and sound lug region were, 1 cm (LugInt-1cm), 3.5 cm (LugInt-3.5cm), and 7 cm (LugInt-7cm), respectively. The residual rate of lug as a whole beam is 50% in the all cases.

### 2.5.2 Investigation on the effect of lug height loss

**Figure 2.24** shows the load-deflection curves and strain distribution for the analysis cases focusing on the effect of lug height loss. In the case of the LugH-75% and LugH-50%, load-deflection curve, maximum load, main rebar strain distribution and crack distribution were nearly same as those of the sound case, while stiffness reduced slightly with lug height decreasing. Until lug height reduction reached to 50%, lug height had almost no influence on the structural behavior of the member.



**Figure 2.24** Analysis results (Effect of lug height loss)



**Figure 2.25** Pull-out test results

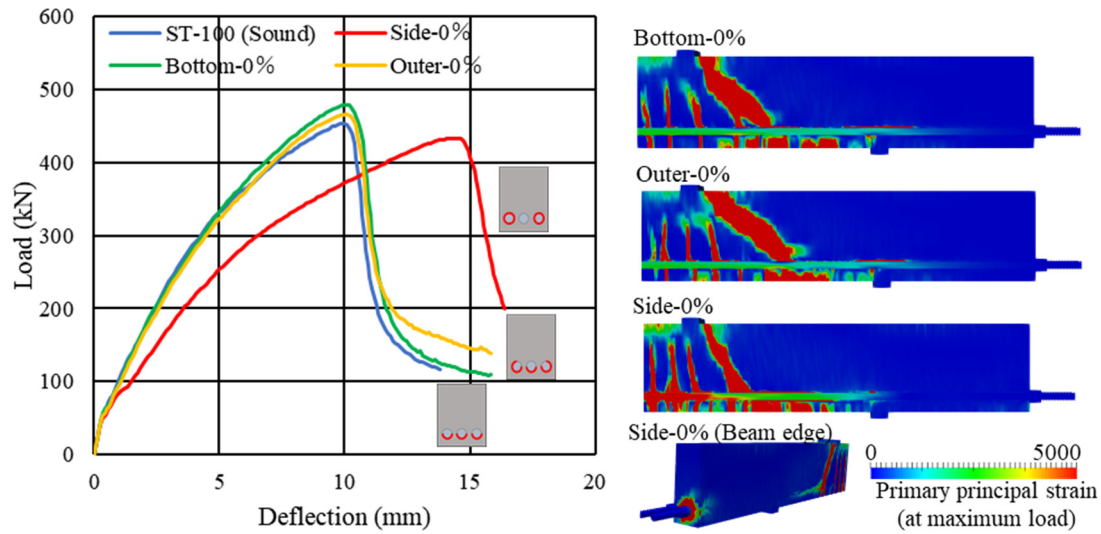
In the LugH-25%, stiffness after flexural cracking was low, crack concentrated in center of the span, and the beam failed by crushing in compression side, not by shear crack opening. This was considered to be due to bond loss caused by the small lug height of 0.5 mm. Bearing area between lug and concrete in the axial direction was extremely low in this state, thus local failure of concrete around rebar resulted bond loss while slipping behavior of main rebar in the case with round bar was not observed.

For more detailed study on the effect of lug height on the bond, the author conducted rebar pull-out tests which used screw rebars with different lug height. This followed the pull-out test sequence described in Chapter 4 and the all lugs of embedded rebar were grinded manually before concrete casting. Same 3 cases reduced lug height as the analysis cases were set, 75%, 50% and 25% of original height. **Figure 2.25** shows the test results of the cases with sound rebar, grinded rebar, and PC rod. It is noted that **Figure 2.25** shows the one of the test results in 2 specimens for each case and they had small scatter as shown in **Figure 2.19**. Pull-out behavior showed same trend as member analysis, the cases with lug height reduced to 75% and 50% showed almost same pull-out stiffness compared with the sound case but rebar having 25% lug height had low pull-out stiffness. Bond strengths became smaller with correlation with lug height reduction because the contact area between lug and concrete became smaller. However, in the beam analysis, these difference in bond strength did not affect the structural behavior because the external force to cause local bond fracture on rebars was larger than that to cause the whole beam failure.

Based on these results, stress transfer in a member can be maintained up to a certain lug height loss while bearing pressure is increasing as the contact area between concrete and rebar is reduced by lug height reduction. When lug loss ratio exceeds a certain level, the concrete at the interlocking surface breaks down locally. If lug height is uniformly de-creased, local bond fracture propagates one after another, and unity between rebar and concrete is lost entirely.

### 2.5.3 Investigation on the effect of non-uniform lug loss region on cross section of rebar

**Figure 2.26** shows the load-deflection curves and strain distribution obtained by FE analysis. In the following figures showing load-deflection curves, the result of sound case (ST-100) is included for comparison. In the case of Side-0%, where two of the three main rebars were perfect round shape, stiffness decreased after the onset of flexural cracks, the cracks were localized, and strain was concentrated at the beam ends, indicating bond loss. On the other hand, in the two cases of Bottom-0% and Outer-0%, the load-deflection curves and strain distributions were almost identical to those of the sound case, so the bond of the entire beam can be almost same condition as sound one. In the Bottom-0% case, lug loss region was the same as ST-50, and the difference between the two cases was whether cover concrete was present or not. However, the two cases clearly differed in behavior. In the ST-50 case of analysis, the main rebar detachment from the upper concrete causes interlock loss, while in Bottom-0%, the concrete under the rebar pushed up the rebar to concrete, so that contact between



**Figure 2.26** Analysis results (non-uniform lug loss region)

the lugs and the concrete was maintained, resulting in sound bond.

Although sound interlock area was 1/2 for Bottom-0% and 1/3 for Outer-0%, behaviors of these beams were almost same as the sound interlock case. As long as some inter-locking region remains on every main rebar, tensile stress can be transferred to the rebars, and they can work as tensile member as it is expected in design.

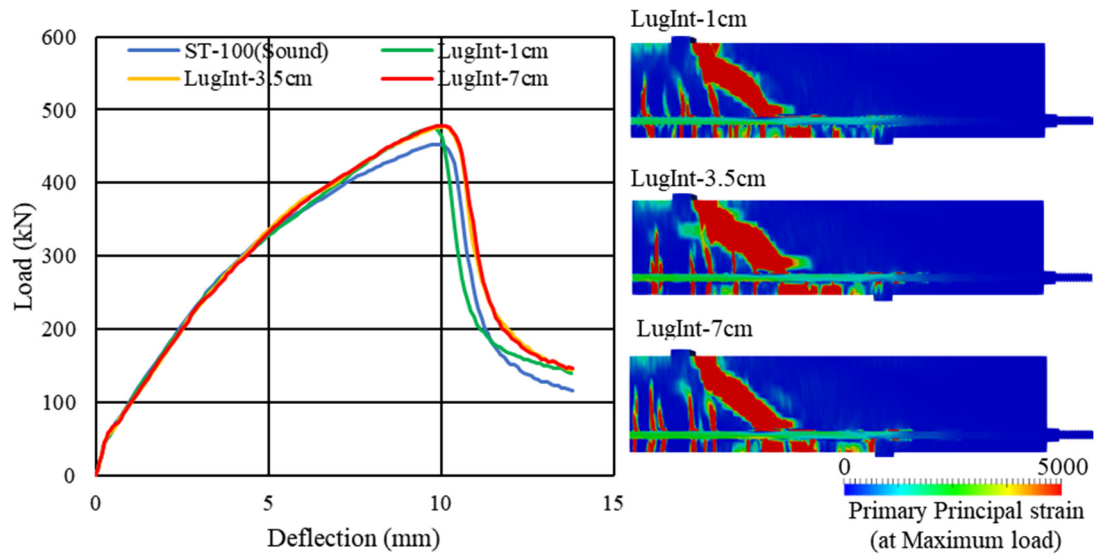
#### 2.5.4 Investigation on the effect of non-uniform lug loss in the axial direction of rebar

**Figure 2.27** shows the load-deflection curves and strain distribution. Regardless of the spacing of the lug loss zones, the maximum load, crack distribution, and failure mode were almost same as those of the sound case. It can be seen that even if there are zones of serious interlock loss in the axial direction of the rebar, bond is maintained for the entire member as long as there are zones where the interlock can work.

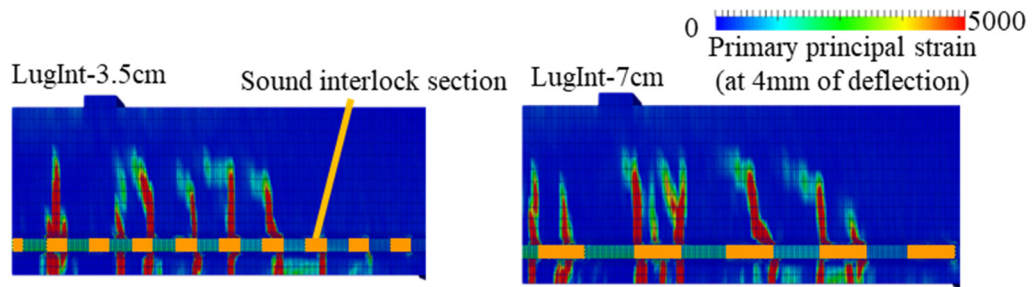
**Figure 2.28** shows the distribution of flexural cracks before shear crack formation in LugInt-3.5cm and LugInt-7cm. The orange parts indicate the sound lug zones, and almost of all flexural cracks occur from sound lug zones or at the boundary between a sound lug zone and a lug loss zone. These positions are considered that there was strong bond between the main rebar and concrete. This has correlation with the result that flexural crack occurs on the stirrups in the experiment.

In actual rebar corrosion, section loss does not occur uniformly in the axial direction. There will be a mixture of zones where the lug to concrete interlock remains sound and zones where it is lost. At this time, unless a part of the rebar due to extreme section loss caused by serious pitting corrosion exists, flexural cracks should be able to disperse in the sound parts and the bond of an entire member can be maintained.





**Figure 2.27** Analysis results (effect of non-uniform lug loss in axial direction of rebar)



**Figure 2.28** Flexural crack distribution before shear cracking

### 2.5.5 Summary of the analytical case study

Analytical case studies about lug height loss, lug loss region on cross section and non-uniform lug loss in axial direction were conducted. Even when the height of the lugs was reduced, sound bond as an entire member was maintained in a certain range of height, which is larger than 0.5mm in this case. On the other hand, as long as stress transfer by interlocks can work in a partial region in cross section or axial direction, rebar slip can be prevented and bond as a whole member can be maintained.

Let us focus on the interlock in a lug based on the Japanese Industrial Standard for deformed steel bars (JIS G 3112 Steel bars for concrete reinforcement). From our analytical results, when concentric section loss ratio reached around 20% to 25%, 75% of contact area between a lug and concrete was lost, which leads bond deterioration. And, when the section loss ratio reached around 25% to 30%, the interlock against pull-out force is completely lost.

On the other hand, when the section loss has non-uniformity, interlock in a partial region of rebars can transfer stress between rebar and concrete. Thus, a member can have bond as a whole member



even when higher averaged section loss occurred. At least, slip and pull-out of an entire rebar can be prevented.

## **2.6 Discussions from experimental and analytical investigations**

In investigations so far, the author tried to separate out the multiple factors of bond deterioration, and focused the interlock, which is dominant factor in bond components. To evaluate the effect of the change in interlock condition on the load bearing mechanism and bond performance of RC beams with different interlock condition, experimental and analytical investigation were conducted. Further, finite element analysis as case studies that simulating the interlock condition that is expected to occur due to rebar corrosion was performed. From these investigations, outcomes are summarized as following:

1. Bond between round bar and concrete is significantly low compared with deformed bar with interlock. It is confirmed that whether interlock can work or not is dominant factor for sound bond rather than chemical adhesion or friction effects. Section loss of rebar causes reduction of contact area between a lug and concrete, but interlock can be maintained until some lug height lost.

2. When unity between rebar and concrete as an entire member is focused, as long as a part of surface has interlock, slip and pull-out of rebar do not occur even if some region in rebar loses interlock completely. Thus, bond performance is insensitive even though the section loss ratio increases by corrosion. As long as the section loss ratio is lower than approximately 20%, stress can be transferred by interlock, and the bond of an entire member can be maintained in an almost sound state.

3. Stirrups can strongly suppress the relative displacement of main rebar against concrete in axial direction and the detachment. As a result, it affects crack location, and keeps interlock between concrete and main rebar, as long as a certain degree of roughness on rebar surface remains even after corrosion crack is formed along rebar or cover concrete is lost.

This investigation focused on interlock effects, which is dominant component of unity between rebar and concrete. Interlock deteriorated with section loss. However, when considering bond deterioration by actual rebar corrosion, corrosion crack also affects bond deterioration. Some points still need more consideration for understanding the correspondence between the actual corrosion condition and bond deterioration.

It might be possible to evaluate bond condition by residual interlocking and to assume almost sound bond until the corrosion ratio reached the point where the interlock between lugs and concrete was significantly lost. More consideration was required for accurate definition of criteria corrosion ratio that serious bond loss occurred. However, the relationship between corrosion process and interlock condition change focusing on local interlock on a lug can be represented as shown in **Figure 2.29** as conceptual diagram. At first, after the onset of rebar corrosion, sound bond is maintained until

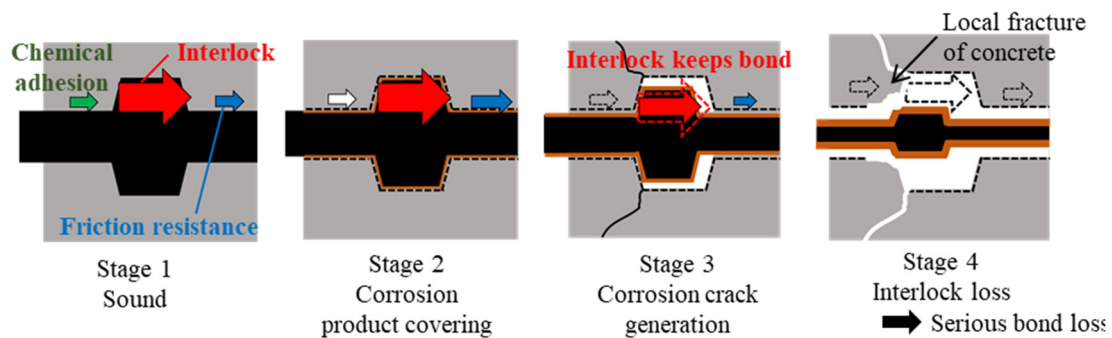
cracks occur in the surrounding concrete while chemical adhesion is lost due to corrosion product (Stage 2). When corrosion cracks occur, it reduces the bearing strength of the concrete contacted with lugs. However, as long as the interlock persists, relative displacement between rebar and concrete can be suppressed (Stage 3). If the interlock was lost owing to serious section loss, the stress transfer will be completely lost (Stage 4). As far as the influence of section loss alone on the bond is concerned, Stage 4 was achieved in 25% of section loss. However, when the rebar was actually corroded, the same state of Stage 4 can occur at a lower corrosion ratio due to local fracture of concrete around rebar caused by small bearing area between lug and concrete. In addition, corrosion cracks, which causes the geometry changes of the concrete surface around rebar influenced the reduction of bearing strength.

When considering bond not in meso scale but in macro scale as a RC member, due to non-uniform corrosion in axial direction, various local interlock condition can be mixed. **Figure 2.30** shows the interlocking condition of the entire corroded rebar. Even if some regions reached Stage 4, as long as other parts were in lighter corrosion degree, interlocks in these regions can maintain bond of an entire member. When rebar corrosion condition is severe and almost every region reaches Stage 4, resistance against pull-out stress by interlock was lost and bond as an entire member seriously deteriorates.

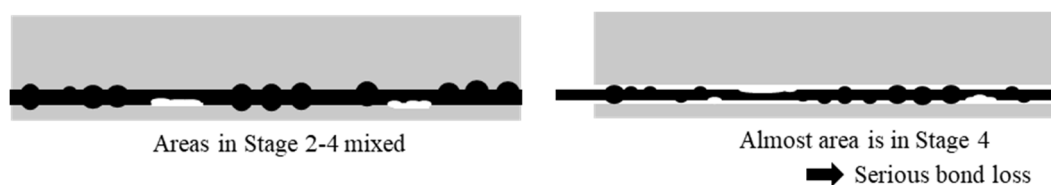
## 2.7 Equivalent modeling of bond deterioration

### 2.7.1 Modeling concept and proposal

Based on the experimental and analytical investigations so far, sound bond condition can be assumed until corrosion ratio as long as parts of region in a member can work. In other word, stress



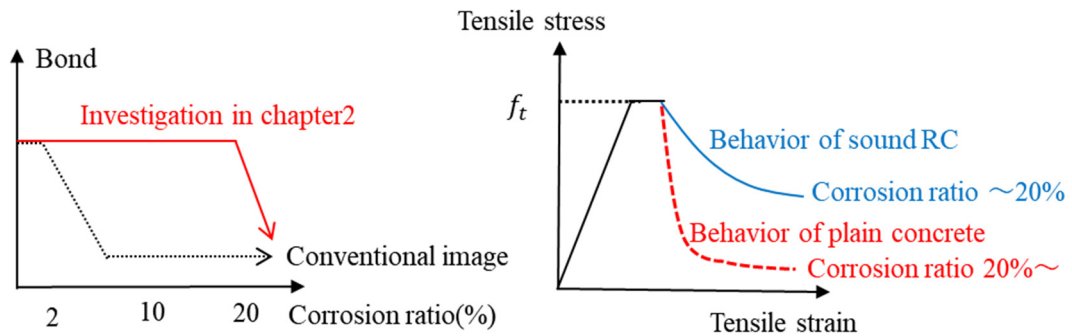
**Fig. 2.29** Interlock loss progress on a lug with corrosion



**Fig. 2.30** Interlock loss progress as an entire member with corrosion

transfer model between rebar and concrete by joint element was not required, but perfect bond can be applied in rough mesh model. Then, rapid bond loss should be modeled in higher corrosion ratio than bond deterioration criteria. **Figure 2.31** shows the concept of proposed bond deterioration model based on investigations in Chapter 2. Bond degree can be represented by tension stiffening, and when the stiffening parameter set at 0.4, a RC element behaves as reinforced concrete with sound bond in the COM3. The behavior of bond deteriorated reinforced concrete becomes close to that of plain concrete, thus the value of stiffening parameter should be increased. This study showed that interlock lost completely at 25% of concentric section loss ratio when focusing local section loss of a lug, and 20% of section loss also affects structural behavior. While 25% was the criteria that complete interlock loss occurred, the behavior of bond performance reduction with section loss at 20% should be considered. Thus, this study set the limit that sound bond can be assumed at 20% of corrosion ratio. When considering nonuniform rebar corrosion in the axial direction, variation of section loss ratio was strongly affected by averaged corrosion ratio. According to the previous researches focusing on the distribution of corrosion ratio in axial direction of rebar [15, 16], all regions of corroded rebar exceeded 20% of section loss ratio in the situation with more than 25% of averaged corrosion ratio, and estimation method of nonuniformity by probability distribution determined by averaged corrosion ratio in a region of rebar as a parameter was suggested. However, consideration of mesh size was required for implementation of nonuniformity probability concept because equivalent averaged corrosion ratio should be defined in a element. While some points have room for more consideration, 20% of section loss was set as the corrosion degree causing sharp bond loss considering the influence of corrosion crack causing reduction of bearing pressure. According to considerations so far, proposed model for bond deterioration in RC zone subjected to rebar corrosion was shown in **Equation 2.3** and **Equation 2.4**.

$$c = 0.4 \quad (R_c < 20\%) \quad (2.3)$$



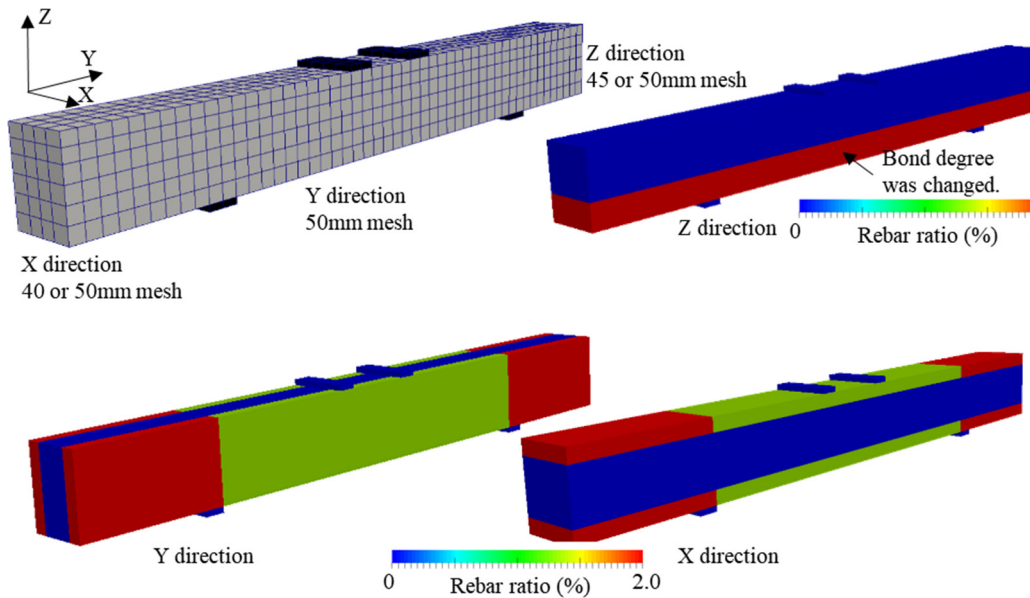
**Figure 2.31** Concept of bond deterioration

$$f_t(\varepsilon_{tu}/\varepsilon_t)^c = \frac{G_f}{l_r} \quad (R_c > 20\%) \quad (2.4)$$

Where,  $R_c$  is averaged corrosion ratio,  $\varepsilon_{tu}$  cracking strain,  $\varepsilon_t$  averaged tensile strain, and  $c$  is stiffening parameter,  $G_f$  is fracture energy of concrete and  $l_r$  is reference length of finite element. The same value of stiffening parameter was applied as sound RC zone until section loss ratio reached 20%, then the same stiffening parameter as plain concrete was set in more than 20% of section loss ratio without gradual change. As future studies, improvement of the accuracy of performance assessment of reinforced concrete structures with rebar corrosion, investigations focusing on cracks around rebar due to were required, and these have contributions for more accurate deterioration behavior of bond in closing to or more 20% of corrosion ratio, which is criteria that bond by interlock as an entire member can be maintained at sound state in this study.

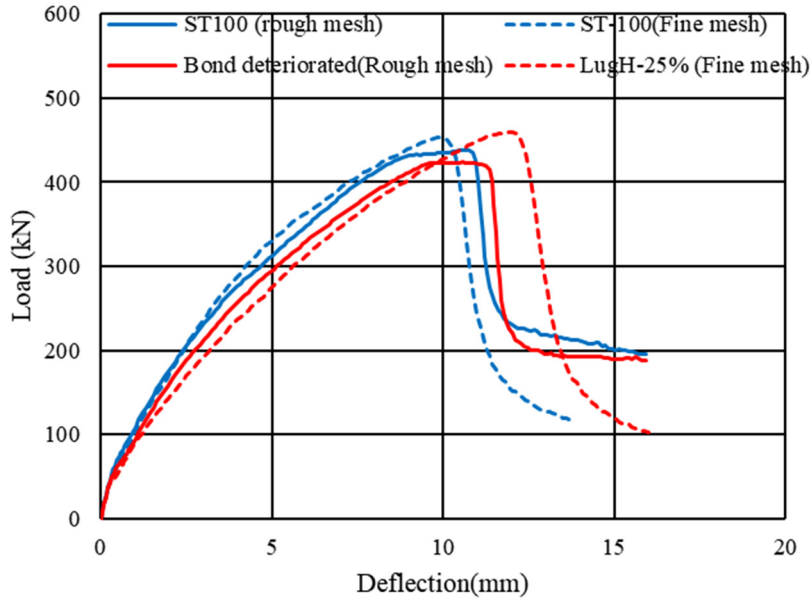
### 2.7.2 The influence of bond deterioration model on structural behavior

In order to investigate structural behavior with proposed bond deterioration model in rough mesh size, the author conducted FE analysis with rough mesh model as shown in **Figure 2.32**. This model reproduced the beam produced in this chapter with approximately 50mm of mesh size, which was the length from center of main rebar to bottom surface of concrete. The both main rebars and stirrups were modeled by distributed rebar ration in RC zone. Two cases were analyzed; sound case simulating the ST-100 case and bond deteriorated case following the **Equation 2.4** for the RC zone in which main rebars were distributed. In the bond deteriorated case, only reduced bond was considered by stiffening parameter and section loss and corrosion crack were ignored. Analytical results are shown in **Figure 2.33**, and the LugH-25% case, which showed bond deteriorated behavior in the case study was also



**Figure 2.32** Analytical model (rough mesh model)

put for comparison. Stiffness reduction due to low bond was reproduced well. Maximum load bond deteriorated case and sound case was same in the both models with rough and fine mesh while there



**Figure 2.33** Analysis results (rough mesh analysis)

was slight difference in the absolute values.

## 2.8 Summary of Chapter 2

Chapter 2 described the investigations on bond performance change caused by interlock loss and development of bond deterioration model. According to the experiment and analytical investigation focusing on the various interlocking condition, it was showed that bond between rebar and concrete as an entire member can be maintained as long as parts of interlock can work even when section loss occurred due to rebar corrosion. Bond deterioration model was proposed based on the investigations with stiffening parameter of reinforced concrete model, and sound degree was kept until 20% of averaged corrosion ratio. Then same stiffening parameter as plain concrete defined by mesh size and fracture energy was applied because rapid bond deterioration due to interlock loss in almost of region of a member. In the current condition, corrosion distribution correlation with expecting mesh size was required as input information for evaluation on existing structure subjected to rebar corrosion. As future studies, investigations on the influence of corrosion crack reducing bearing strength of concrete on bond deterioration or bond deterioration behavior with high corrosion ration causing pit corrosion or large nonuniformity of corrosion can improve accuracy of bond deterioration model and support the equivalent bod deterioration model as averaged corrosion ratio as a member requesting rough

investigation on corrosion condition of rebars of existing structures with rebar corrosion.

## References in Chapter 2

- [1] 石灰石鉱業協会, 石灰石骨材とコンクリート, 石灰石鉱業協会, 2005
- [2] Asamoto, S., Ishida, T., Maekawa, K., (2008), Investigation into volumetric stability of aggregates and shrinkage of concrete as a composite, *J. Adv. Concr. Technol.*, 6(1), 77-90, doi: 10.3151/jact.6.77
- [3] Hashin, Z., (1962), The Elastic Moduli of Heterogeneous Materials, *J. Appl. Mech.*, 29(1), 143-150
- [4] Hansen, T. C., (1965), Influence of Aggregate and Voids on Modulus of Elasticity of Concrete, Cement Mortar, and Cement Paste, *ACI Journal Proceedings*, 62
- [5] Maekawa, K., Fukuura, N., Soltani, M., (2008), Path-Dependent High Cycle Fatigue Modeling of Joint Interfaces in Structural Concrete, *J. Adv. Concr. Technol.*, 6(1), 27-242, doi: 10.3151/jact.6.227
- [6] Baltay, P., Gjelsvik, A., (1990), Coefficient of friction for steel on concrete at high normal stress, *J. Mater. Civ. Eng.*, 2(1), 46-49, doi: 10.1061/(ASCE)0899-1561(1990)2:1(46)
- [7] Ito, Y., Chijiwa, N., The influence of the liquid water on fatigue performance at embedded joint of corrugated steel web PC bridge, 8th Regional Symposium on Infrastructure Development in Civil Engineering (RSID8). 2A-5, 2018.10, Philippines
- [8] Fujiyama, C., Maekawa, K., (2011), A Computational Simulation for the Damage Mechanism of Steel-Concrete Composite Slabs under High Cycle Fatigue Loads, *J. Adv. Concr. Technol.*, 9(2), 193-204, doi: 10.3151/jact.9.193
- [9] 米津薫, 藤山知加子, 土屋智史, 牧剛史, 斉藤成彦, 渡辺忠朋, (2016), 非線形解析に基づく各種合成部材及び接合部の損傷評価, 土木学会論文集 A1, 第 72 巻 5 号, pp.II\_124-II\_134
- [10] L.A. Lutz, P. Gergely, (1967), Mechanics of bond and slip of deformed bars in concrete, *ACI Journal*, 64(11), 711-721
- [11] Y. Goto, (1971), Cracks formed in concrete around deformed tension bars, *ACI Journal*, 68(4), 244-251
- [12] 水野高明, 渡辺明, (1963), 丸鋼, 異形丸鋼および異形ねじり鉄筋の付着に関する研究, 第 93 号, pp.23-30, 土木学会論文集
- [13] 島弘, 周礼良, 岡村甫, (1987), マッシュなコンクリートに埋め込まれた異形鉄筋の付着応力 - すべり - ひずみ関係. 土木学会論文集, (378), 165-174.
- [14] Muthulingam, S., Rao, B. N., (2015), Non-uniform corrosion states of rebar in concrete under chloride environment, *Corros. Sci.*, 2015 93, 267-282, doi: 10.1016/j.corsci.2015.01.031
- [15] Biswas, R., Iwanami, M., Chijiwa, N., Uno, K., (2020), Effect of non-uniform rebar corrosion on structural performance of RC structures, A numerical and experimental investigation, *Constr. Build Mater.*, 230, 116908, doi: 10.1016/j.conbuildmat.2019.116908

[16] Zhang, W., Zhou, B., Gu, X., Dai, H., (2014), Probability distribution model for cross-sectional area of corroded reinforcing steel bars, J. Mater. Civ. Eng., **2014**, 26(5), 822-832., doi: 10.1061/(ASCE)MT.1943-5533.0000888

### ***Annotation***

Contents from 2.2 to 2.6 in chapter 2 have been published as follows.

Kurihara, R, Ito, Y, Cai, Q, Chijiwa N., The Influence of Interlock Loss between Rebar and Concrete on Bond Performance of RC Member, Appl. Sci., **2022**, 12(3):1079, doi: 10.3390/app12031079

# Chapter 3

Investigation on the influence of various scale cracks on structural performance and development of shear transfer model subjected to corrosion crack

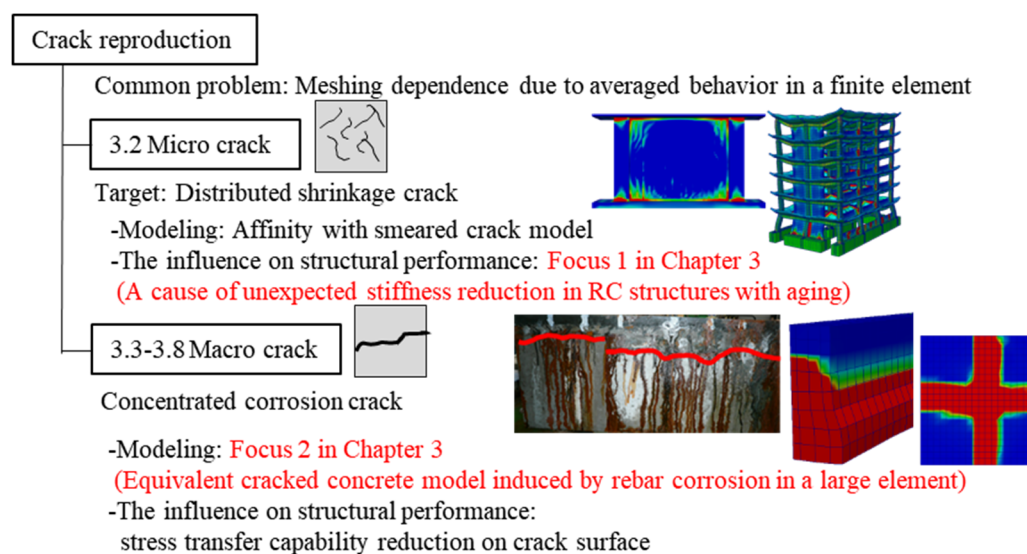
- Analytical investigation on distributed cracks
- Analytical investigation on the difference of behavior change of shear transfer by mesh size
- Experimental and analytical investigation on the shear stiffness until corrosion crack penetration
- Analytical investigation and development of modified shear transfer model considering nonuniformity



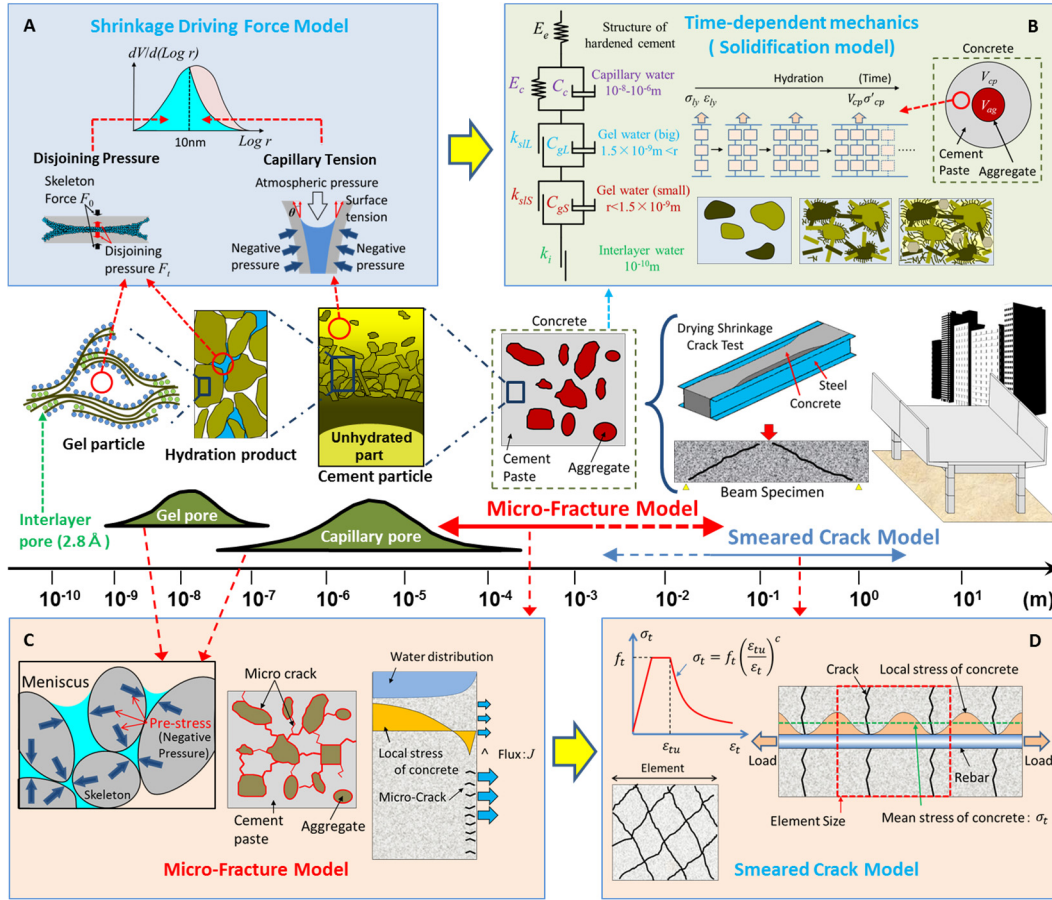
### 3.1 Abstract of chapter 3

This chapter aimed the development of equivalent model for corrosion crack focusing on shear transfer reduction. Shear transfer at crack surface had been developed based on investigations on cracks by external force with high accuracy, but application for corrosion crack considering the specificity such as anisotropy, crack elongation behavior from inside of concrete, and progress of crack width had the room for more development. In addition, assumption of shear transfer model in large mesh for corrosion crack had possible to deviate from actual condition, thus difference by mesh size had to be considered and implemented to structural analysis model. When considering the FE analytical evaluation for real scale structure subjected to rebar corrosion, direct FE model with large mesh size had great contribution for the purpose to reproduce overall structural behavior with low computation load. Thus, the equivalent corrosion model as averaged behavior was required for more effective and efficient structural performance evaluation. Another advantage of modeling as averaged behavior was the reduction of scattering. When analytical models tend to reproduce phenomena in detail with fine mesh, it was required to model various local nonuniformity explicitly such as interfacial zone between different materials as showed in chapter 2, while analytical results were also output as averaged value.

The author discussed on a reproduction method for cracks induced by various factor with separating out. Cracked concrete model has developed for external force and applicability for other cracks such as shrinkage crack or corrosion crack should be verified dividedly as shown in **Figure 3.1**. Fine distributed cracks were seemed to have high affinity with smeared crack model, and these cracks were caused by shrinkage, such as moisture move in skeleton pore of concrete or hydration. However, the influence of cracks on structural performance and applicability for reproduction of fine cracks in



**Figure 3.1** Focuses in Chapter 3



**Figure 3.2** Schematic platform of multi-scale thermo-hygral analysis (Yoneda *et al.*[8, 9]).

full-scale model should be confirmed before the development of model for corrosion crack with deviation in modeling concept. The author applied the multi-scale thermo-hygral analysis summarized in **Figure 3.2** [1, 2] for integrating shrinkage crack effects and structural effects in member scale and full-scale structure. In this analysis, influences of drying shrinkage crack on structural stiffness was focused on, and distributed shrinkage reduced structural stiffness of RC structures. These results suggested that the reduction of RC structure stiffness, which had been reported for past 30 years, was thought to mainly attribute to the drying effect. Dried region gradually progressed from concrete surface, thus degrees of the drying effect on structural performance highly depended on dimension of structures. When considering FE analytical investigation on drying effects, mesh size was one of the important factors for accurate evaluation because analytical calculation was averaged in a finite element.

When focusing on for corrosion crack, characteristic of corrosion crack such as concentrated crack with specific direction along rebar might be deviated from the concept of smeared crack model, and it should be considered for modeling. Corrosion crack in structural FE model was induced as initial crack with rebar direction, thus unevenness or uncertainty of crack progress was averaged in

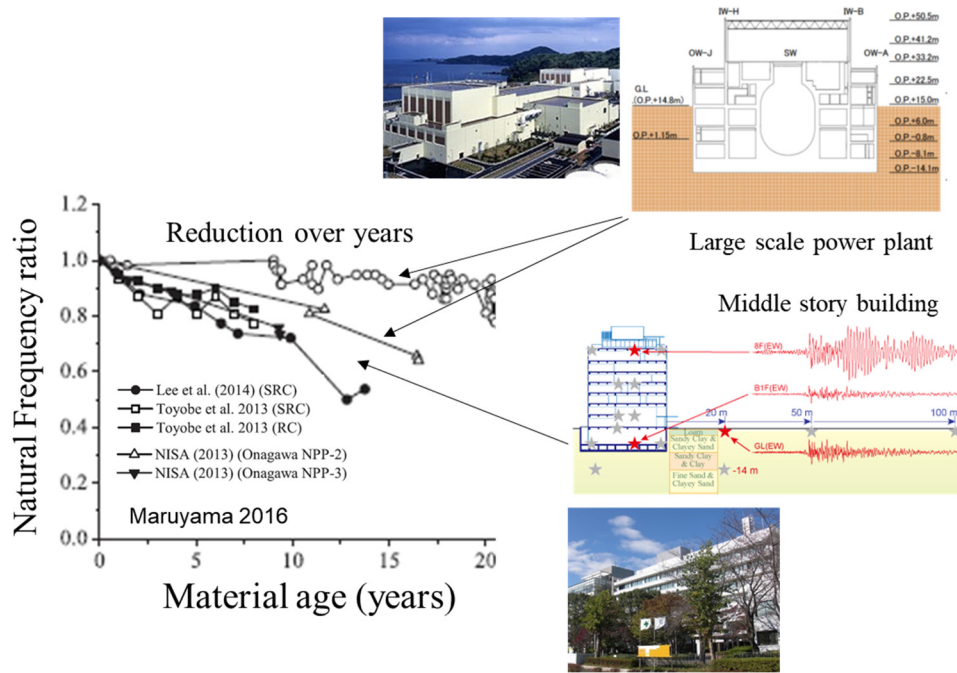
a element while cracks elongation due to external force was based on analyzed strain as the output results. Averaged behavior of corrosion crack in a element had dependence of mesh size on accuracy of analysis and applicability of conventional model for corrosion cracks should be investigated for analysis with large mesh size. In order to make clear the problems, The author conducted analysis the focusing on the corrosion crack elongation and shear transfer by conventional corrosion model with different size of mesh on concrete plate. Corrosion crack was applied by expansion strain in RC element with rebar corrosion, and expansion strain was calculated rebar ratio, rebar diameter and mass loss ratio in the conventional model. The shear stiffness reduction behavior in the conventional model was deviated from actual condition in the case with large mesh size, and the author divide development of modified model into two state, with non-penetrated and penetrated of crack. In the state with non-penetrated crack, conventional model cannot be applied basically because the model considers cracked or uncracked state, not partially propagated crack in one element. Shear experiment for concrete block with partial pre-crack in shear surface was conducted. The author proposed new shear transfer model based on the area ratio of cracked and un-cracked region in shear surface of concrete, and function  $k$  determining area ratio from corrosion ratio of rebar and the ratio of rebar diameter to mesh size.

For the development of shear transfer model after crack penetration, it was required to catch the difference of crack inducing and structural behavior induced by forced expansion strain by mesh size. The author conducted reproduction FE analysis for beam loading test failed in shear with and without corrosion crack by different mesh size. Corrosion crack was induced by accelerated corrosion test. Beam model with large mesh size overestimated stiffness reduction by corrosion crack. It is led from two factors, averaged corrosion crack strain with unevenness in large mesh and neglect of discharge of corrosion gel from penetrated crack. The author proposed equivalent model for unevenness of corrosion crack in large mesh and induction of expansion limit by discharge of corrosion gel. Reproduction analysis for beam test used proposed model in large mesh can describe experimental results well.

## 3.2 The influence of distributed cracks on RC structures

### 3.2.1 Drying shrinkage effects on structural performance in full scale structure

The monitoring for RC structures such as middle or high story buildings or nuclear power plant has been conducted and its natural frequency has been reported to gradually decrease for past 30 years [3-6]. The decrease of natural frequency means the reduction of structural stiffness under the small vibrations. Maruyama reported an advanced investigation from a multi-scale views of material as moisture loss by evaporation and stiffness change, and drying shrinkage induced cracking [7]. **Figure 3.3** shows the natural frequency ratio of various RC structures including middle story RC buildings and buildings in ONAGAWA nuclear power plant [3-7]. There are different rates of reduced natural



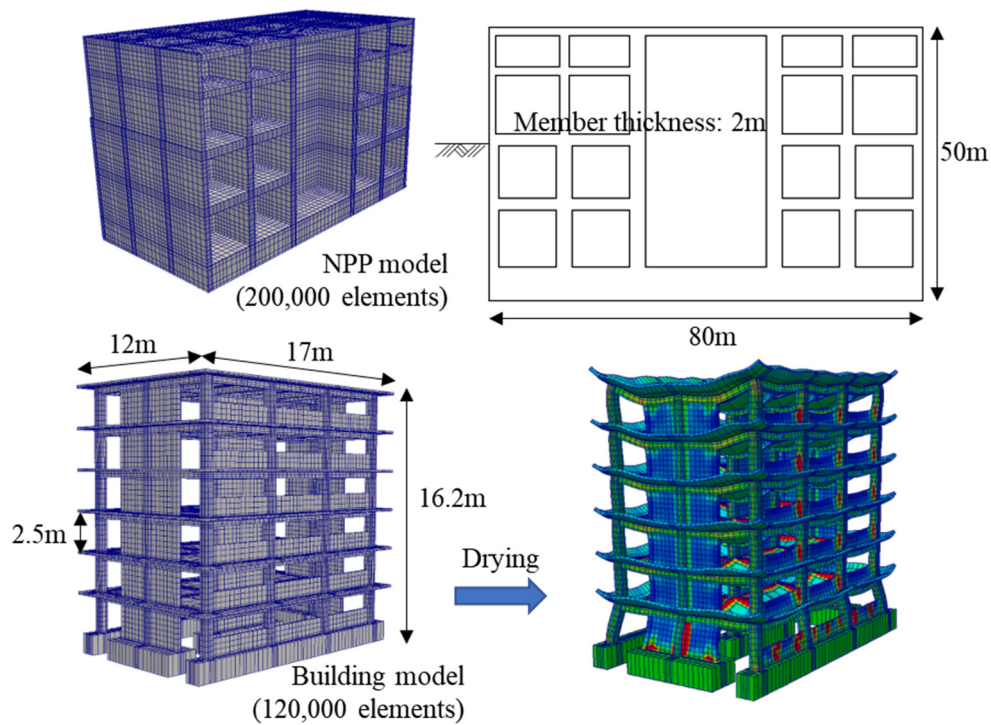
**Figure 3.3** Reduced natural frequency of RC structures with different dimensions (Maruyama [7])

frequency by scale of structure. The power plants whose walls have large thickness of 1~2m produces slower reduction of natural frequency than the middle story buildings with much smaller dimensions of columns and slabs.

The author applied the thermo-hygral analysis [1, 8, 9] over several decades by full-scale mockup model of multi-story buildings and nuclear power plants in service. This analytical system can consider moisture transport and related shrinkage, self-equilibrated stresses, crack nonlinearity, deformation by sustained stresses as long-term actions and mode of deformation with integration of each effects. Applicability of this system were confirmed in past researches [10-14]. In the analyses, cracking due to mechanical restriction in elements close to neighboring members with different shapes and dimensions numerically represents the kinetics of junction. As this crack was the indirect and weak expression of localized junction planes with small sized finite elements, the multiplication of shear strain and the element size was mechanically equivalent to the shear slip of the junction plane. Then, the shear transfer model of RC elements results in the model of junction planes.

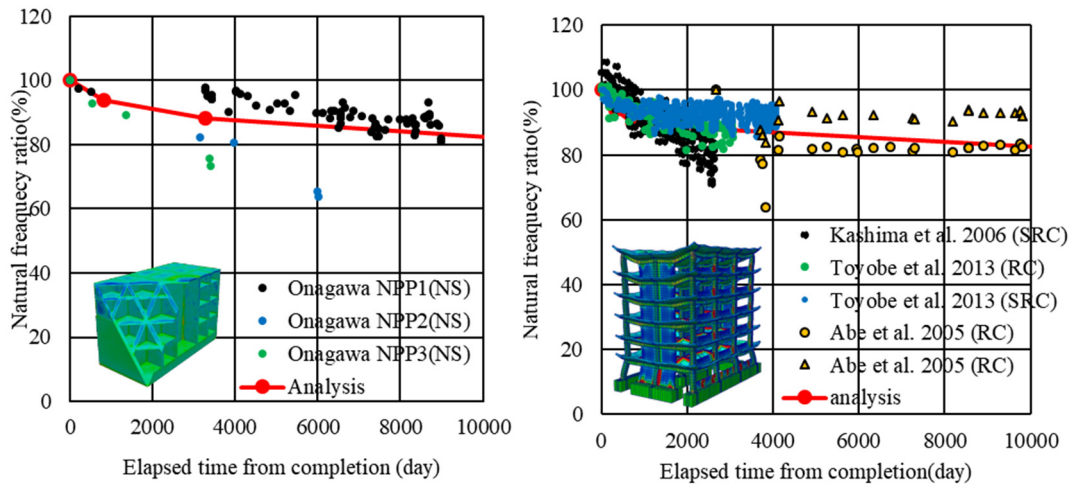
Analytical models for nuclear power plant and multi-story RC building are shown in **Figure 3.4**. 6-story building base on previous full-scale experiment, and the dimension and shape of nuclear power plant model are plainly decided in reference to power plants [7]. In the nuclear power plant model, reinforcement of all member is arranged to be smeared out. RC walls are designed to function against in-plane shear with distributed cracking, and its reinforcement ratio is set as 1.2%. For the base slab, orthogonal reinforcement of 1.0% is assumed as well. For the both model, one-time casting of fresh concrete is numerically assumed to make a simultaneous start of cement hydration and micro-pore formation at all finite elements under zero gravity. During this period of initial hydration, perfect sealed conditions were set up. After 7 days curing, the whole structure was exposed to 60% relative humidity (RH) and the vertical gravity of 980 gal. The mix proportion of concrete simulated is listed in Table 1. At each elapsed time, the horizontal gravity of 10 Gal, constant equivalent static force proportional to the mass of concrete, was fictitiously applied and the horizontal drift was computed. Thus, the averaged shear stiffness was calculated.

The long-term natural frequency reduction with aging was numerically reproduced as shown in **Figure 3.5** [3-6]. Crack concentration near joint area among structural members in multi-story buildings due to restriction of drying shrinkage and cracks close to the surfaces of RC thick walls of nuclear power plants due to drying progress from concrete surface were observed. The reduction of

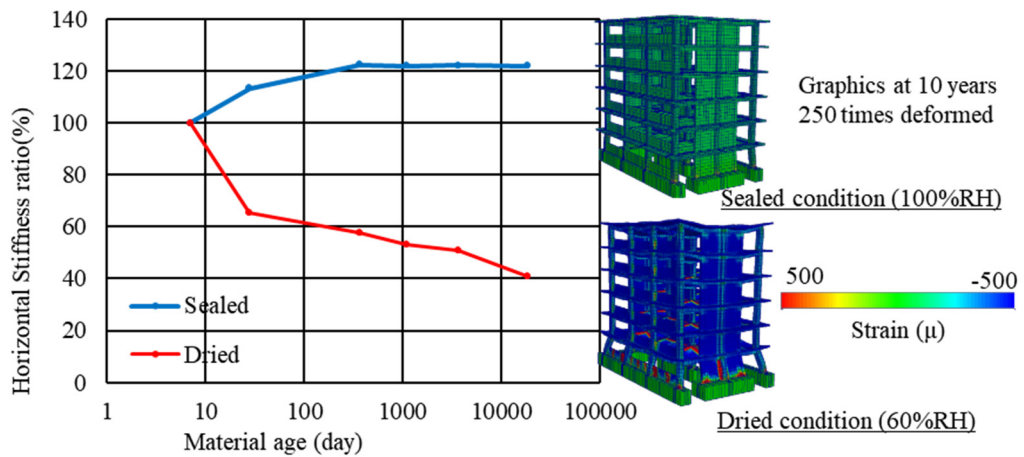


**Figure 3.4** Mock-up model of nuclear power plant and multi-story building





**Figure 3.5** Mock-up model of nuclear power plant and multi-story building



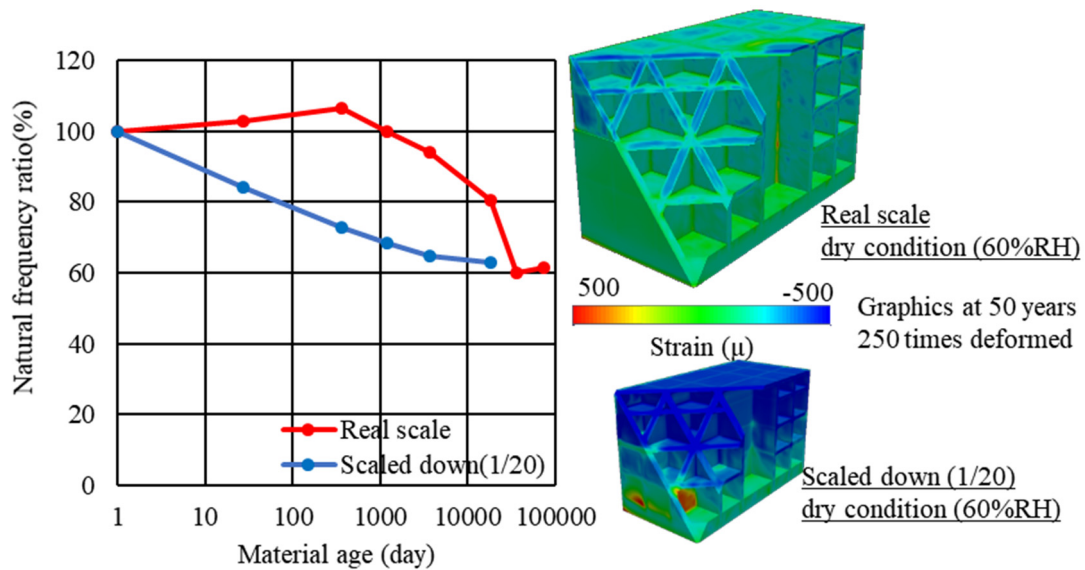
**Figure 3.6** Difference by environmental condition on multi-story building model

RC building stiffness was thought to mainly attribute to the drying effect. **Figure 3.6** shows that the comparison with environmental condition in the building model. If the perfect sealing would be continued for the whole lifetime, the stiffness of concrete gradually increases by progressive hydration of cement, the overall stiffness of structure comes up to the maximum at about 200 days. In construct, the overall structural stiffness is gradually declining if drying and moisture loss are numerically allowed. Within the limited information, the author may conclude at least that the moisture loss and associated structural cracking may play some substantial role on the decay of natural frequency of structural concrete owing to both cracking and hydration degree.

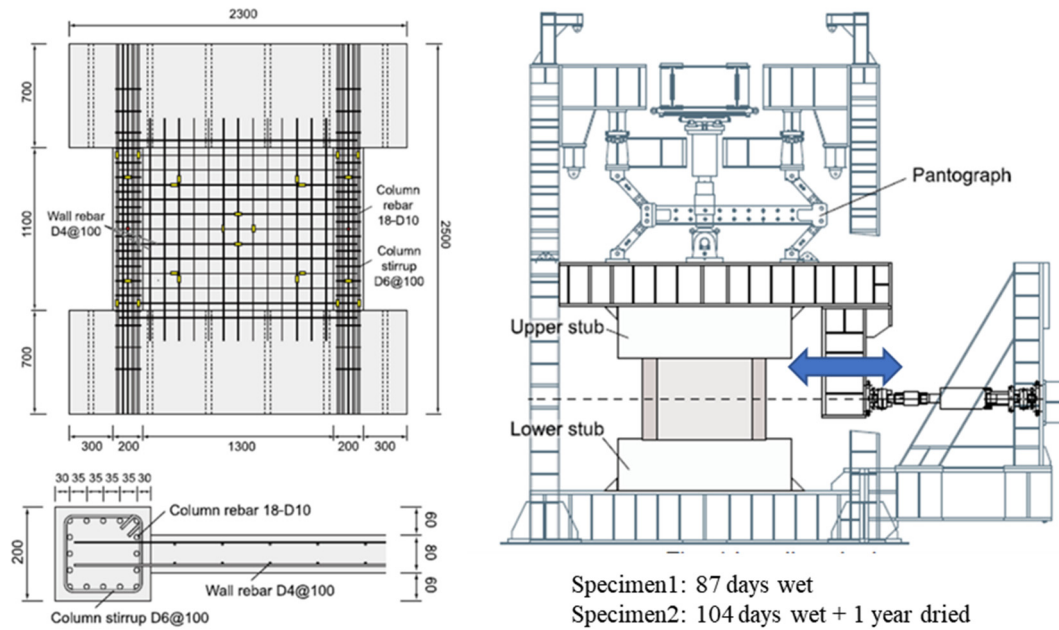
### 3.2.2 Drying shrinkage effects on structural performance in member scale structures

For discussing the scale effect, the small model with 1/20 dimension is also produced with the same material and the reinforcement ratio and comparison of stiffness reduction ratio with size was showed in **Figure 3.7**. In the full-scale nuclear power plant model, as the thickness of walls is more than 1.0m, the rate of moisture loss normalized by volume is much less at the beginning of drying. Even after the exposure to the natural environments, water loss from concrete accompanying the retardation of cement hydration is concentrated only nearby the surfaces. Then, the strength continued to increase for large volume of core concrete, and the overall structural stiffness is increasing up to almost 200 days. After this period, the gradual decline of the global stiffness can be seen in **Figure 3.7**, similar tendency to the case of RC building. Drying of concrete and stiffness reduction greatly affected by member thickness, thus the author focused on the member scale for more precise understanding. In this research, RC shear wall was focused as RC member. RC shear wall should be subject to drying effects because member thickness is smaller and its surface area exposed to air is larger than other members such as column or beam. Sasano *et al.* conducted the shear cyclic loading test on the RC shear walls in the previous research [15]. In this study, this shear wall is numerically reproduced and used to discuss the drying effect on concrete member especially in the effects of size.

**Figure 3.8** shows the outline of experiment in previous research and mix proportion of concrete is given in **Table 3.1** [15]. The RC wall was designed as 1/3 scale of wall in real buildings. The thickness of the wall was 80 mm and mesh reinforcement at 0.35% of the reinforcement ratio was produced. There were 2 cases of environmental condition named “Sealed” and “Dried”. Both specimens were in moisture curing until the age of 87 days (Sealed specimen) and 104 days (Dried



**Figure 3.7** Mock-up model of nuclear power plant and multi-story building



**Figure 3.8** Outline of loading test on the shear wall (Sasano *et al.* [15])

specimen) after 7 days of sealed curing. Shear cyclic loading test on “Sealed” was conducted after moisture curing. The other specimen was exposed to ambient air in experimental room for 1 year until the age of 462 days, and then loaded. The shear span was fixed at 0.32, and axial force of 360 kN was applied during loading. The value of axial force is designed as 15% for the designed compressive strength of 30MPa. Experimental result is showed in **Figure 3.9**. Drying shrinkage cracks in whole region in shear wall were observed only in dried specimen, and cracks were concentrated in the edge area of the wall and columns. Looking at the envelopes from the relationship between applied load and relative displacement between the bottom and top of wall, the initial stiffness of dried specimen shows 54% of lower value than that of sealed specimen. The initial stiffness was obtained from linear least-squares method at first cycle response, and the stiffness of each cycle was defined as the average of the 2 slopes from the origin to the peaks. In contrast, the ultimate strength was almost same, and the difference in the stiffness became smaller with higher stress loading cycle.

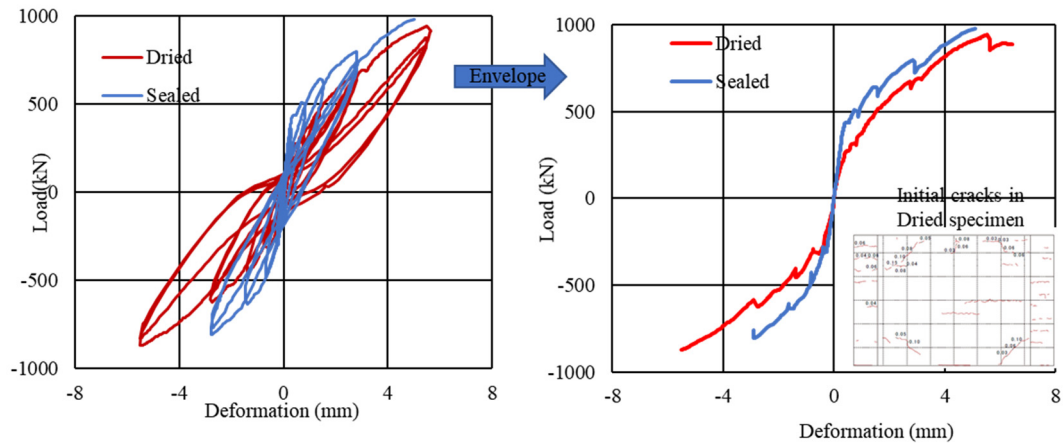
The author applied the thermo-hygral analysis for reproduction. Analytical model and strain distribution caused by exposure in ambient environment is shown in **Figure 3.10**. Same mix proportion, environmental condition and loading cycle as that of experiment were applied. In order to track drying progress from concrete surface accurately, approximately 10 mm of element size was applied in the wall part, thus 8 elements were placed for wall thickness. Distributed drying shrinkage and concentration of crack in the restriction region among members could be reproduced well. **Figure 3.11**



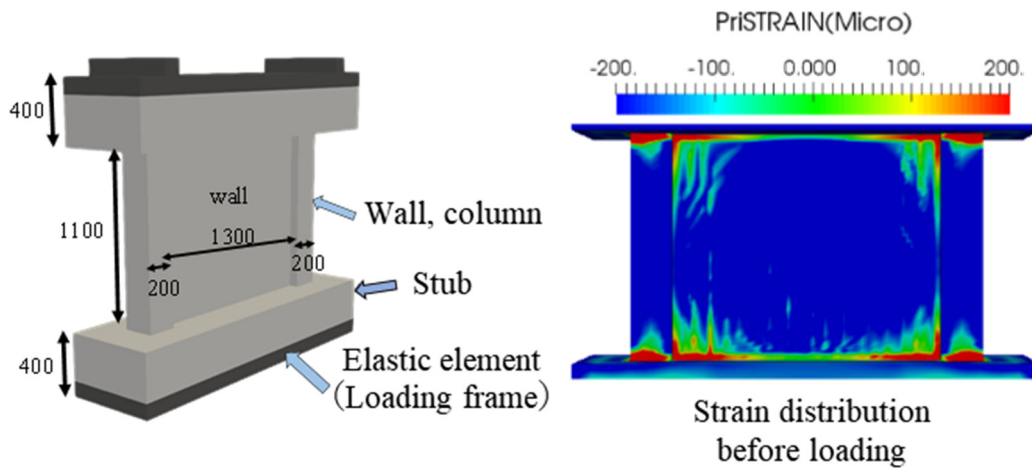
**Table 3.1** Mix proportion of concrete (Sasano *et al.* [15])

W.C (%)	s/a (%)	Unit weight (kg/m <sup>3</sup> )			
		Water	Cement	Gravel	Sand
5.3	50	182	324	854	864

Note) Specific gravity: normal Portland cement=3.15, gravel=2.55, sand=2.58

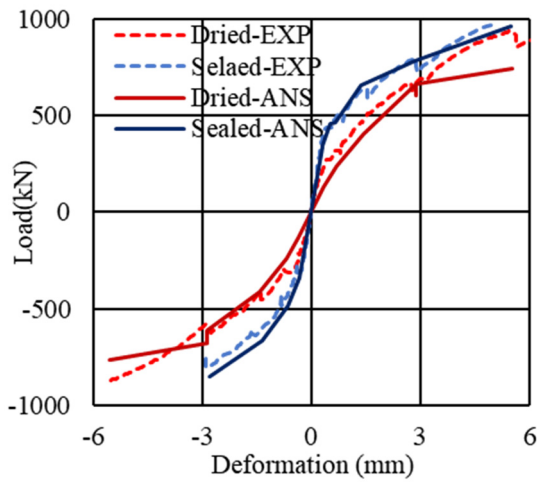


**Figure 3.9** Experimental results (Sasano *et al.* [15])



**Figure 3.10** Analytical model and strain distribution by thermo-hygral analysis

shows the comparison of analytical result with experimental one in the envelope of load-displacement curve. Initial stiffness reduction due to drying can be reproduced by thermo-hygral analysis and the analysis also can track stiffness reduction behavior in each loading cycle as shown in **Table 3.2**. In order to investigate the scale effect, the author produced scaled up models in two degree, 3 times larger and 5 times larger with same shape. Each scale aims the investigation on real scale structure and huge



**Figure 3.11** Result of reproduction analysis

**Table 3.2** Stiffness in each drift cycle

Sealed	ANS	EXP	A/E
Initial stiffness	1109	1226	0.90
Stiffness (1/800)	527	459	1.15
Stiffness (1/400)	321	289	1.11
Stiffness (1/200)	192	196	0.98
Dried	ANS	EXP	A/E
Initial stiffness	629	663	0.99
Stiffness (1/800)	349	333	1.04
Stiffness (1/400)	247	236	1.04
Stiffness (1/200)	133	165	0.80

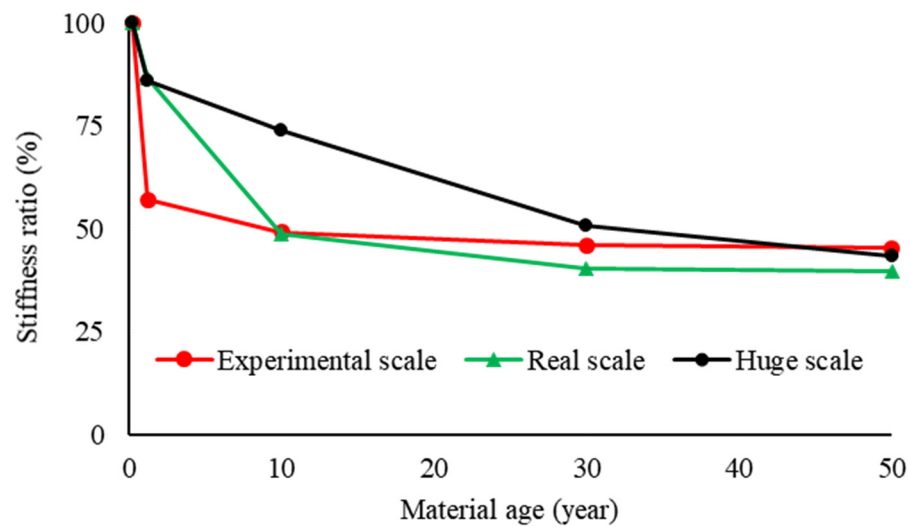
structure such as nuclear power plant, respectively. Mesh placing for each size model were same, in other word, mesh size were also 3 times and 5 times larger in real scale and huge scale, respectively in order to evaluate under equal condition of drying progress. For investigation on long-term behavior, shear cyclic loading were applied in each model at the age of 94days (moisture cured), 462 days, 10 years (3650days), 30 years (10950 days), 50 years (18250 days). Exposure to stable environmental condition, 50% of relative humidity and 20 °C of air temperature, was set after same environmental condition as reproduction analysis of experiment until the age of 462days. **Table 3.3** shows initial stiffness ratio and maximum load ratio at each age based on the age of 94 days in each case. Initial stiffness reduced gradually with aging in all scale models, while maximum load was not so different by material age. **Figure 3.12** shows the initial stiffness change of each case with aging. In the same scale model as experiment, initial stiffness reduction converged in 10 years at 30% of reduction degree. Convergence time became longer with higher scale, 30 years for real scale and 50 years huge scale, respectively, even though dried region might be overestimated due to larger mesh size. Stiffness reduction ratio after convergence was almost same in all scale models, approximately 30%. Under the condition with equilibrium of vapor pressure between inside of concrete and ambient air, member stiffness had been declined at same degree because drying shrinkage cracks were distributed on overall region of the member.

### 3.2.3 Outcomes from analytical investigations on distributed fine cracks

The mockup model of RC power plant buildings and the multi-story building was affected by the moisture loss and drying shrinkage, and structural stiffness declined. The rate of stiffness reduction is slower in huge structure with thick member. It is shown that the drying shrinkage of concrete was one of the key factors to predict the structural stiffness of the whole buildings with different dimensions,

**Table 3.3** Initial stiffness ratio and ultimate load ratio based on that at the age of 94 days

Age (day)	Experimental scale		Real scale		Huge scale	
	Ultimate load	Initial stiffness	Ultimate load	Initial stiffness	Ultimate load	Initial stiffness
94 (Wet curing)	100	100	100	100	100	100
462 (1 year)	94.9	57.0	99.6	86.6	102	85.9
3650 (10 years)	96.4	49.2	93.5	48.8	103	73.9
10950 (30 years)	93.5	46.0	92.0	40.5	99.0	50.8
18250 (40 years)	92.0	45.3	90.3	39.8	98.1	43.4



**Figure 3.12** Initial stiffness change with aging with different dimension

and the scale of structural members is confirmed to be a critical factor for drying. When drying effects for member was focused, shear stiffness in RC member was degraded by drying shrinkage cracks distributed in an entire member. Stiffness reduction caused by distributed fine cracks can be reproduced well in smeared crack model. From the viewpoint of mesh size, distributed crack could be evaluated in various scale model equivalently, but drying progress from concrete surface had mesh size dependence because drying condition was averaged in a element.

### 3.3 The influence of concentrated crack due to corrosion expansion

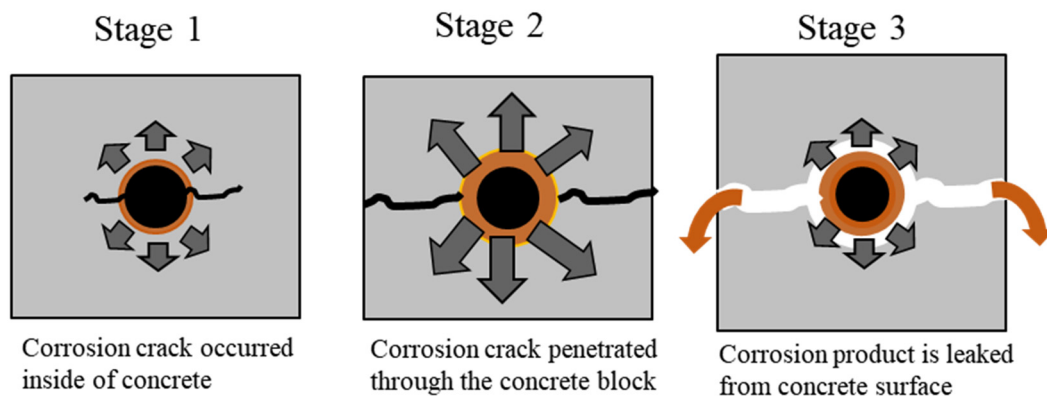
#### 3.3.1 Organization of issues on modeling of corrosion crack

Corrosion crack is meso-scale crack along rebar, not assembly of distributed fine cracks. Smeared crack model treats a element as cracked concrete with many fine cracks. when the element has higher tensile strain than tensile strength along strain direction. Thus, cracked or uncracked condition or unevenness of crack surface is averaged in a element. When large mesh size is applied for real scale

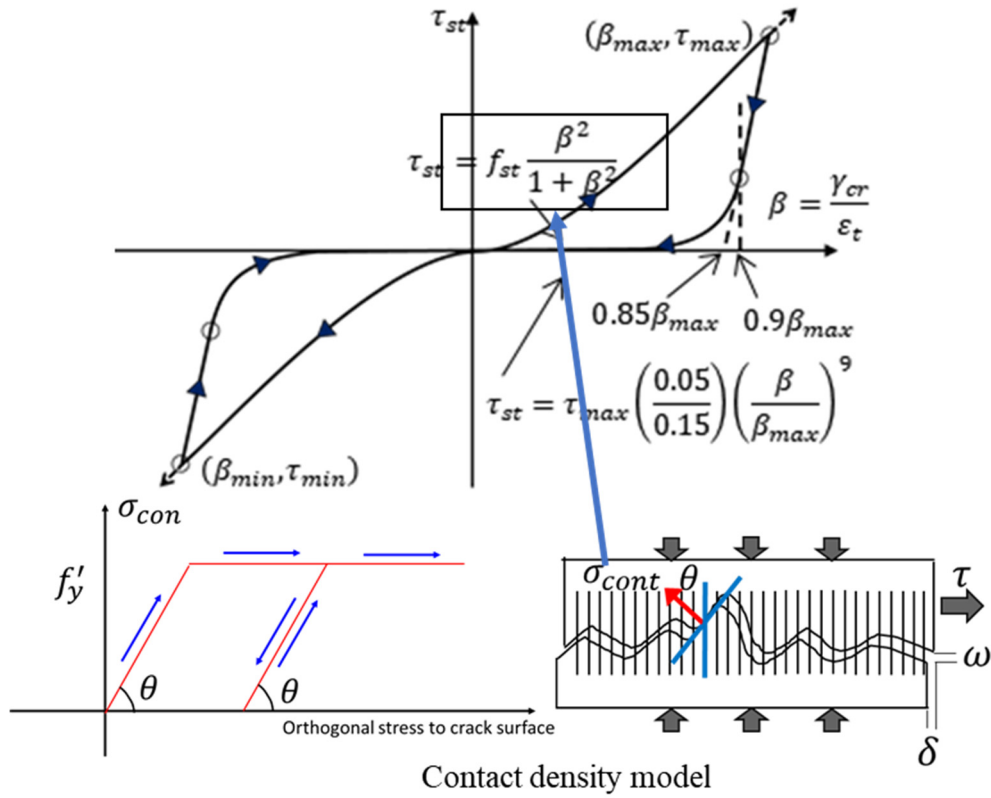
structure, the behavior with averaged crack should have deviation from actual condition. Here, the author divided the discussion into three stages by corrosion process as shown in **Figure 3.13**. Stage 1 focused the condition until corrosion crack penetrates through concrete block. In large mesh, cracked and uncracked region were existed at the same time. In stage 2, the condition that corrosion crack has penetrated was considered. Completely cracked concrete can be assumed in this stage and in the conventional model, corrosion crack is induced straightly based on rebar direction. Actual corrosion crack should have unevenness and these effects may produce the deviation of model from actual condition especially in large mesh size. In stage 3, corrosion product can discharge from penetrated crack in concrete surface, thus expansion behavior due to corrosion process should be changed. Basic numerical models for cracked concrete was described in chapter 1, and corrosion crack modeling should have greatly influence in shear transfer model because corrosion crack occurs along rebar. Section 3.4 focuses on the stage 1, and Section 3.5.1 and 3.5.2 discussed on stage 2 and stage 3, respectively.

### 3.3.2 Conventional model for shear transfer on crack surface of concrete

This section describes constitutive law of shear transfer between crack surface. **Figure 3.14** shows the basic shear model of cracked concrete. In this study, initial shear stiffness was focused and shear stiffness model is based on the contact density model [16, 17]. Contact density model considers surface angle in crack for each contact density unit (1mm in COM3), integral along crack surface. Shear stiffness of cracked concrete  $G$  is described in **Equation 3.1** and **Equation 3.2** below [15]. This shear model describes only from shear transfer ratio of shear displacement to opening displacement without crack width. Thus, shear stiffness is varied along the route shown in **Figure 3.14** under various stress field such as crack opening by corrosion, crack closing by dead load, or shear gap



**Figure 3.13** Discussion division for corrosion crack modeling



**Figure 3.14** Basic model of shear in cracked concrete

by seismic load.

$$\frac{1}{G} = \frac{1}{G_c} + \frac{1}{G_{crk}} \quad (3.1)$$

$$G_c = \frac{E_c}{2(1+\nu)}, \quad G_{crk} = f_{st} \left( \frac{\beta}{1+\beta^2} \right), \quad \beta = \delta/\omega \quad (3.2)$$

Where,  $G_c, G_{crk}$ : shear stiffness of sound concrete and cracked surface,  $f_{st}$ : shear strength of concrete,  $\delta$ : shear displacement, and  $\omega$ : opening displacement.

When cracks closed, cracked concrete should have high shear stiffness and that phenomena can be considered by taking uncracked shear stiffness into account. Because the value of  $G_c$  was greatly higher than  $G_{crk}$ , the value of  $G_{crk}$  becomes dominant in the high tensile strain normal to crack surface condition.

### 3.3.3 Conventional model for corrosion expansion induction

Corrosion expansion model was developed by Toongoenthong *et al.* [17, 18], and it can reproduce the expansion of corrosion products into the surrounding concrete. Concrete crack was formed with induced expansion strain, and section loss of rebar also can be considered with mass loss ratio of rebar due to corrosion. The amount of mass loss has linear relationship with induced tensile stress for

surrounding concrete. Scheme of corrosion model is shown in **Figure 3.15**. When rebar corrosion occurs, the corrosion product expands feely in the situation without any restraint from surrounding concrete. Volume loss of the corroded rebar from mother steel  $V_{loss}$  can be represented by **Equation 3.3**.

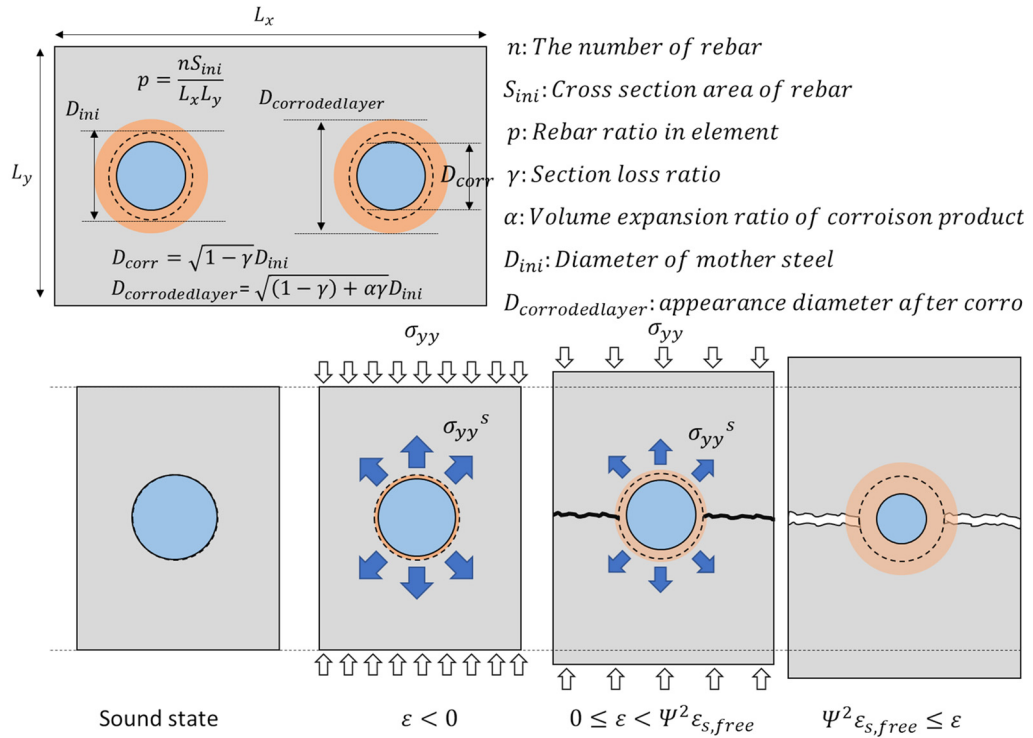
$$V_{loss} = \pi \gamma \alpha D_{ini} / 4 \quad (3.3)$$

Where,  $\gamma$  denoted volume fraction loss of steel per unit length ranging from 0 to 1 as non-dimensional factor. The value of 0 for  $\gamma$  shows sound state and 1 means complete section loss of rebar.  $\alpha$  is the coefficient of expansion of corrosion product ranging from 0.02 to 14. Under the assumption of consequently formation of the corrosion product around the mother rebar, the diameter of the corroded reinforcement  $D_{corrodedlayer}$ , which consists of mother steel and its corrosive product, can be described as **Equation 3.4**, and **Equation 3.5** shows the reinforcement free-expansion strain,  $\varepsilon_{s,free}$ .

$$D_{corrodedlayer} = D_{ini} \sqrt{1 + \gamma(\alpha - 1)} \quad (3.4)$$

$$\varepsilon_{s,free} = \sqrt{1 + \gamma(\alpha - 1)} - 1 \quad (3.5)$$

Expansion strain causing tensile stress can be induced in a finite element as initial state correlating with rebar diameter, rebar ration and corrosion mass loss ratio. Thus, cracked concrete model is called when induced tensile stress exceeds tensile strength. This Maekawa-Toongoenthong corrosion model had been developed and approved in previous researches [17-21].



**Figure 3.15** Concept of corrosion expansion model

### 3.3.4 Variation of shear stiffness reduction behavior with dependence on mesh size

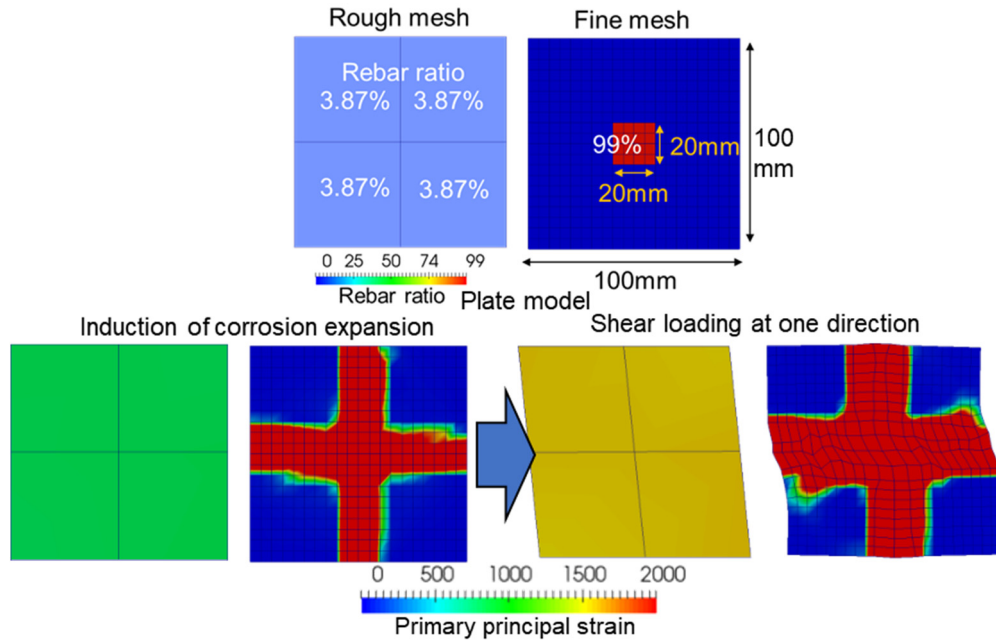
In order to catch the problems caused by different mesh size, shear loading analysis was conducted for plate model composed from concrete and a rebar with different mesh size as shown in **Figure 3.16**. Cross section of plate model was square of 100mm on a side and width was 10mm by 1 mesh. In large mesh, 4 elements of hexahedron with the size of 50mm composed the model, while 5mm of mesh size was applied for the fine mesh case. Considering the condition that a rebar of D22 was placed in the center of the square cross section, rebar ratio of 3.87% was smeared in the all of cross section for the large mesh case. 99% of rebar ratio was applied in center area of square with 20mm on a side in the fine mesh case. 10cases for each mesh was set as the parameter of mass loss due to corrosion, 0, 0.001, 0.006, 0.01, 0.025, 0.05, 0.075, 0.1, 0.2, and 0.3 g/cm<sup>2</sup>, respectively. Mass loss can be conversed to corrosion volume ratio by **Equation 3.6** and basically corrosion ratio was set as parameter showing corrosion degree for following discussion.

$$R_c = \frac{4M_l}{\rho_s D} \quad (3.6)$$

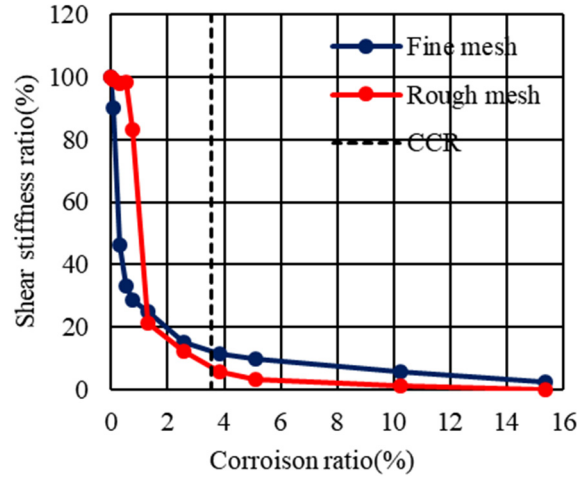
Where,  $R_c$ : corrosion ratio in volume,  $M_l$ : Mass loss ratio per surface area (g/cm<sup>2</sup>),  $\rho_s$ : density of rebar (g/cm<sup>3</sup>),  $D$ : Diameter of rebar (cm).

After inducing expansion strain in each case, shear strain in one direction was applied and initial stiffness was calculated from the slope of averaged shear stress to averaged shear strain under the 0.0002 micro of averaged shear strain.

**Figure 3.17** shows the shear stiffness ratio to sound shear stiffness in each mesh, and Y-axis shows the corrosion ratio calculated from the input amount of mass loss and section area of rebar.



**Figure 3.16** Scheme of shear loading analysis



**Figure 3.17** Shear stiffness ratio with corrosion ratio progress

Where, critical corrosion ratio (CCR) is also put on the graph. CCR means the corrosion ratio at when corrosion crack reaches the concrete surface proposed by Oh et. al. [22]. CCR can be determined only from the cover thickness of concrete as shown in **Eq. 3.7**.

$$CCR = 0.0018c^{2.07} \quad (3.7)$$

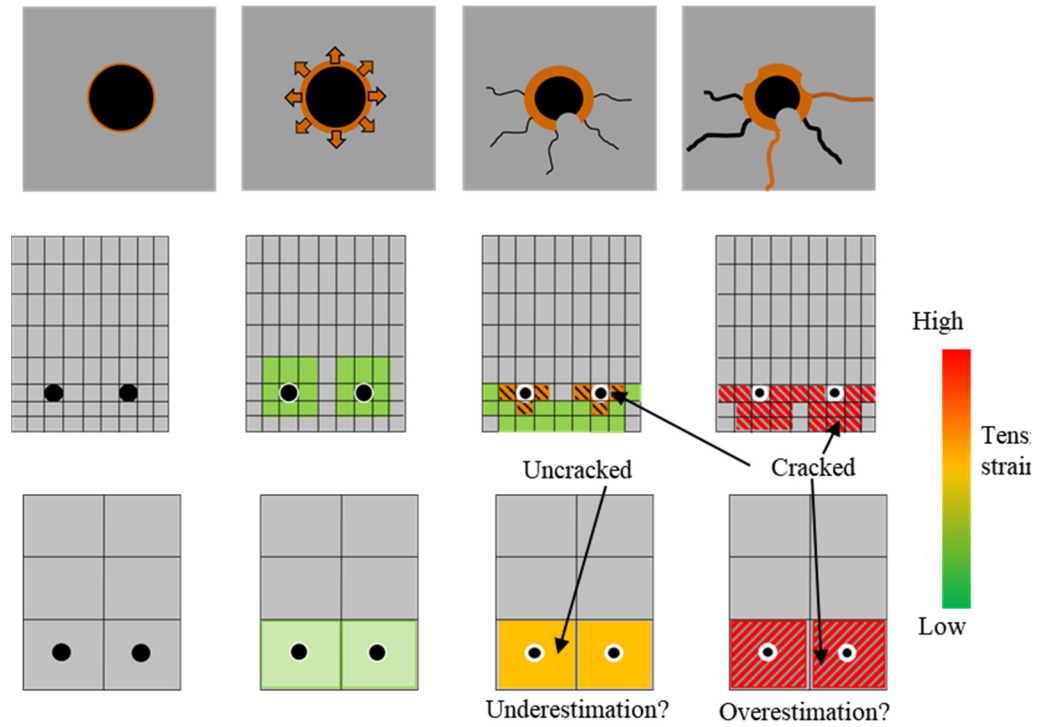
Where, *CCR*: critical corrosion ratio (%), *c*: cover thickness of RC.

Looking at the analytical results, shear stiffness in the state with slight corrosion ratio under 1.3% was stable at the almost same value as sound stiffness in large mesh. In the state with higher corrosion ratio, shear stiffness of large mesh rapidly decreased and the value kept lower than that of fine mesh. On the other hand, stiffness reduction of fine mesh was monotonous decrease and smooth curve. This difference was caused by expanded area. Distributed tensile strain in all the cross section was given in large mesh, thus uncracked model was applied in the slight corrosion state and shear stiffness of 4 elements was taken from cracked model after expansion strain reached cracked tensile strain, 0.0002 micro. In the fine mesh case, concentrated expansion strain was given in the center elements, and expansive strain propagated to surround concrete as actual expansion stress propagation by corrosion product. Expansion strain caused crack and crack elongation can be reproduced because there were many meshes elements in the direction of crack elongation to concrete surface. From these results, the author divided investigations into two parts mainly, with non-penetrated crack before reaching CCR and with penetrated crack.

### 3.4 Development of shear transfer model before crack penetration

Problems before crack penetration was presented in **Figure 3.18** When expansion strain due to corrosion was applied, fine mesh could track the crack elongation but large mesh cannot and shear



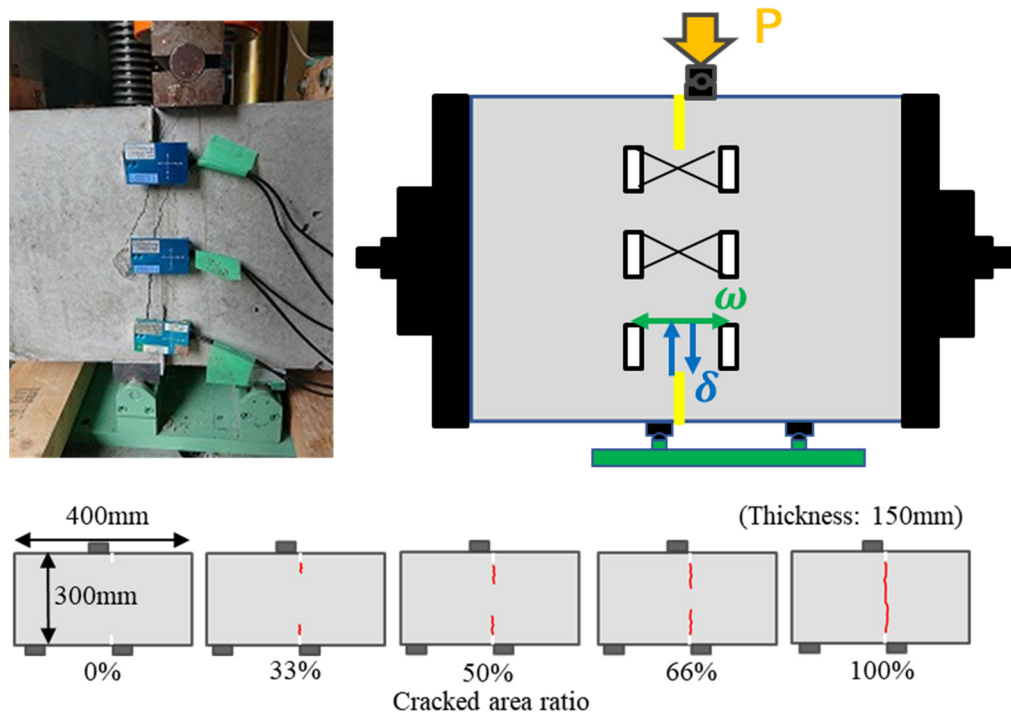


**Figure 3.18** problem presentation diagram before crack penetration

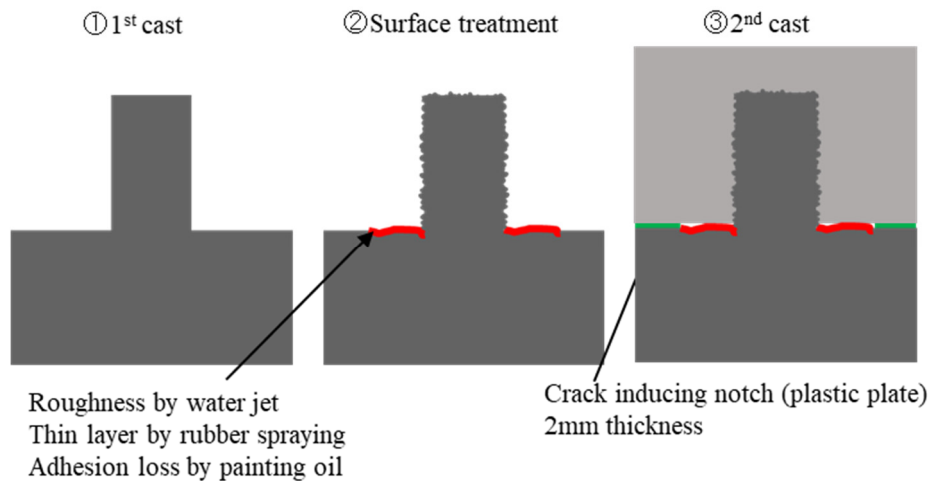
stiffness greatly depends on uncracked or cracked state under applied tensile strain. Shear stiffness of uncracked concrete was described by  $G_c$  in **Equation 3.2**, and that of cracked concrete is given by **Equation 3.1**. Shear transfer between crack surface given by  $G_{crk}$  was greatly lower than the value of  $G_c$ , thus rapid reduction of shear stiffness of cracked state occurred. The author conducted shear test for concrete block with partial pre-crack in order to investigate shear stiffness reduction behavior with crack elongation.

#### 3.4.1 Experimental program on shear stiffness with non-penetrated crack

Experimental setup is shown in **Figure 3.19**. Shear loading test for concrete block specimens with 400mm\*H300mm\*W150mm, which close value to the mesh size applied for real scale FE analysis in general was conducted. 5 cases with different pre-cracked area were set and 2 specimens for each case were tested. Noted that 4 sound specimens (0% of pre-cracked) were tested in order to confirm the scatter of this test program. Measurement targets were applied load by load cell, crack opening displacement, and shear displacement by 2-directional crack gauge. For averaging open and shear displacement in blocks, total 6 gauges, 3 gauges on each front and back surface were attached. Production method of pre-cracked block specimens is shown in **Fig. 3.20** At first, convex shape concrete was casted, and surface roughness was performed by water jet 5 hours after first casting. Surface roughness by water jet aimed to reproduce corrosion crack surface. Rubber film for producing



**Figure 3.19** Experimental setup



**Figure 3.20** Production method of pre-cracked block specimens

thin layer was produced by rubber spray after wiped and dried to remove water in the surface of concrete. It took 8 hours for drying of rubber paint, then the other part of concrete was casted after painting of oil for removing the effects of chemical adhesion between concrete and rubber. Shear loading test was performed after 7 days under sealed curing. Compressive and tensile strength at shear loading were 40.7 MPa and 2.57 MPa, respectively.

### 3.4.2 Experimental results and proposal of the shear stiffness model

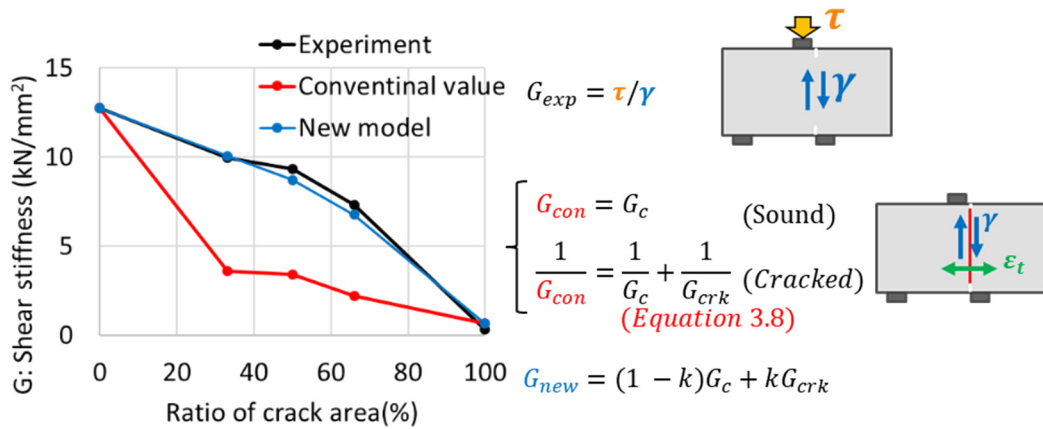
**Figure 3.21** show the experimental results and comparison of conventional and proposal shear stiffness model in this chapter. Y-axis shows the shear stiffness of concrete block and experimental shear stiffness can be taken from slope of applied load to averaged shear displacement in elastic range at first stage of loading. Conventional model as shown in **Equation 3.1** and **Equation 3.2** was also calculated and plot from shear and open displacement in experimental value. Shear stiffness by conventional model in the condition that cracked and uncracked area were mixed in shear surface was clearly lower than experimental value. Here, the author suggested the new shear stiffness model in **Equation 3.8**. It was based on the assumption that shear stiffness could be calculated from the area ratio of cracked region to uncracked region,  $k$ .

$$G = (1 - k)G_c + kG_{crk} \quad (3.8)$$

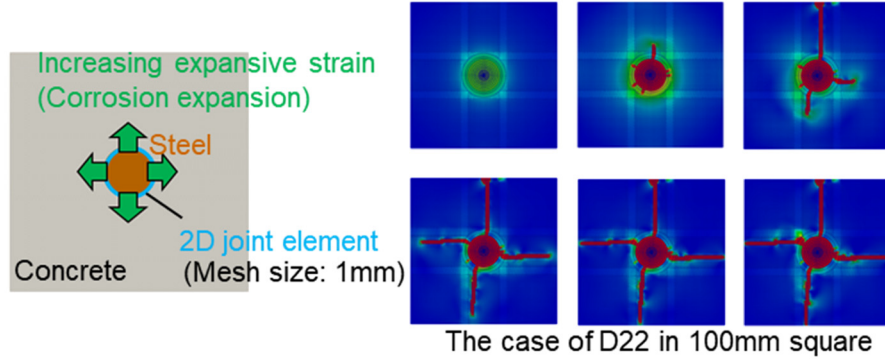
The proposal model has good agreement with experimental results while conventional model overestimated stiffness reduction because the influence degree of  $G_c$  is greatly lower compared with  $G_{crk}$  due to high difference of absolute value.

### 3.4.3 Determination method of cracked area ratio to uncracked area in a finite element

For practical application new shear stiffness model for corrosion crack,  $k$  had to be defined by corrosion ratio. Crack elongation and cracked area might be influenced by mesh size and rebar diameter because concrete area in a mesh can be given from these two factors. For investigation on crack elongation with corrosion expansion process, analysis tracking crack elongation induced by forced expansion of inside steel with very fine mesh size, 1mm as shown in **Figure 3.22**. This analysis did not use the conventional corrosion model but just induced expansion strain into center steel element. 5 micro of expansion strain was induced per a step and monotonously increased for 600 steps, thus 3000 micro of expansive strain was applied finally. Total 8 cases were set, D10 and D22 of rebar



**Figure 3.21** Experimental results and proposal of new shear stiffness model



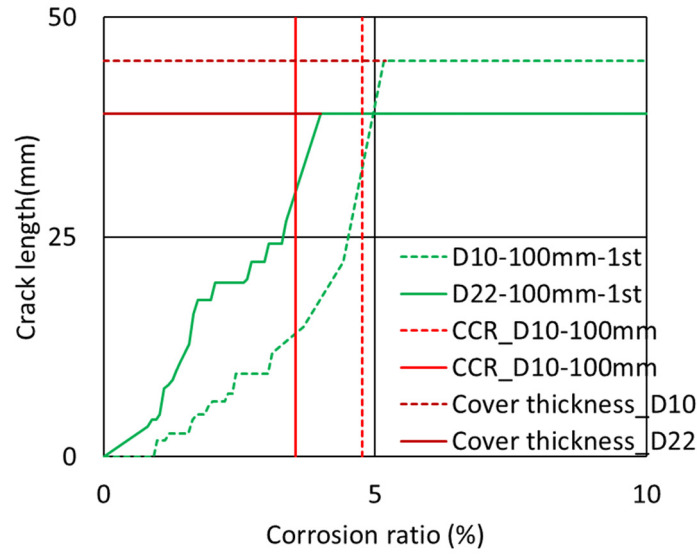
**Figure 3.22** Analytical tracking of crack elongation due to steel expansion

diameter, and 50mm, 100mm, 200mm of one side length, and square of 200mm of one side length with confinement of displacement in each edge for orthogonal direction. Edge confined cases reproduced infinite mesh size. Two dimensional joint element was applied between steel and concrete element. Joint element was necessary because perfect rigid connection was reproduced and crack opening was suppressed strongly when joint element was not placed. Joint element had large stiffness in closure direction and extremely small stiffness for open direction for normal direction, and Shear resistance were zero considering the situation corrosion product was produced around mother steel. To avoid the effect of body motion of mesh, displacement in center node of rebar was restricted.

Crack elongation was judged by tensile strain in gauss points. When tensile strain exceeded 0.0002, the point was judged as cracked. Where, it was required to define relationship forced expansion strain and corrosion ratio. Because elastic modulus of corrosion gel was greatly smaller than that of steel, equivalent corrosion ratio was need to be conversed by the ratio of elastic modulus of steel to that of corrosion gel as shown in **Equation 3.9**.

$$R_{cor} = 100 \frac{E_s}{E_{cr}} \gamma(\%), \gamma = \frac{\varepsilon_{expd}}{(\alpha - 1)} \quad (3.9)$$

Where,  $R_{cor}$ : equivalent corrosion ratio,  $E_s, E_{cr}$ : Elastic modulus of steel (200 GPa) and corrosion product,  $\gamma$ : section loss ratio,  $\varepsilon_{expd}$ : Forced expansion in steel element,  $\alpha$ : Expansion ratio of corrosion product.  $E_{cr}$  and  $\alpha$  is widely different by environmental condition such as oxygen or water content. The value of  $E_{cr}$  has been reported 0.02GPa, 2-4GPa, or 14GPa as maximum value. [23, 24].  $\alpha$  in actual environmental is assumed as 2-4, and this study fixed  $\alpha$  to 2.5 [25, 26].  $E_{cr}$  has wide range and it is difficult to determine and varied with corrosion process. However, exact value depends on mainly environmental condition, thus structural analysis cannot consider that. In this study,  $E_{cr}$  was treated as fixed value and it is determined by expansion strain at crack reaching to concrete surface and CCR. **Figure 3.23** shows  $E_{cr}$  determine. At first, CCR point in this analysis was defined



**Fig. 3.23** Determine of  $E_{cr}$

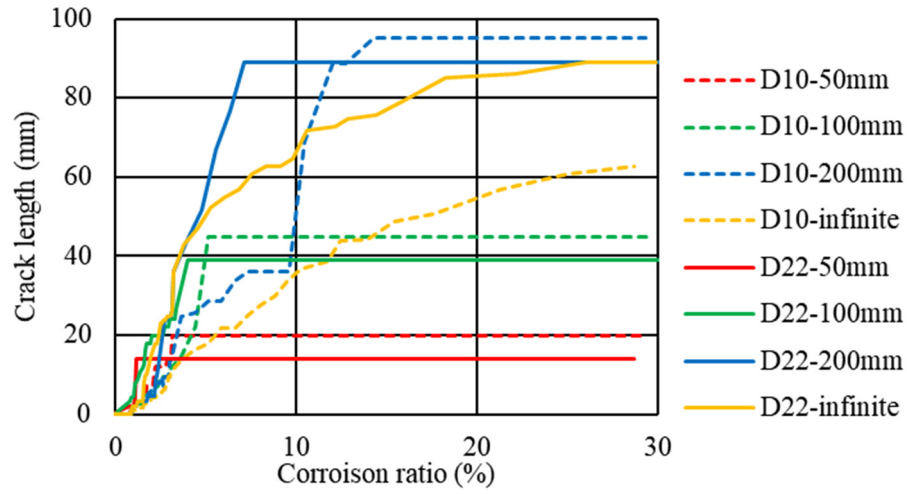
as reach of fastest crack to concrete surface.  $E_{cr}$  was determined by fitting of CCR in analytical result with calculated CCR by cover thickness.  $E_{cr}$  can also change depending on confine by concrete, thus difference of mesh size has effects of  $E_{cr}$ , strictly speaking. In this study  $E_{cr}$  was defined base on the cases with 100mm of on side length, which have almost same cover thickness as actual structures. As a result, 4GPa is defined as  $E_{cr}$ , and this value has agreement with previous researches focusing on corrosion crack elongation before surface crack occurred.

**Figure 3.24** and **Figure 3.25** shows crack length of 1st and 2nd elongation. In the edge-restricted cases, crack elongation is almost linear, and initial elongation of other cases are also linear. However, crack tip became closer to concrete surface, crack elongation speed became higher because confinement against crack opening is low. Looking at 2nd clack behavior, elongation speed became slow after 1st crack reached the concrete surface because penetrated to one side can easily open. Finally, the both 1st and 2nd crack, 6 cases except for restricted case, reached concrete surface. **Figure 3.26** shows the ratio of cracked to concrete area except for steel element of each case. Cracked area was given summation of 1st and 2nd crack length.

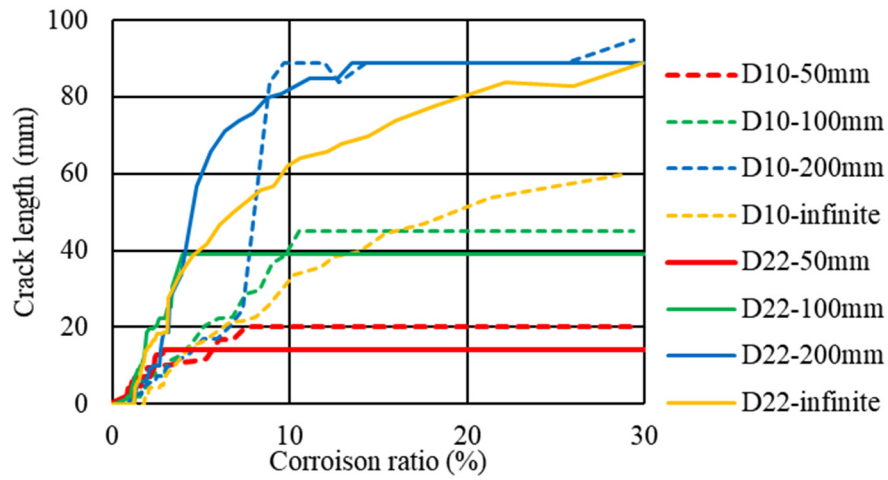
**Equation 3.10** was proposed as function  $k$  based on crack elongation tracking analysis. Crack elongation was linear in first stage and accelerated with closing to concrete surface, thus the author defined  $k$  as quadratic function of corrosion ratio, and the ratio of rebar diameter to mesh size which means concrete area in a element was used as primary coefficient.

$$k = \frac{L_{cr} + D}{l_r}, L_{cr} = \alpha \left( \frac{D}{l_r} \right) (R_{cor})^2 \quad (3.10)$$

Where,  $L_{cr}$ : mesh size(mm),  $D$ : rebar diameter(mm),  $L_{cr}$ : crack length,  $R_{cor}$ : corrosion ratio (%),  $\alpha$ :



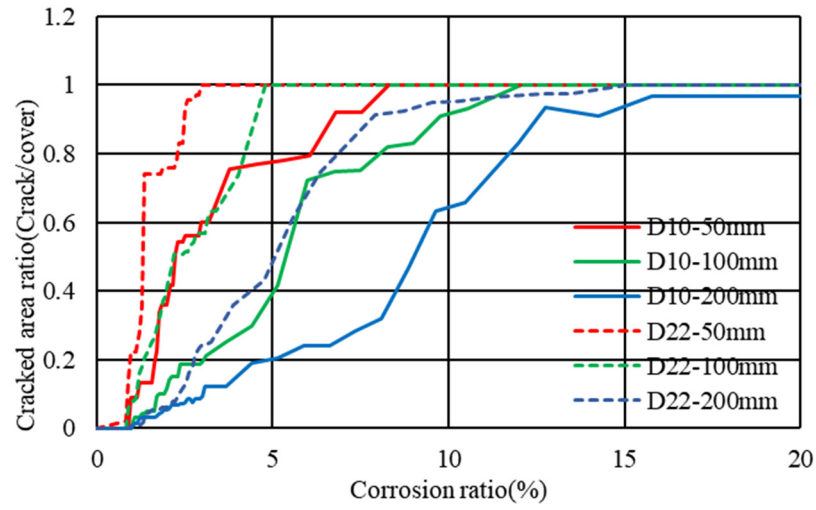
**Fig. 3.24** Crack elongation of 1st crack



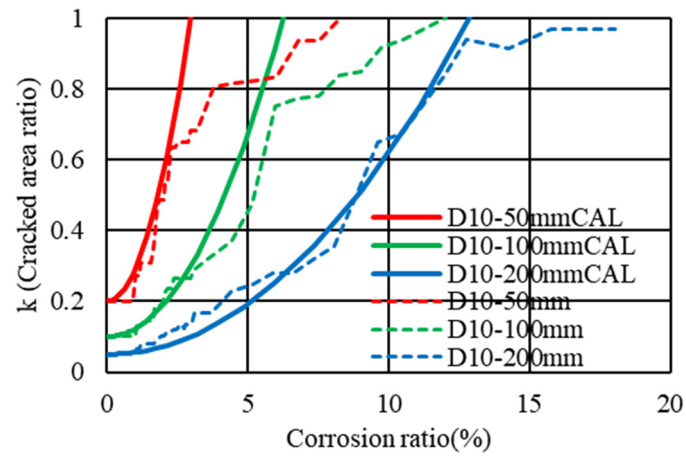
**Fig. 3.25** Crack elongation of 2nd crack

constant coefficient 15.

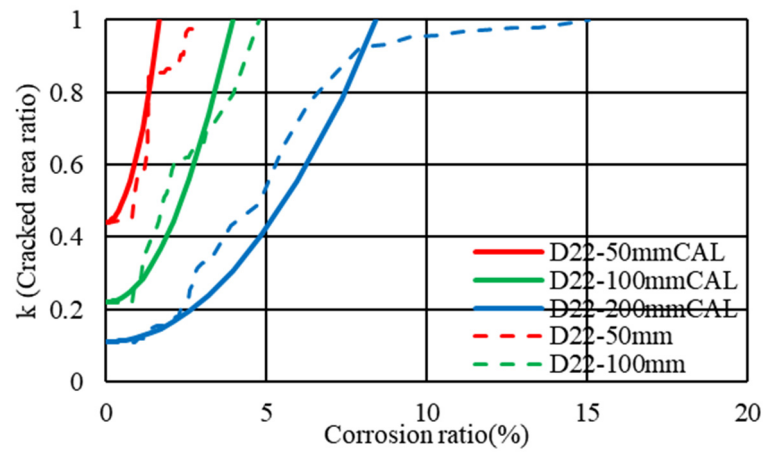
Comparison of proposed  $k$  with experimental cracked area ratio was showed in **Figure 3.27** and **Figure 3.28**. Noted that rebar was treated as crack surface because chemical adhesion was lost immediately after rebar corrosion started, and rebar diameter in practical use can be deemed as a part of roughness of crack surface. Thus, cracked area was defined even in 0% of corrosion ratio by rebar in this graph. Here, proposed  $k$  had good agreement with experimental results, while reduction of 2nd crack elongation speed cannot reproduce especially in the case  $D/L_r$  was high. However, it was safe side evaluation from the view point s of shear stiffness reduction. Analytical expansion neglected the decreasing of  $E_{cr}$  due to change from gel behavior to liquid behavior due to water ingress from



**Fig. 3.26** cracked area ratio per cover thickness



**Figure 3.27** Comparison of proposed  $k$  with experimental cracked area ratio(D10)



**Figure 3.28** Comparison of proposed  $k$  with experimental cracked area ratio(D22)

surface reached crack, or absorption of  $E_{cr}$  into opening crack in elongation stage.

For more precise tracking of corrosion elongation, these effects should be taken into account. Noted that  $L_{cr}$  in the **Equation 3.10** was defined to fit the analytical results with extreme fine mesh and experiments in previous researches for tracking corrosion crack progress. Thus, it was required to verify the accuracy of the crack elongation model into various conditions such as multiple rebars, various rebar diameters, different corrosion speed, bended rebar, or larger concrete block for expanding the applicable range while property of concrete did not have large effects on corrosion crack elongation in the previous research [22]. In the sequence, such as the number of rebar or concrete length in a block might be required to be implemented into the model.

### 3.5 Development of shear transfer model after crack penetration

According to **Figure 3.17**, which was comparison with fine and large mesh size in corrosion expansion model, shear stiffness of large mesh is lower than that of fine mesh. This section focuses on the shear transfer model after crack penetration and suggests modification model. The author considered two deviations between actual phenomena and analytical model as the reason; unevenness of crack surface and angle in a large element, and crack width limitation due to discharge of corrosion gel.

#### 3.5.1 Equivalent crack width model considering nonuniformity of crack

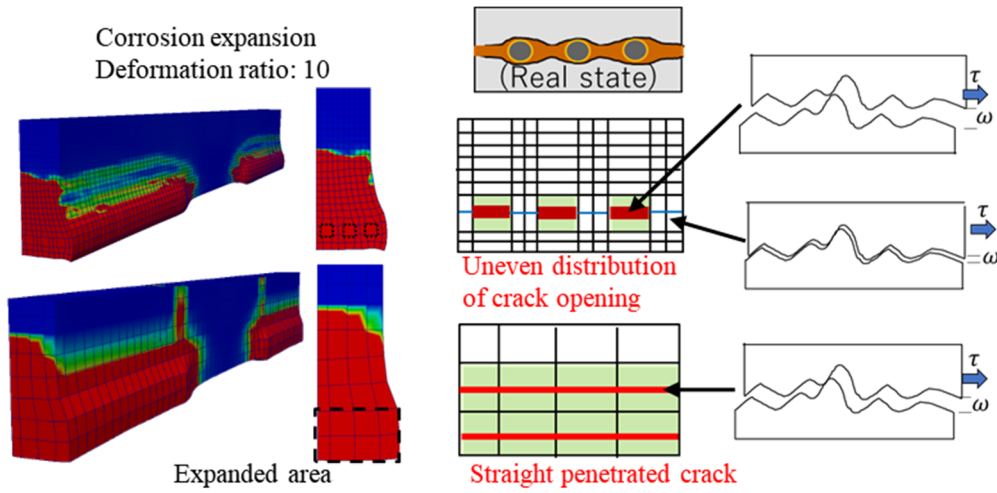
Crack induced by corrosion expansion was averaged straightly in a element. Especially in the case of rough mesh, unevenness in cross section and axial direction of member cannot be neglected. When corrosion crack occurs, crack width should have distributed in cross section of member. Fine mesh model may be able to reproduce but rough mesh cannot because averaged expansive strain is applied in entire RC zone of member as shown in **Figure. 3.29**. In this condition, closed point has greatly high shear stiffness especially in the case that contact is recovered. and that in opened point is low. According to shear stiffness model based on contact density function described in **Equation 3.2**, crack width and shear stiffness is not linear, thus averaged crack width has lower stiffness than uneven opening state. When unevenness in axial direction is focused on, uneven crack angle should have high stiffness due to interlock between crack shape. Contact density function was based on the roughness of the crack surface in small region that is able to be assumed straight crack. Rough mesh includes and can not neglect the crack shape, but shear stiffness based on the contact density between straight crack



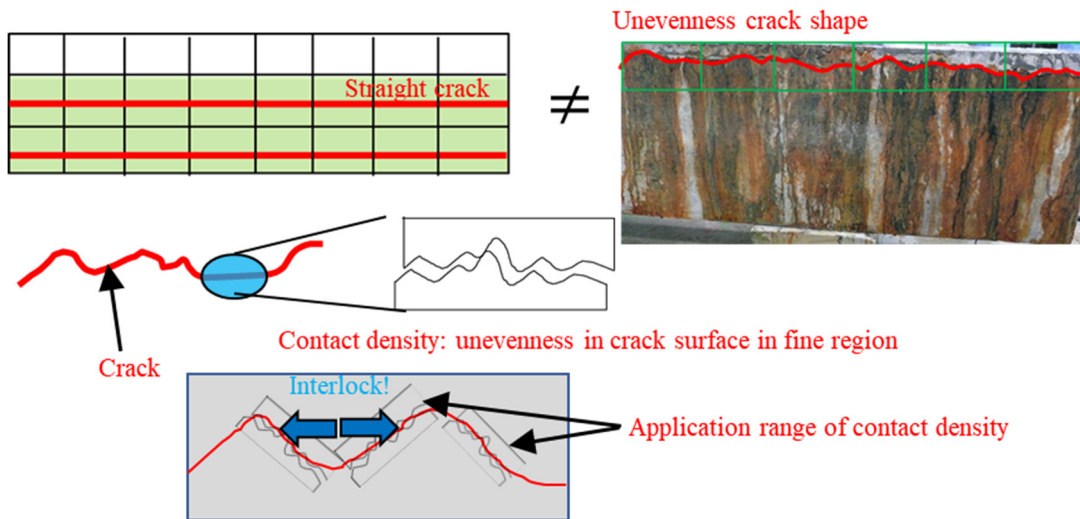
along input rebar ratio is applied as shown in **Figure 3.30**. Concept of equivalent crack width for unevenness of crack is shown in **Figure 3.31**. The distribution of corrosion crack width is not considered and crack width caused by expansion strain calculated from input value is applied in large mesh. However actual corrosion crack has various crack width and minimum width  $w_{min}$  is assumed as the half value of maximum crack width as shown in **Equation 3.11**.

$$w_{min} = 0.5w_{max} \quad (3.11)$$

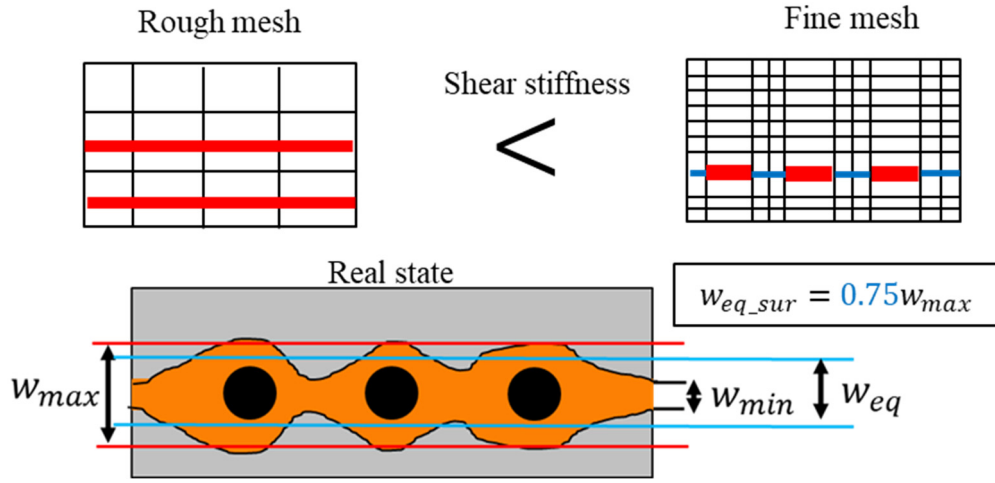
$w_{eq\_suf}$  is considered as average crack width along crack surface. Strictly speaking, integral of crack width in the all surface should be defined as should be described as  $w_{eq\_suf}$ . However, this study



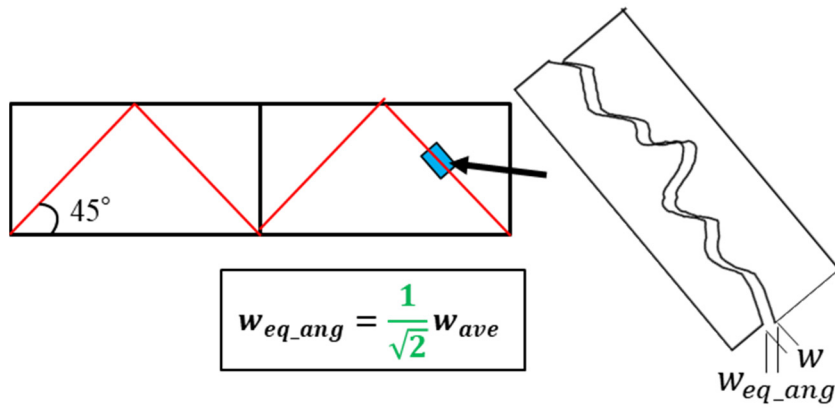
**Fig. 3.29** Reproduction of unevenness of crack surface



**Fig. 3.30** Reproduction of unevenness of crack surface



**Fig. 3.31** Scheme of equivalent crack width for unevenness crack surface



**Fig. 3.32** Scheme of equivalent crack width for unevenness crack angle

assumed various crack unevenness can be described from averaged value of maximum and minimum crack width, and equivalent crack width in this study is shown in **Equation 3.12**.

$$w_{eq\_suf} = \frac{1}{2}(w_{max} + w_{min}) = 0.75w_{max} \quad (3.12)$$

Concept of equivalent crack width considering the unevenness of crack angle in rough mesh is shown in **Figure 3.32**. In this study, simply 45 degree of crack angle is assumed and projected crack width  $w_{eq\_ang}$  can be given in **Equation. 3.13**.

$$w_{eq\_ang} = \frac{1}{\sqrt{2}} w \quad (3.13)$$

Therefore, unevenness by crack surface and crack angel is integrated and equivalent crack width  $w_{eq}$  can be given in **Equation 3.14**.

$$w_{eq} = \frac{0.75}{\sqrt{2}} w = w_{eq\_suf} \times w_{eq\_ang} \quad (3.14)$$

For direct representation of unevenness, inducing of equivalent crack width  $w_{eq}$  is suit as shown in **Equation 3.14** below, but according to the investigation in previous section, corrosion ratio and crack width are linear relationship in large mesh size, thus authors applied this consideration as corrosion ratio because  $R_{cor}$  can be common input parameter in this chapter. Thus, the author suggests equivalent corrosion ratio described in **Equation 3.15**.

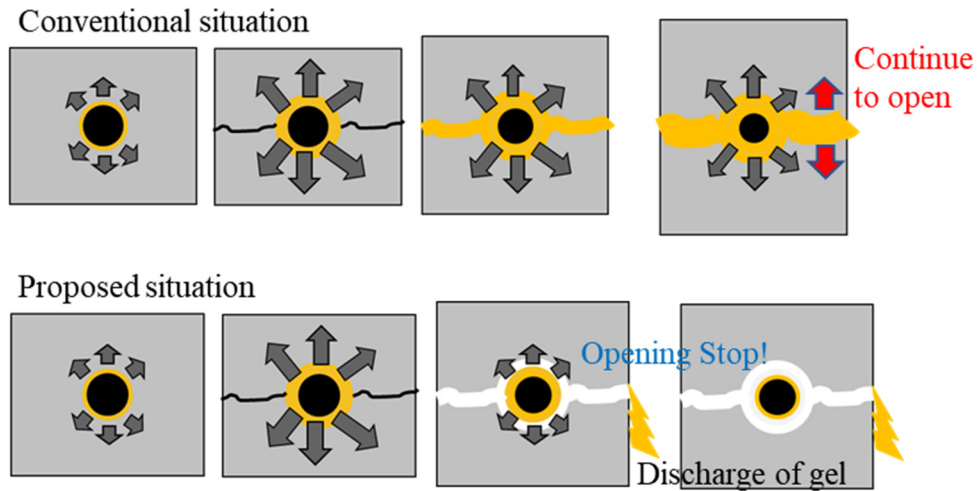
$$R_{cor\_eq} = \frac{0.75}{\sqrt{2}} R_{cor} \quad (3.15)$$

Where,  $R_{cor\_eq}$ : equivalent corrosion ratio (%),  $R_{cor}$ : actual corrosion ratio (%).

### 3.5.2 Crack width model considering crack opening limit

According to shear loading analysis by conventional corrosion model, shear stiffness continued to decrease with corrosion ratio increasing even after corrosion ratio exceeded 10%. In general, discharge of corrosion gel occurs from surface reached crack, whose width is more than 0.3mm. Thus, corrosion product does not hold in cracks, but leak from cracks on concrete surface. In this state, expansion strain generation due to corrosion product should be stopped and expansive stress can release as shown in **Figure 3.33**. While opened crack cannot be closed because corrosion crack propagation can be deemed to be plastic deformation, crack width should be converged. In other word, crack width by corrosion expansion has limit.

In order to implement the crack width limit, named as discharge limit, the author referred the critical corrosion ratio, CCR [22]. According to the paper for development of CCR, concrete surface strain at CCR is 125-130 micro. While CCR shows the crack reaching to concrete surface, discharge of



**Fig. 3.33** Comparison of analytical result with experimental results

corrosion gel does not start immediately because crack width is too small to cause leak of gel, not liquid. The author set discharge limit as almost 2 times higher value than CCR, 250 micro by **Equation 3.16**.

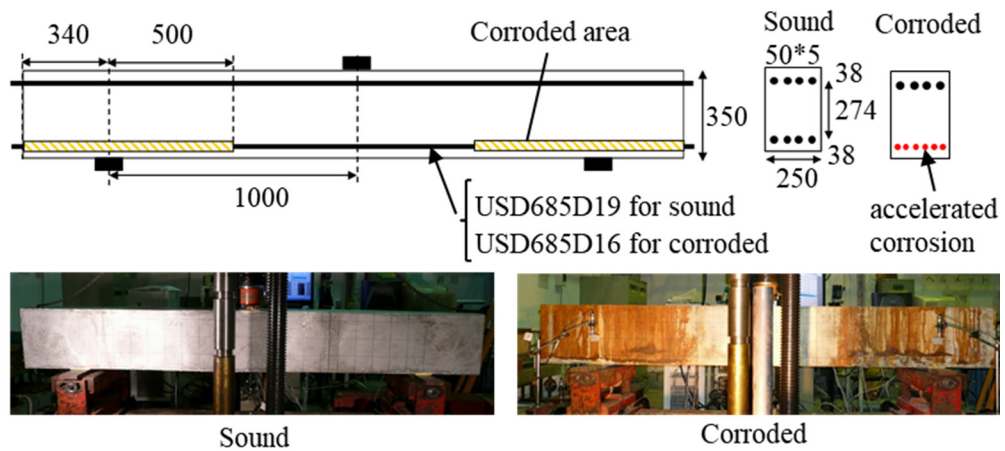
$$L_d(\%) = 2.0CCR, CCR(\%) = 0.0018c^{2.07} \quad (3.16)$$

Where,  $L_d$ : discharge limit,  $CCR$ : critical corrosion ratio,  $c$ : cover thickness (mm). Strain discharge limit (250 micro) is the close point that surface strain increases rapidly in previous researches [22]. This strain increasing means rapid crack opening, which is seemed to be allow gel leak, therefore this value was set as discharge limit.

### 3.6 Structural behavior change by proposed shear transfer model on a RC member

#### 3.6.1 The target member and outline of static loading test

In order to understand the influence of overestimation of shear stiffness on structural behavior of member, reproduction analysis for beam loading test with rebar corrosion in previous research was conducted. Chijiwa et al. conducted static loading test on the beam with rebar corrosion and compared with sound behavior. **Fig. 3.34** shows experimental setup [27]. The RC beam has 1000mm of shear span, 350mm of height, and 250mm of width. For achieving shear failure, high strength rebar (USD685) was used as main rebar and 4 rebars of D19 and 6 rebars of D16 were used for sound and corroded specimen, respectively. Rebar ratios were almost same between 2 specimens and increase of the number of rebars in corroded beam aimed to emphasize corrosion crack effect. Accelerated corrosion was conducted for 837 hours with 1.5A of constant current, resulting 254mg/cm<sup>2</sup> of corrosion mass loss. Electrical circuit for accelerated corrosion test was produced by saline pool by mortal on reversing of beam and stainless mesh connected to rebar. Compressive strength and tensile strength of concrete was 48.0MPa and 3.64MPa for corroded specimen, and 34.7MPa and 2.70MPa



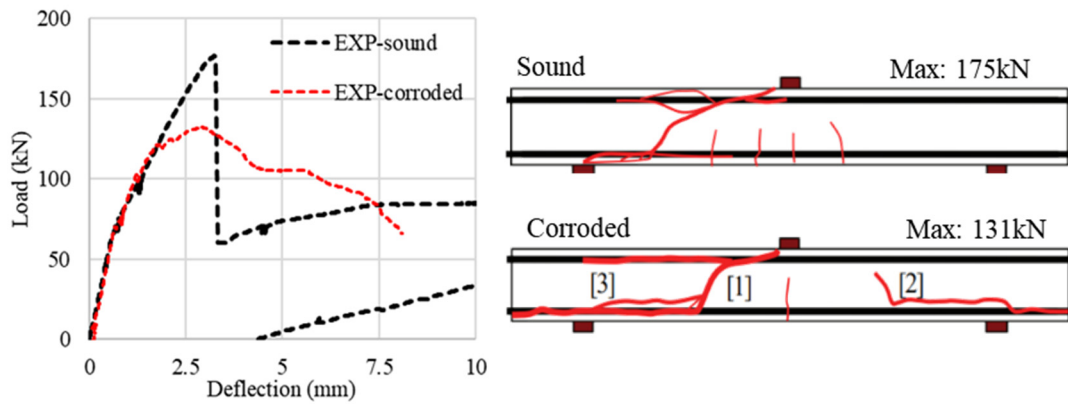
**Figure 3.34** Experimental setup (Chijiwa *et al.* [27])

for sound specimen.

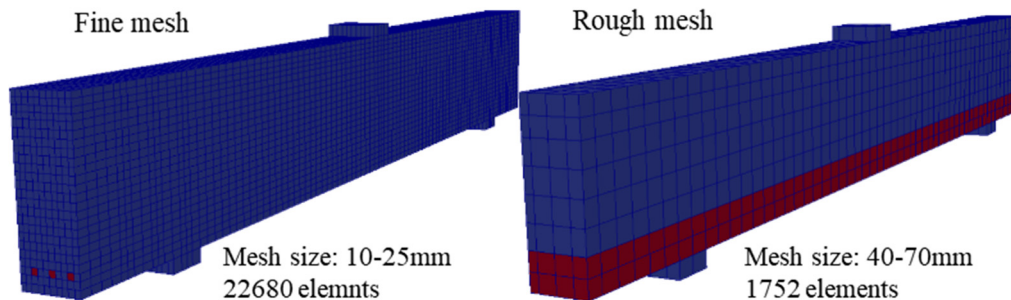
Load-Deflection curve and crack pattern in the experiment are summarized in **Figure 3.35**. Ultimate load is 175 kN and 131 kN for sound and corroded specimen, respectively. Maximum load of corroded beam reduced to 75% of that of sound specimen, and dominant damage for failure is crack along compression rebar rather than shear crack. Shear slip along corrosion crack did not be observed. Shear crack angle of corroded specimen was larger than sound one and shear crack origin was influenced by corrosion crack end, which was assumed to be caused by arch mechanism in corroded specimen.

### 3.6.2 Reproduction FE analysis by the conventional corrosion crack induction model

Reproduction analysis model is shown in **Figure 3.36**. Considering the symmetry of geometry, half model in beam width was produced. In order to catch the effects of mesh size, 2 models were produced. In fine mesh, rebar ratio was concentrated in the mesh in same location and surround concrete elements did not have rebar ratio. Thus, expansion force from inside can be reproduced. Based on the investigations in Chapter 2, rebar concentrated element and surrounded element were fixed with sharing the nodes. Rough mesh applied smeared rebar ratio in RC zone, and the entire of this area expanded in corroded analysis.

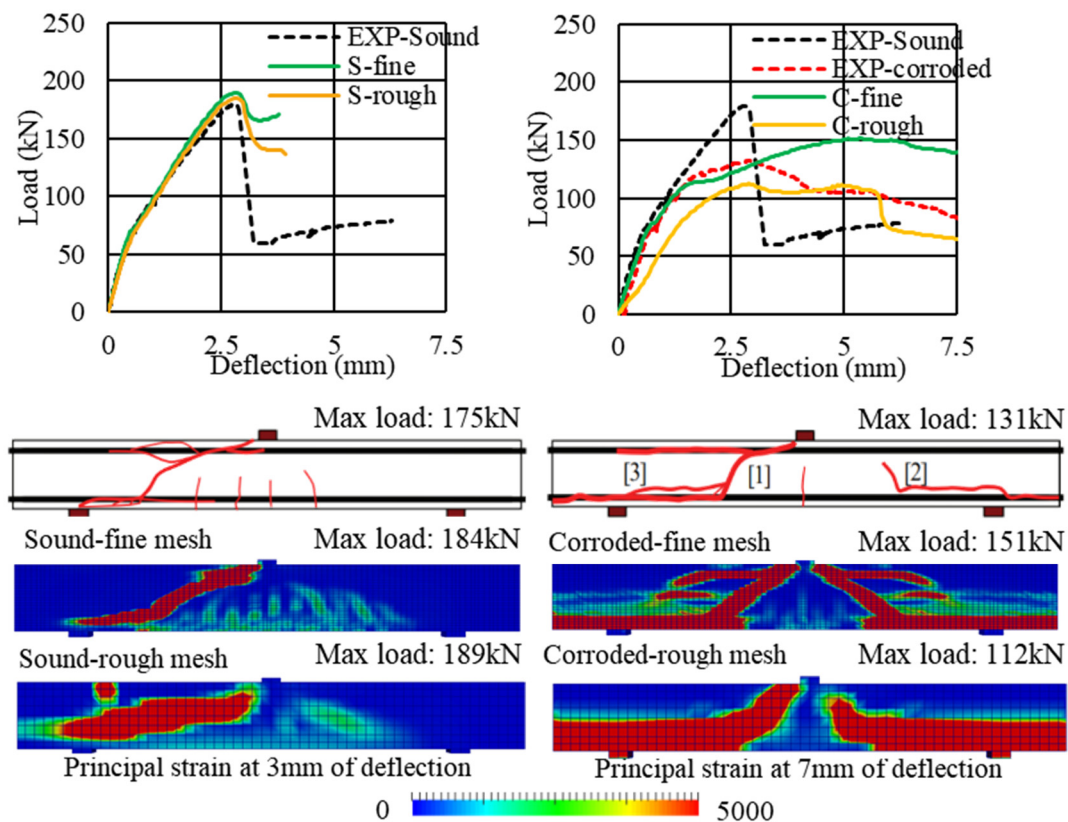


**Figure 3.35** Experimental results (Chijiwa *et al.* [27])



**Figure 3.36** Reproduction analysis model

Comparison of analytical results with experimental results are shown in **Figure 3.37**. In the sound case, FE analysis succeeded to reproduced the structural behavior in static loading test well in load-displacement relationship and crack pattern. While post-peak behavior was varied between the experiment and the analysis with different mesh size, failure mode of all the cases were sharp load drop by shear crack formation. Maximum load in the experiment, analysis with fine mesh, and with rough were 179kN, 180kN, and 175kN, respectively while calculated shear strength based on JSCE code was 154kN, thus variation in the maximum load was in the range of 5%. In the corroded case, there are clear difference by mesh size. Fine mesh model can reproduce the experimental results in the initial stiffness, stiffness with flexural crack, and sharp deflection increasing at 120 kN of applied load. In the experiment, deflection increasing was caused by shear crack formation, then load was dropped with formation of crack along compression rebar. Shear crack and crack along the compression bar was reproduced in the analysis case with fine mesh as shown in the strain distribution, but post-peak behavior differed from experimental results. This deviation between analytical results and experiment was caused by sudden shear crack formation in the compression field although change of crack angle due to corrosion crack could be reproduced well. Analysis with smeared crack model reproduced cracks as stiffness reduction of finite element and complete separation could not be reproduced directly,



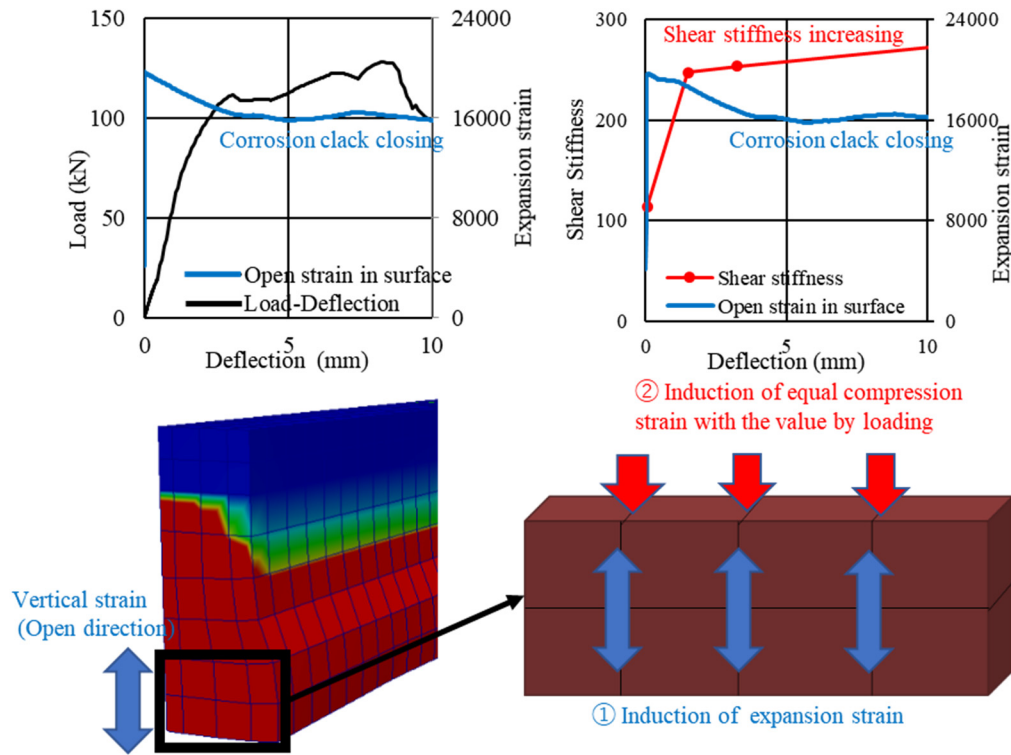
**Figure 3.37** Comparison of analytical result with experimental results

thus sharp reduction of tension resistance should be assumed. However, tension stiffening was considered due to compression rebar in this analytical model, and fluent deflection increasing was observed. It was also supported by deviation of post-peak behavior only in the corroded case. Shear crack in this case was propagated from the edge of corrosion crack and crack angle to beam axis was larger than sound case. Therefore, shear crack was almost orthogonal direction to compression rebar which was assumed as distributed rebar and tension stiffening in this analytical model. As a results resistance against shear crack opening was considered to be high only in the corroded case analysis. When focusing on the analytical behavior in corroded case, member stiffness was lower than experimental value from initial stage to failure even while fine mesh can reproduce the experimental results. Totally, FE analysis except rough mesh model with rebar corrosion can track the structural behavior well while post-peak behavior has difference due to spoiling or dynamic crack propagation which cannot be reproduced in FE analysis. Therefore, it is confirmed that conventional corrosion model in the case applying rough mesh overestimated the stiffness reduction between corrosion crack. Focusing on the point of 40 kN of applied in load load-displacement curve of corroded beam with rough mesh, initial stiffness was recovered. It was because that compression stress in vertical direction closed the corrosion crack along main rebar, then high shear stiffness can be applied in the elements. It is one of the proofs that shear stiffness reduction was higher than assumption in model development. In order to confirm the crack closing effects, the author conducted the sensitivity analysis as shown in **Figure 3.38**. First, vertical strain in expanded area by corrosion expansion in beam loading analysis was picked up, and crack closing behavior with increasing of applied load was confirmed. For getting shear stiffness in this region, the author produced the analytical model simulating only expanded area. Equal compression strain with the value induced by loading was applied after induction of same corrosion expansion, then shear stiffness for axial direction of beam was got from pure shear loading. **Figure 3.38** clearly shows the shear stiffness increase of expanded area by loading.

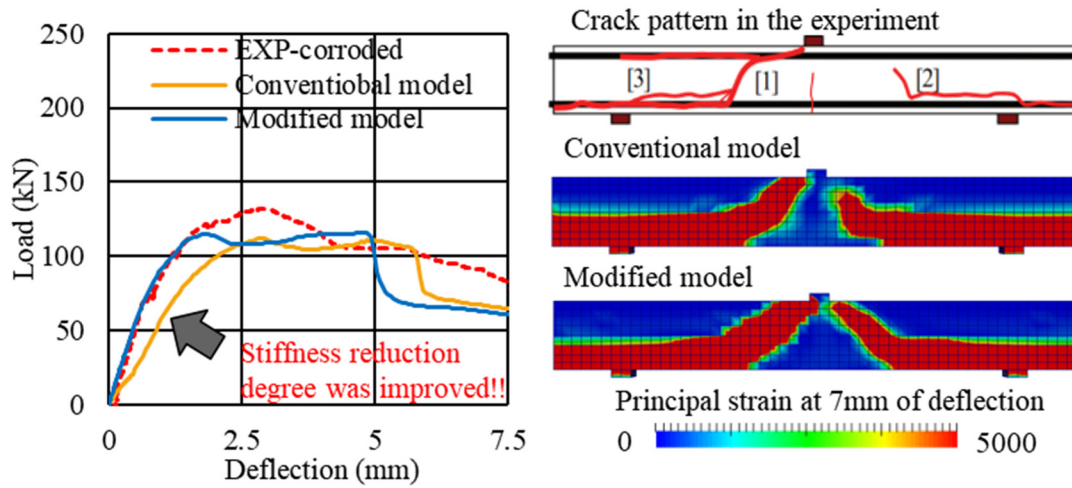
### 3.6.3 Application of the proposed model considering the discharge limit

According to the development of corrosion model in section 3.6, the author conducted reproduction analysis for static loading test on corrode beam conducted in previous section. Analysis model was same, but equivalent corrosion ratio and discharge limit were set newly. Corrosion ratio by electrical accelerated corrosion was 8.06% and this value exceeded discharge limit proposed in section 3.5. Discharge of corrosion product was also confirmed visually as shown in **Figure 3.32**. Thus, smaller crack width than conventional analytical model was applied at discharge limit. Analytical result is shown in **Figure 3.39**. Deviation in stiffness reduction by overestimation of crack width can be improved and analysis with rebar corrosion by new model had good agreement with experimental results. Equivalent corrosion model had enough accuracy for large mesh analysis with 70mm of mesh size in high corrosion ratio, exceeding discharge limit.





**Figure 3.38** Investigation on crack closing effects in loading

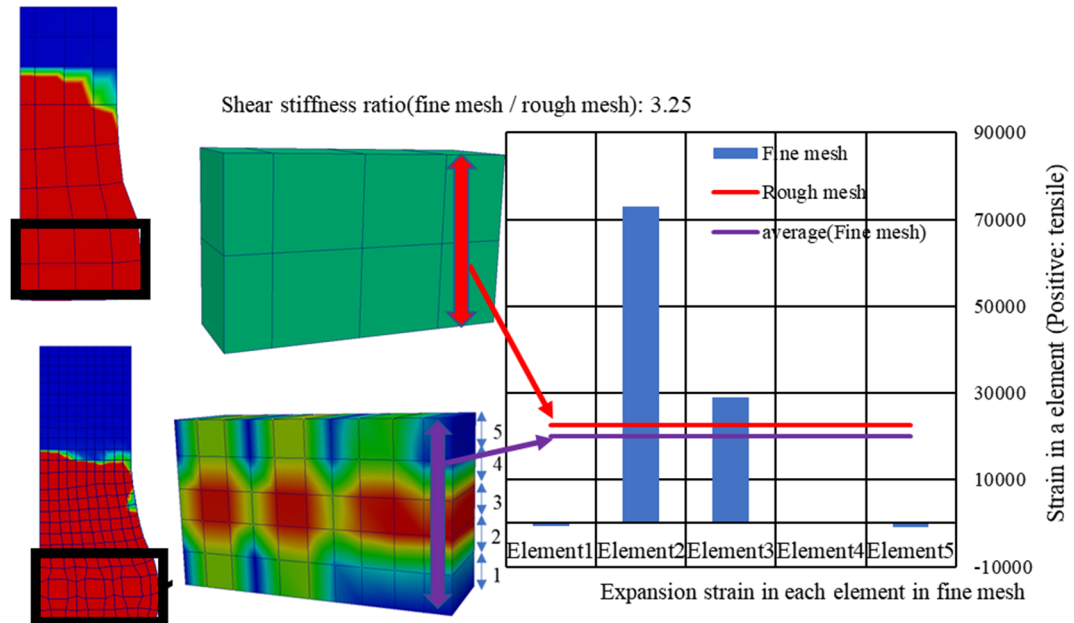


**Figure 3.39** Comparison of analytical result with experimental results

### 3.6.4 The influence of equivalent crack width model on shear transfer

The author conducted parametric analysis for corrosion ratio base on corroded beam. The analytical model simulating only expanded area in the both fine mesh and rough mesh size. **Figure 3.40** shows the analytical model and comparison of crack opening behavior in fine and rough mesh.



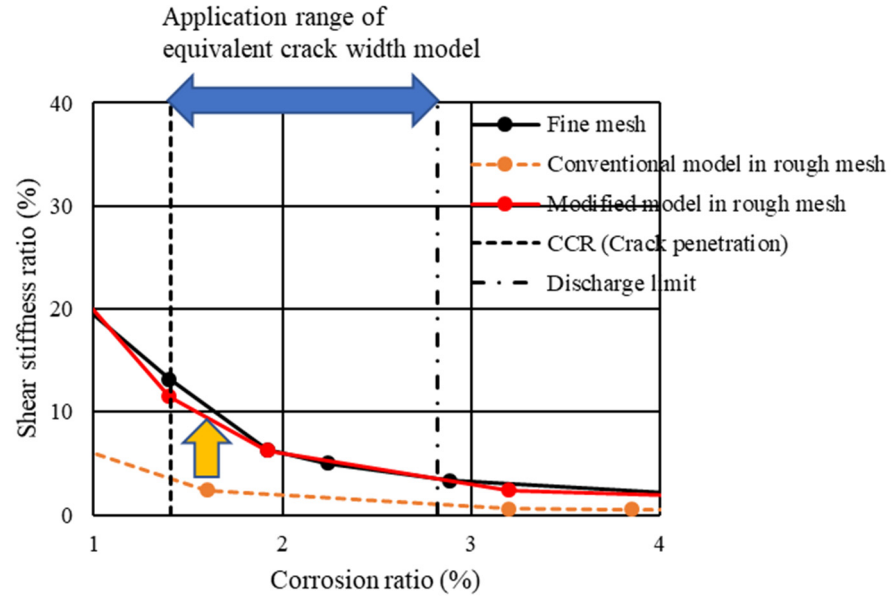


**Figure 3.40** Crack opening behavior difference in fine mesh and rough mesh

Both models showed average strain value by corrosion expansion, but each element in fine mesh model has high variation in strain. According to former investigation focusing on shear stiffness of a element with expansion strain, shear stiffness rapidly decreased at higher strain than cracking, 200 micro. Looking at strain distribution in normal direction to beam axis, uneven strain distribution was reproduced as assumption in the **section 3.5.1**. Thus, fine mesh model had 3.25 times higher value of shear stiffness than rough mesh model. The author applied shear loading with various corrosion ratio in the both fine mesh and rough mesh, and two crack width model, conventional and proposed equivalent crack width model in rough mesh. Here, comparison of initial shear stiffness by proposed equivalent crack width model and fine mesh is shown in **Figure 3.41**. By applying equivalent crack width model, shear stiffness in expanded region became close value to that from fine mesh analysis, which could reproduce the assumed situation of uneven crack width distribution, in the application range of equivalent crack width model.

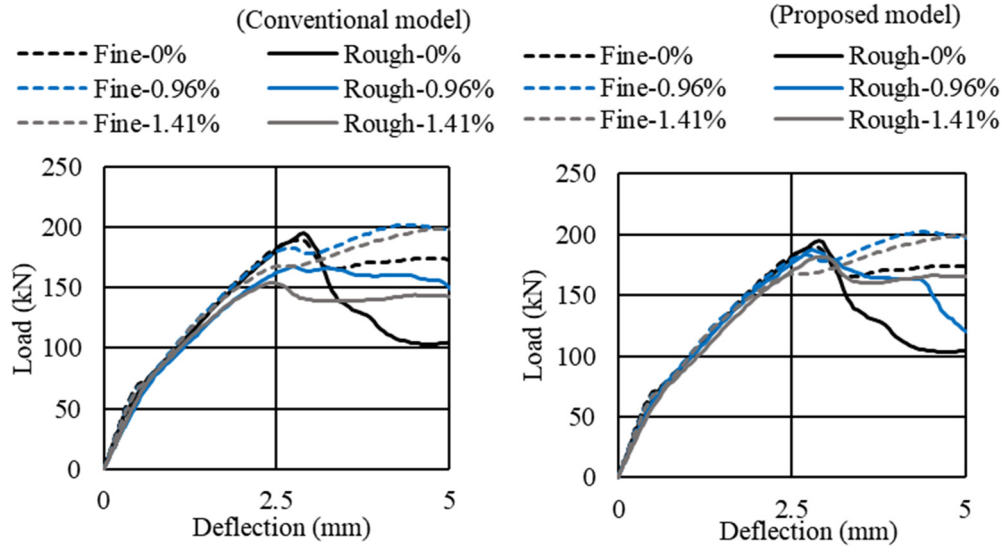
### 3.6.5 Structural behavior change with corrosion progress

In order to investigate the influence of the proposed model on the structural performance of a member, analysis on static loading for a beam was performed. The target beam was shown in **Figure 3.34**, and two FE analytical models were produced by the both rough and fine mesh size as shown in **Figure 3.36**. Corrosion ratio was set as the parameter, and total 48 cases (16 degrees of corrosion ratios from 0% to 18.2% for 3 models, fine mesh, rough mesh with the conventional model, and rough mesh with the proposed model) were analyzed. Corrosion ratio was set 6 degrees for stage 1 including sound state without rebar corrosion, 4 degrees for stage 2, and 6 degrees for stage 3 including the

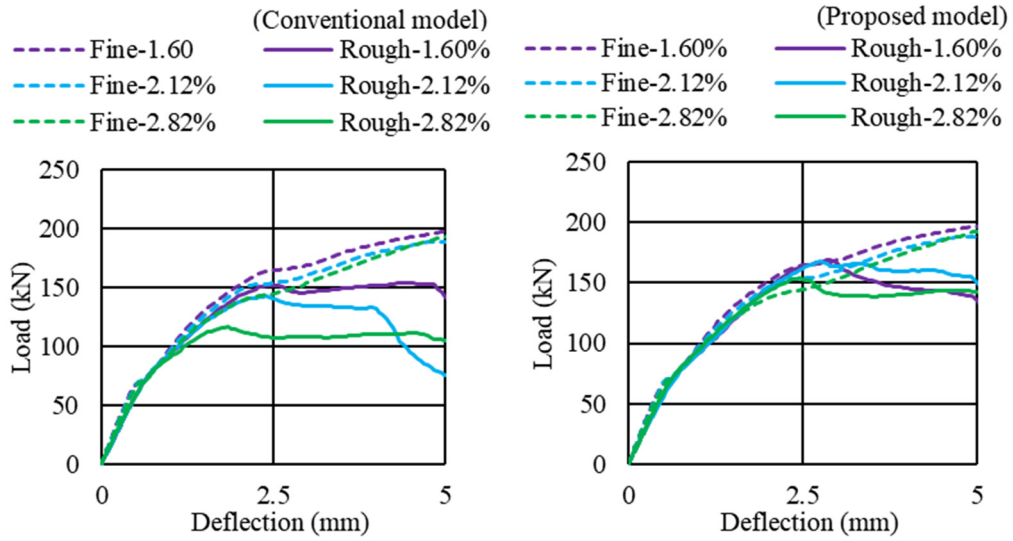


**Figure 3.41** Improvement of shear stiffness by equivalent crack width model

reproduction of experimental situation performed in section 3.6.3. According to the rebar arrangement shown in **Figure 3.34**, CCR (Critical Corrosion Ratio) which showed the corrosion ratio at crack penetration was 1.41%, thus discharge limit proposed in this chapter was 2.82% according to the proposal in section 3.5.2. **Figure 3.42**, **Figure 3.43**, and **figure 3.44** shows the comparison between analytical results with fine and rough mesh in load-displacement curves focusing on the stage 1, stage 2, and stage 3, respectively. In the all Figures, left side graph shows the comparison between the result by fine mesh model and that by rough mesh with conventional model, and right side one compares fine mesh model with proposed model in rough mesh size. Noted that discharge limit proposed in section 3.5.2 was also applied in the model with fine mesh because limit of expansive strain was common phenomena without the dependence on mesh size. Bond deterioration was not considered in all cases according to the investigation in Chapter 2 because corrosion ratio kept less than 20% in this investigation in order to focus on the effects of corrosion crack. When corrosion ratio was exceeded 20%, the effects of low substantial rebar amount or pit corrosion seemed to be significant. Corrosion crack model mainly caused change of the shear transfer degree around rebar, and member stiffness was influenced by shear transfer behavior, thus initial stiffness change with increase of corrosion ratio was summarized and showed in **Figure 3.45**. Initial stiffness was defined as the slope of applied load to deflection until deflection of beam reached 0.2mm, and it was confirmed that principal strain in any finite elements was under 200 micro which was judged as cracked in this FE analytical system.

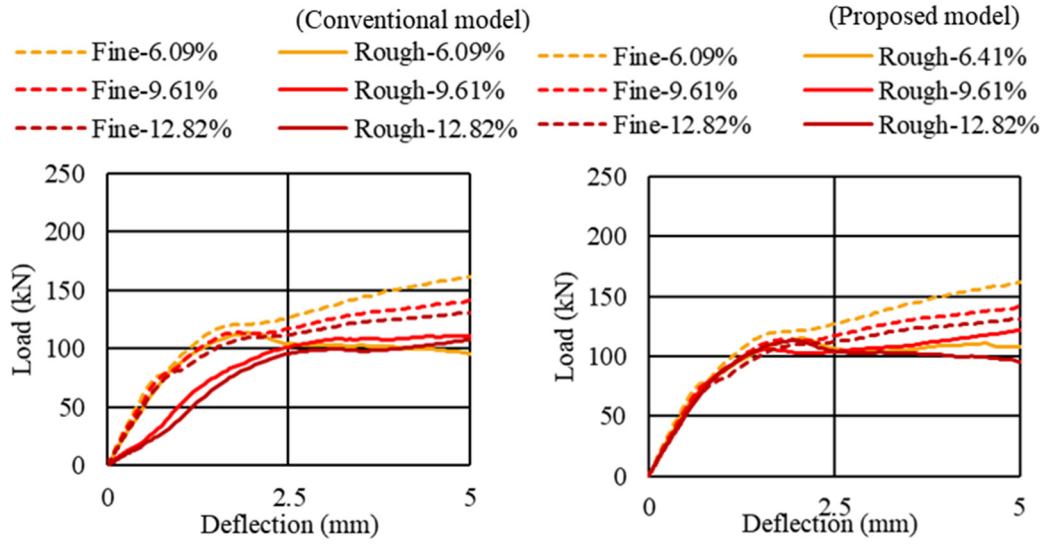


**Figure 3.42** Comparison between conventional and proposed model (Stage 1)

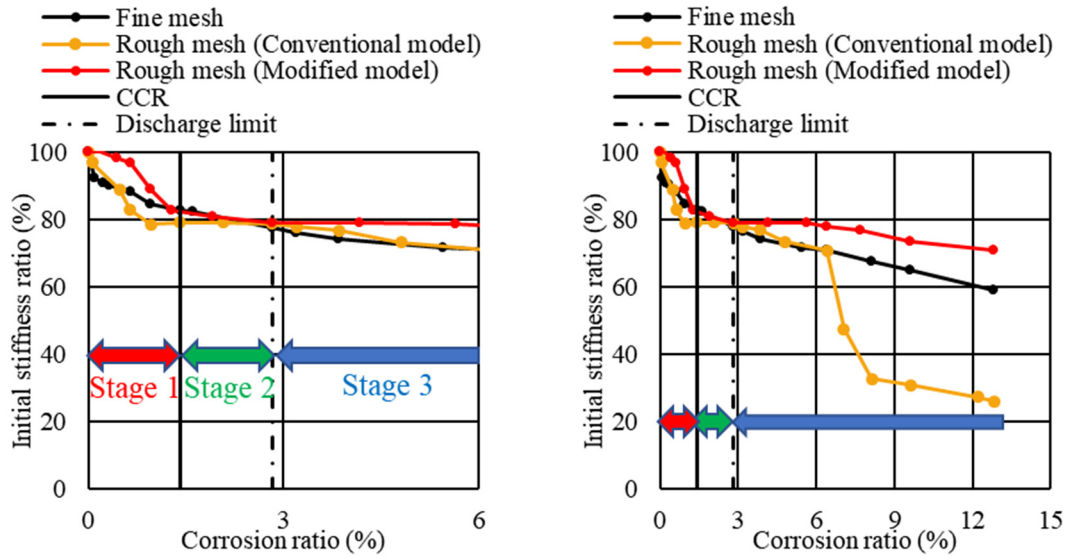


**Figure 3.43** Comparison between conventional and proposed model (Stage 2)

When focusing on the stage 1, load-deflection relationship was not influenced well by corrosion because crack was not penetrated and enough stress transfer for load bearing was maintained. Rough mesh with conventional model overestimated crack elongation and shear transfer with penetration crack was reproduced. Thus, initial stiffness and load capacity was lower than that with fine mesh. Accuracy of analytical results with the proposed model considering non-penetrated condition of corrosion crack was improved. Here, initial stiffness in this stage was larger than fine mesh. Beam model with fine mesh had only 2 elements between rebar and concrete surface, thus crack elongation was also seemed to be overestimated. The initial stiffness of the member was almost same value



**Figure 3.44** Comparison between conventional and proposed model (Stage 3)



**Fig. 3.45** Shear stiffness change due to modified corrosion crack model

between fine mesh and rough mesh with the proposed model at the CCR. In the stage 2, fine mesh model could represent actual crack distribution as discussed in section 3.6.4, thus the author set fine mesh as target structural behavior. The conventional model overestimated reduction of load capacity and member stiffness, and the proposed model can improve the match with the results by fine mesh. Stiffness improvement was also supported from the investigation on the shear stiffness on model applied region shown in **Figure 3.41**. Member stiffness of conventional model in the stage 3 had rapid reduction from 8% of corrosion ratio. It is because that applied expansive strain was exceeded 20000 micro as shown in **Figure 3.40**, then stiffness of a whole rebar distributed region was extremely low.

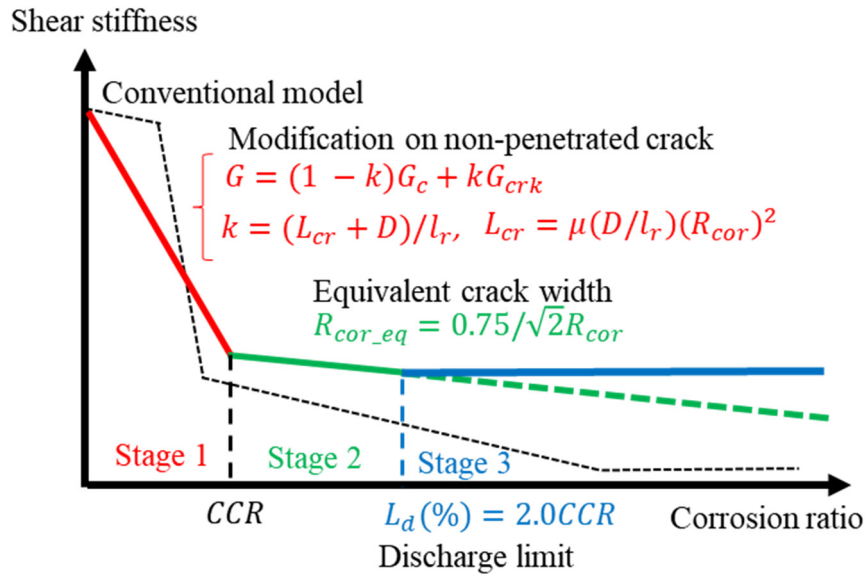
In the stage 3, the accuracy of member stiffness before and after propagation of flexural cracks was improved while ultimate load had been reproduced well because section loss of rebar which had been considered in the both conventional and proposed model was dominant. The proposed discharge limit induced only slight stiffness reduction due to progress of section loss of rebar in the stage 3. Member stiffness reduction behavior with fine mesh considered unlimited expansive strain, thus reduction rate with the proposed model became slighter than that by fine mesh with the conventional expansion model. Through all the stages, post-peak behavior of members had room for improvement of accuracy for reproduction because the ultimate state of shear failure mode had variation such as shear crack propagation region, unbalancing of shear span with or without shear crack, or the influence of compression rebar even in experiments. In the FE analysis conducted in this chapter had a trend that fine mesh model had more resistance against applied load even after shear crack formed while rough mesh model showed drop of load immediately with shear failure especially in the situation with high corrosion ratio causing penetrated crack. It was mainly considered to be caused by damage compression side of the beam, namely, damage was averaged in a element and rough mesh model had 1 or 2 elements for compressed region in the ultimate state. Furthermore, the angle of shear crack to beam axis was large due to corrosion crack in this target beam, thus smeared compression rebar influenced. Shear crack induced local tensile strain in compression side dynamically at failure, thus equivalent tension softening behavior in compression field depending on the mesh size might improve reproduction of actual phenomenon. Modeling method considering these effects required more consideration.

### **3.7 Summary of chapter3**

The goal of this chapter was the development of structural model for corrosion crack. When considering modeling by smeared crack concept, discussion on cracks should be divided by scale, distributed cracks and concentrated crack. Thus, the author focused on not only the development of corrosion crack model but the influences of distributed fine cracks on structural performance and its structural modeling in FE analysis while distributed cracks had affinity with smeared crack model. First, the author conducted the thermo-hygral analysis for the mockup model of RC power plant buildings and the multi-story building, which had been reported that structural stiffness declined with aging. Analysis considering moisture loss by environmental condition could reproduce the stiffness reduction behavior well, thus it is shown that the drying shrinkage of concrete is one of the key factors to predict the structural stiffness of the whole buildings with different dimensions, and the scale of structural members is confirmed to be a critical factor for drying. The author focused on the member scale, and the thermo-hygral analysis was also conducted for the shear wall whose structural performance change caused by drying was tested in the previous research. Three degree in member scale was set as parameter aiming laboratory scale, real scale, and scale in huge structures such as

nuclear power plant. The rate of stiffness reduction was slower in huge structure with thick member while converged reduction ratio was insensitive with structural scale. When drying effects for member was focused, shear stiffness in RC member was degraded by drying shrinkage cracks distributed in an entire member. Stiffness reduction caused by distributed fine cracks can be reproduced by conventional smeared crack model.

The model of corrosion crack had difficulty in deviation between smeared crack model and specific characteristic of corrosion crack such as concentration or specific direction along rebar. In order to make clear conventional model, the author conducted the corrosion induced analysis for concrete plate with a rebar with fine or rough mesh size, and the shear stiffness in the model with rough mesh size was underestimated or overestimated with corrosion ratio. For more accurate reproduction, the corrosion crack model was developed with division into three state, state that corrosion crack did not penetrated, the crack was penetrated but corrosion product was kept around rebar, and corrosion product was discharged from concrete surface by penetrated crack. Corrosion model was developed as shown in **Fig. 3.46**. Conventional corrosion model cannot represent non-penetrated crack condition, thus this study proposed new model for shear stiffness, which is reproduced by area ratio of cracked to uncracked. Area ratio  $k$  was described by only two parameter, corrosion ratio  $R_{cor}$  and ratio of rebar diameter to mesh size  $D/l_r$ . After crack penetration, expansion in an entire RC zone by rough mesh with corrosion cannot consider the uneven crack width in cross section and axial direction. Equivalent corrosion ratio  $R_{cor\_eq}$  can solve this deviation from actual condition. Under severe corrosion state, conventional model neglected the discharge of corrosion gel from penetrated crack. Implement of discharge limit which means limit value of crack



**Figure 3.46** Summary of model development for corrosion crack

opening can consider this phenomenon. Validation of the proposed model was performed by the reproduction analysis for the static loading test on the beam subjected to severe rebar corrosion exceeding discharge limit and parametric analysis by fine and rough mesh model with various corrosion ratio. Shear transfer declination of damaged concrete due to corrosion crack can be evaluated precisely and stiffness of a member could be reproduced with high accuracy as member scale structural response. There was room for more consideration on the reproduction of the structural response around failure or in post-peak especially for shear failure, but the proposed model was insensitive in this stage. Instead, the structural behavior around shear failure was determined by momentary shear crack penetration behavior in compression edge, thus it was considered that fracture behavior under compression influenced greatly with high dependence with mesh size. More validations were also required for wide applicability range and high precision by reproducing actual behavior of member on flexural and shear mode. In this study, from 50mm to 200mm of mesh size is main target, but real scale analysis with foundation or ground requires larger mesh size, 300mm or 500mm. Multiple rebar in a mesh or more direct implement of crack angle has large contribution.

### References in Chapter 3

- [1] Maekawa, K. Ishida, T., Kishi, T., (2008). Multi-scale modeling of structural concrete. CRC Press
- [2] Maekawa, K., Ishida, T., Kishi, T. (2003). Multi-scale modeling of concrete performance integrated material and structural mechanics. *Journal of Advanced Concrete Technology*, 1(2), 91-126
- [3] Ogata, Y., Hirotsu, K., Aizawa, N., Inoue, N., Nozawa, T., (2011), A study of initial stiffness on the building changed by passing age at small and medium-sized earthquake motion by ARX model, *Summaries of technical papers of annual meeting, AIJ, B-2, Structure II*, 983-984
- [4] Abe, Y. and Mori, K., (2005), Research study on degradation of natural frequency of reinforced concrete buildings by micro tremor measurement. *Proc. Architecture Institute of Japan Tohoku Branch, Structure* (68), 89-92
- [5] Kashima, T. and Kitagawa, Y., (2006), Dynamic characteristics of a building estimated from strong motion records using evolution strategy, *Journal of Structural and Construction Engineering*, 602, 145-152.,
- [6] Toyobe, R., Kojima, H., Tobita, H. and Fukuwa, N., (2013), Long-term seismic response observation for evaluation of dynamic properties of low and midium-rize building, *AIJ Tokai Branch*, 51, 177-180
- [7] Maruyama, I., (2016), Multi-scale review for possible mechanisms of natural frequency change of reinforced concrete structures under an ordinary drying condition, *Journal of Advanced Concrete Technology*, vol.14, 691-705
- [8] Yoneda, T., Ishida, T., Maekawa, K., Gebreyouhannes, E., Mishima, T., (2015), A micro-cracking

model coupled with micro fracture and water status in micro pore structures, Journal of Japan Society of Civil Engineers, Ser. E2 (Materials and Concrete Structures), 71(3), 263-282

[9] Yoneda, T., Ishida, T., Maekawa, K., Gebreyouhannes, E. Mishima, T. 2013, Simulation of early-age cracking due to drying shrinkage based on a multi-scale constitutive model, Poromechanics V: ASCE, 579-588.

[10] Chijiwa, N. and Maekawa, K., (2015), Thermo-hygral case-study on full scale RC building under corrosive environment and seismic actions, Journal of Advanced Concrete Technology, 13(10), 465-478

[11] Maekawa, K., Zhu, X., Chijiwa, N., Tanabe, S., (2016), Mechanism of long-term excessive deformation and delayed shear failure of underground RC box culverts. Journal of Advanced Concrete Technology, 14(5), 183-204

[12] Maekawa, K., Ishida, T., Chijiwa, N., Fujiyama, C., (2015). Multiscale coupled-hygro mechanistic approach to the life-cycle performance assessment of structural concrete.” Journal of Materials in Civil Engineering, ASCE, 27(2), A4014003, 1-9

[13] Kurihara, R., Chijiwa, N., Maekawa, K., (2017). Thermo-hygral analysis on long-term natural frequency of RC buildings with different dimensions. Journal of Advanced Concrete Technology, 15(8), 381-396.

[14] Gebreyouhannes, E., Maekawa, K., (2016)., Nonlinear gel migration in cracked concrete and broken symmetry of corrosion profiles. Journal of Advanced Concrete Technology, 14(6), 271-286.

[15] Sasano, H., Maruyama I., Nakamura, A., Yamamoto, Y., Teshigawara, M., (2018), Impact of Drying on Structural Performance of Reinforced Concrete Shear Walls, Journal of Advanced Concrete Technology, vol.16, pp. 210-232

[16] 李宝禄, 前川宏一. (1988). 接触面密度関数に基づくコンクリートひびわれ面の応力伝達構成式. コンクリート工学, 26(1), 123-137.

[17] Maekawa, K., Okamura, H., & Pimanmas, A., (2003), Non-linear mechanics of reinforced concrete. CRC Press.

[18] Toongoenthong, K., Maekawa, K., (2005)., Simulation of coupled corrosive product formation, migration into crack and propagation in reinforced concrete sections. Journal of Advanced Concrete Technology, 3(2), 253-265.

[19] Toongoenthong, K., Maekawa, K., (2005)., Multi-mechanical approach to structural performance assessment of corroded RC members in shear. Journal of Advanced Concrete Technology, 3(1), 107-122.

[20] Biswas, R. K., Iwanami, M., Chijiwa, N., & Uno, K. (2020). Effect of non-uniform rebar corrosion on structural performance of RC structures: A numerical and experimental investigation. Construction and Building Materials, 230, 116908.

[21] Chijiwa, N., Suryanto, B., Kurihara, R., FORENSIC ANALYSIS OF REINFORCED



CONCRETE HALF-JOINTS. Technology, 6(1), 215-226, 2020

- [22] Oh, B. H., Kim, K. H., Jang, B. S. (2009), Critical corrosion amount to cause cracking of reinforced concrete structures. ACI Materials Journal, 106(4), 333.
- [23] Molina, F. J., Alonso, C., Andrade, C. (1993), Cover cracking as a function of rebar corrosion: Part 2—Numerical model. Materials and structures, 26(9), 532-548.
- [24] Amleh, L., Ghosh, A. (2006), Modeling the effect of corrosion on bond strength at the steel-concrete interface with finite-element analysis. Canadian Journal of Civil Engineering, 33(6), 673-682.
- [25] 高谷哲, 西澤彩, 中村士郎, 山本貴士, 宮川豊章, (2015), コンクリート中における鉄筋の腐食生成物の生成プロセスおよび電気化学的特性. 土木学会論文集 E2 (材料・コンクリート構造), 71(3), 235-247.
- [26] 高谷哲, 中村士郎, 山本貴士, 宮川豊章. (2013), コンクリート中の鉄筋の腐食生成物の違いがひび割れ発生腐食量に与える影響. 土木学会論文集 E2 (材料・コンクリート構造), 69(2), 154-165.
- [27] 千々和伸浩, 川中勲, 前川宏一. (2011), 引張鉄筋定着部に腐食劣化を有する RC 梁の残存耐力と未損傷領域への面的補強. 土木学会論文集 E2 (材料・コンクリート構造), 67(2), 160-165.

### ***Annotation***

Contents in section 3.2 and section 3.3 in chapter 3 have been published as follows.

Kurihara, R., Chijiwa, N., Maekawa, K., (2017). Thermo-hygral analysis on long-term natural frequency of RC buildings with different dimensions. Journal of Advanced Concrete Technology, 15(8), 381-396., doi: 10.3151/jact.15.381

# Chapter 4

## Conclusions

- Conclusions
- Future recommendations

## 4.1 Conclusions

This study focused on the influence of rebar corrosion on bond between rebar and concrete and stress transfer behavior change due to concrete crack. Implementation into structural analysis models was also aimed and FE analytical model which was applicable in FE analysis with large mesh size was developed by averaged structural behavior considering spatial nonuniformity. The advanced point of this study was implementation of meso scale phenomenon into macro scale model under the social demand of FE modeling which was applicable for the analytical evaluation on real scale structures subjected to rebar corrosion. The main conclusions are summarized as followings.

- (1) Whether mechanical interlock can work or not was dominant factor for sound bond rather than chemical adhesion or friction resistance. Section loss of rebar causes reduction of contact area between a lug and concrete, but interlock can be maintained until a certain degree of lug height loss.
- (2) Stirrups strongly suppressed the relative displacement of main rebar to surrounded concrete in the both axial direction and orthogonal direction. As a result, it affected location of crack propagations, and kept interlock between concrete and main rebar. Stirrups had great contribution to prevent detachment and slip of main rebar.
- (3) When parts of rebar surface had interlock, slip and pull-out of rebar did not occur even if some region in rebar lost interlock completely. Thus, bond performance was insensitive even though the section loss ratio increased by corrosion. As long as the section loss ratio was lower than approximately 20%, and the bond as an entire member can be assumed as sound state.
- (4) Stiffness reduction caused by bond deterioration in the state with high section loss ratio was reproduced by the proposed model defined by the degree of tension stiffening by the structural analysis ignoring section loss and corrosion crack with large mesh size.
- (5) Smeared crack model can reproduce the influence of distributed cracks on the structural performance properly. Stiffness of structures with various scale was declined due to shrinkage crack formed by moisture loss with environmental condition. It suggested the cause of natural frequency decline measured in existing structures. Scale of members had large influences on the speed of drying progress, and there was mesh size dependence in the analytical reproduction of drying effects.

- (6) When elongation of corrosion crack before penetration was focused on, shear stiffness could be calculated by the summation of uncracked and cracked stiffness with the area ratio. Area ratio can be described by the squared corrosion ratio of rebar and the ratio of rebar diameter to mesh size.
- (7) Shear stiffness after crack penetration in large mesh based on the contact density function in the conventional model had deviation from actual value. It was required to consider the unevenness of crack surface in the both normal and parallel direction to rebar axis. Equivalent crack width model considering averaged crack width and macro scale contact was proposed. Equivalent crack width also can be described as equivalent corrosion ratio. Overestimation of shear stiffness reduction after crack penetration was modified by the proposed model.
- (8) Maximum crack width should be implemented into the model of corrosion expansion because discharge of corrosion product from cracked concrete surface released expansive strain. Corrosion ratio at the discharge limit was considered as 2 times larger value. Overestimation of shear stiffness reduction at the high corrosion ratio was modified.
- (9) Change of stress transfer behavior of concrete around rebar and member stiffness before and after formation of flexural crack with corrosion progress up to 12% of section loss ratio was reproduced well by the proposed model even when large mesh size was applied.

This study investigated and developed the equivalent corrosion models in large mesh size, and practical FE model for analytical evaluation on real scale structures with corroded rebar was developed. Through the investigation, this study gave the important suggestion on bond deterioration. In general, bond was regarded as deteriorated after corrosion crack became visible at concrete surface. However, this study showed that bond between rebar and concrete can be maintained as long as interlock in parts of region in a member worked. These suggestions were given by separating out various bond components which are complicatedly influenced. Corrosion crack declined the performance of RC structures in member stiffness influencing seismic response. Before the development of equivalent corrosion crack model, the author focused on the influence of drying shrinkage of concrete on structural performance. Drying shrinkage crack was distributed crack in a whole member and have a high affinity with smeared crack model. It was showed that the conventional smeared crack model had enough accuracy to evaluate the distributed crack, and it was suggested that drying of concrete was a cause of problem in existing RC structures. Conventional model for induction of corrosion expansion in large mesh was deviated from actual phenomenon, thus equivalent corrosion crack model was developed in this study. The proposed model produced improvement in the prediction of the behavior damaged concrete as averaged behavior of FE mesh with corrosion crack. Totally, this study had

contribution in the evaluation of residual structural performance for deteriorated structures by rebar corrosion for effective and efficient maintenance.

#### **4.1 Future recommendations**

This study proposed the limit value of corrosion ratio that sound bond can be assumed, and development of bond deterioration model after the limit as sharp loss of bond. Applicable range of bond deterioration model by tension stiffening with high rebar corrosion state was required because more than 20% of corrosion ratio can be observed on severe condition against rebar corrosion such as coastal structures. Investigation on the influence of crack around rebar was also required for more accurate bond deterioration model. Corrosion crack changed the geometry of concrete around rebar, thus it was equivalent as section loss of rebar.

Equivalent corrosion crack model had a room for investigation on more precise description. Equivalent crack width model was based on the minimum crack width in uneven crack surface as assumed fixed value. Inducing of function which can consider instability or uncertainly such as probability distribution on crack opening, crack elongation direction or meso-scale interlock between cracks may improve the accuracy of the proposed model.

The proposed model required corrosion ratio as a input data, and the corrosion ratio should be estimated from destructive or non-destructive inspection on existing structures. It is difficult to get accurate corrosion state of nonuniform rebar corrosion while inspection technology is now developing. Interrelationship between averaged region defined by finite element and inspection was considered for application on existing structures. Changing property of corrosion product fixed in this study can be evaluated properly in the analysis. For improving that, time dependent model with multi-scale structural model which can reproduce chemical reaction causing corrosion process is highly recommended. It makes possible to track overall life cycle of newly established structure and future behavior of existing structure. Development of integrated analysis requires investigations on variation of property of corrosion product affected environmental condition, the effects of stress state on corrosion crack elongation with time dependence considering creep behavior, induction of pit corrosion, and implementation of pit corrosion as averaged behavior. Estimation of airborne chloride environment or rinse of adhered salt by rainfall is also called for.

## 謝辞

博士學位論文の提出にあたり、多くの方々にご指導・ご支援いただきました。

千々和伸浩博士には學位論文の主査として、また、学部4年の研究室所属以来、研究内容に関するご指導にとどまらず、進路、研究哲学、様々なことについて、終始あたたかいご指導をいただきました。ありがとうございました。これからも先生の背中を追い、精進してまいります。學位論文審査にあたっては、岩波光保博士、高橋章浩博士、佐々木栄一博士、河野進博士、牧剛史博士には副査をお願いし、数多くの貴重なご助言を賜りました。謹んで感謝申し上げます。

岩波光保博士、中山一秀博士には、研究室所属以後、常日頃から、研究にとどまらず様々なことについてご指導、ご助言いただきました。先生方の多大なる支援をうけ、6年間を通して大変有意義な研究室生活を送ることができ、大きく成長できました。感謝申し上げます。二羽惇一郎博士、中村拓郎博士、大窪一正博士、にはコンクリート研合同ゼミの場を中心に、貴重なご意見を数多くいただき、ありがとうございました。先生方から吸収させていただいたことは貴重な財産となりました。

本研究は日本学術振興会 特別研究員奨励費(課題番号: 19J22658)の助成を受け実施したものであり、ここに記して御礼申し上げます。

研究室メンバーをはじめ、家族、友人、数多くの方より、本研究の遂行にあたり多大なるご協力、ご支援をいただきました。皆様に深く御礼申し上げます。

令和4年2月 栗原 遼大